Water-Based Polymeric Nanostructures for Agricultural Applications

Priyanka Bansal

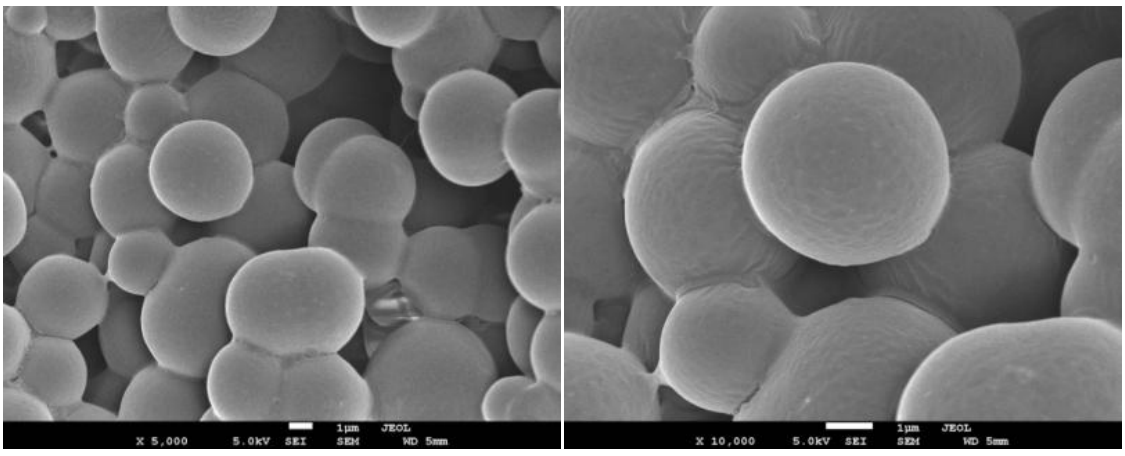

Marburg/Lahn 2010

Water-Based Polymeric Nanostructures for Agricultural Applications

Dissertation

zur

Erlangung des Doktorgrades

der Naturwissenschaften

(Dr. rer. nat.)

dem

Fachbereich Chemie

der Philipps-Universität Marburg

vorgelegt von

Priyanka Bansal

aus

Neu Delhi, Indien

Marburg/Lahn 2010

Vom Fachbereich Chemie der Philipps-Universität Marburg als Dissertation angenommen:	12.11.2010
Erstgutachter:	Prof. Dr. Andreas Greiner
Zweitgutachter:	Prof. Dr. Andreas Seubert
Tag der mündlichen Prüfung:	22.11.2010

Table of Contents

List of symbols and abbreviations

APCI	Atmospheric pressure chemical ionization
a.u.	Arbitrary units
cm	centimeter
cm^{-1}	Wavenumber
Conc.	Concentrated
$CDCl_3$	Deuterated chloroform
CMC	Critical micelle concentration
Da	Dalton
DSC	Differential scanning calorimetry
DA	(E,Z)-7,9-dodecadien-l-yl acetate
DMF	Dimethyl formamide
e.g.	For example
et al.	et alii
FTIR	Fourier transform infrared spectroscopy
GPC	Gel permeation chomatography
g	gram
h	Hour
hν	Radiation
HCl	Hydrochloric acid
i.e.	That is
K	Kelvin
kDa	KiloDalton
km	Kilometer
kV	Kilovolt
m	mass
m	Multiplet (NMR)
mg	Milligram
mol	Mole
M_w	Weight average molecular weight

M_n	Number average molecular weight
min	Minute
mN	Millinewton
mL	Milliliter
mm	Millimeter
MWCO	Molecular Weight Cut-Off
NMR	Nuclear magnetic resonance
nm	Nanometer
OLA	Oligolactide
ppm	Parts per million
PVA	Poly(vinyl alcohol)
PLA	Polylactide
PEO	Polyethylene oxide
PU	Polyurethane
Pa	Pascal
s	Second
s	Singlet (NMR)
SEM	Scanning electron microscope
T_g	Glass transition temperature
TGA	Thermogravimetric analysis
T	Temperature
THF	Tetrahydrofuran
UV	Ultraviolet
vol.	Volume
wt%	Weight percentage
WAXD	Wide angle X-ray diffraction
z	Charge
µm	Micrometer
δ	Chemical shift

1. Introduction and aim of this work

Electrospinning of biodegradable polymers for the preparation of nanofiber-based non-wovens has many potential applications in medicine, drug-delivery and agriculture. Among the biodegradable polymers, mainly aliphatic polyesters have been used for nanofiber preparation by electrospinning. The solubility of these biodegradable polymers like polylactides (PLA), polyglycolide (PGA), and polycaprolactones (PCL) is mostly limited to harmful solvents like chloroform and dichloromethane, which is critical for processing and certainly restricts the potential of biodegradable polyesters, in particular for coating applications for solutions.[1-3]

Other biodegradable and water soluble polymers like poly(vinyl alcohol) along with water soluble, biodegradable polyesters[4, 5] are less useful for applications as mentioned above, as the resulting coatings etc. will also be water-soluble, if not, otherwise a laborious and harmful crosslinking step is involved after processing.

Water could be the most promising solvent for processing if the encapsulation of additives such as drugs, enzymes, pheromones, bacteria, viruses, cells in biodegradable polyester for release applications is required for particular applications. However, encapsulation of additives in biodegradable polyesters for controlled release applications in the case of water-soluble polyesters would result in burst release of additives which is mostly unwanted. Therefore, disintegration of the polyester matrix, although processed from water, should not occur upon contact to water immediately and thereby requires water-insoluble polyesters dispersed in water. For example, burst release of pheromones would occur in biotechnical plant protection upon contact with water if the polyesters used for encapsulation would be too hydrophilic. Here, retarded release of pheromones is of outmost importance for successful plant protection. An answer to this problem could be dispersions of water-insoluble biodegradable polyesters in water.

Electrospinning of aqueous dispersions of biodegradable polyesters alleviates concerns regarding safety, toxicology, and environmental problems, which are associated with spinning of such polyesters from harmful organic solvents and thereby offers novel

perspectives for applications in medicine, pharmacy and agriculture. Electrospinning of polymers from aqueous dispersions is termed as "green electrospinning".[6]

The aim of this work is to prepare stable aqueous dispersions using biodegradable materials followed by subsequent electrospinning to get water-stable nanofibers.

The work consists of three parts:

First part involves the preparation of water stable poly(vinyl alcohol) (PVA) fiber mats for various applications including microencapsulation. In this part, various chemical crosslinking methods, photocrosslinking methods and physical methods are tried to bring about water insolubility of PVA. Crosslinking PVA with another polymer, polyurethane (PU) is also carried out. Electrospinning of polyurethane dispersion in water with PVA produced nanowebs with excellent water resistance both at low as well as high temperatures. Furthermore, the water absorbancy of the insoluble PVA fiber mats is altered by a simple sol-gel treatment. The mats thus obtained show excellent hydrophobicity.

Second part involves the preparation of microcapsules loaded with an additive, a pheromone, using biodegradable polymers for mating disruptions in *Lobesia Botrana*, the European Grapevine Moth. Various microencapsulation techniques like coacervation, solvent evaporation are tried and polyester microcapsules containing as high as 60 wt% pheromone are produced.

Third part involves the preparation of stable secondary dispersions of sufficiently hydrophilic oligolactide (OLA) as a matrix for encapsulation of the pheromone. The concept of miniemulsions is applied to use the pheromone as a secondary dispersion hydrophobe to stabilize the dispersions of a polymer like OLA in water. Dispersions with high solid content containing OLA, pheromone and a surfactant Brij® S20 are prepared by a combination of solvent displacement method and osmosis. The resulting dispersion is electrospun by combination with the dispersion of a biodegradable blockcopolyester resulting in all-biodegradable water-stable nanofibers.

2. Theoretical background

2.1. Electrospinning

2.1.1. Introduction

Electrospinning[7-13] is the process of producing continuous fibers from the submicron diameter down to the nanometre diameter. Till now, the electrospinning method has been successfully employed to prepare fibers from a wide range of polymers, including conventional polymers, biodegradable polymers, proteins, and peptides. The electrospinning process has attracted great attention not only because of its versatility in spinning a wide range of polymeric fibers but also because of its consistency to produce fibers with submicron diameters. Electrospun fibers show many outstanding properties such as large surface area, tunable surface morphologies, flexible surface functionality, and better mechanical performance. The various applications of nanofibers include filtration, textiles, drug delivery[14, 15], wound dressings, tissue scaffolds[16-18], plant protection and so on. Incorporation of carbon nanotubes[19, 20], biological materials such as bacteria[21] and virus[22] into the polymer matrix to obtain multifunctional nanofibers has also been possible.

Apart from polymers, electrospinning has been used to produce nanofibers of composites, semiconductors and ceramics[23, 24], metals[25]. Fabrication of electrospun nanofibers via different nanofiber assembling techniques has also been reported for various applications such as continuous nanofiber yarn[26], uniaxial aligned nanofiber mats[27, 28], aligned fibrous arrays[29] and so on.

2.1.2. Electrospinning technique

A schematic diagram to interpret the electrospinning of polymer nanofibers is shown in **Figure 1**. The electrospinning process requires the presence of a high voltage supply, a capillary tube or needle of small diameter, a grounded metal collector. In the electrospinning process, a high voltage is used to create an electrically charged jet of polymer solution or melt out of the needle. Before reaching the collector, the solution jet evaporates or solidifies and is collected as a web consisting of interconnected fibers. One electrode is placed into the spinning solution or melt and the other is attached to the

collector. The end of the needle is subjected to an electric field. This needle contains the polymer solution held by its surface tension. This induces a charge on the surface of the liquid. Mutual charge repulsion and the contraction of the surface charges to the counter electrode cause a force directly opposite to the surface tension. As the intensity of the electric field is increased, the hemispherical surface of the fluid at the tip of the capillary tube elongates to form a conical shape known as the Taylor cone. Further increasing the electric field, a critical value is attained with which the repulsive electrostatic force overcomes the surface tension and the charged jet of the fluid is ejected from the tip of the Taylor cone. The discharged polymer solution jet undergoes an instability and elongation process, which allows the jet to become very long and thin. Meanwhile, the solvent evaporates, leaving behind a charged polymer fiber. In the case of a melt, the discharged jet solidifies in air.[30, 31]

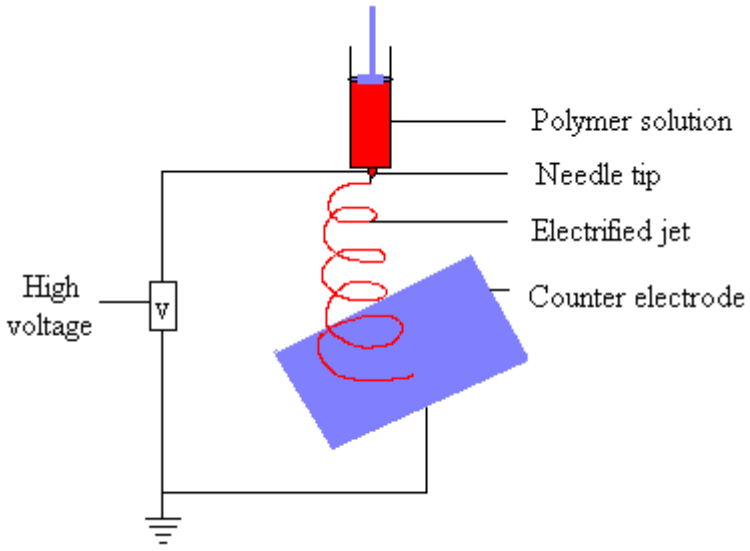

Figure 1. Schematic representation of the electrospinning set-up.

The formation of nanofibers by electrospinning can be controlled by various parameters like applied voltage, solution feeding rate and solution properties like conductivity, viscosity, and surface tension. Therefore, these electrospinning parameters can be tuned to produce nanofibers with varying diameters.[32]

2.2. Degradable polymers

2.2.1. Introduction

Since the first developments of polymeric materials, scientists and engineers have intensively tried to increase the stability of these materials against the environmental influences. As a result, these polymeric materials (plastics) are being used in all sectors of life as durable products with tailor-made properties. However, since the last decade the enormous use of these materials has created serious problems of degradation owing to their excessive stability. As a consequence, a lot of initiative has been taken since the early 1990s to develop novel polymers which have the same properties as conventional polymers but are more susceptible to degradation and hence are more environmental friendly. Since the main bulk of the domestic waste is made of plastics, there is a great deal of interest in recycling plastics and in producing plastic materials that can be safely and easily disposed of in the environment. Current degradable polymers are designed to degrade either biologically, photolytically, or chemically, depending on the disposal environment that they will encounter after use.

Table 1. Classification of biodegradable polymers.[33]

Natural Polymers		Synthetic Polymers	
Sub-classification	Examples	Sub-classification	Examples
1. Plant origin		1. Aliphatic polyesters	
1.1. Polysaccharides	Cellulose, Starch, Alginate	1.1. Glycol and dicarbonic acid polycondensates	Poly(ethylene succinate), Poly(butylene terephthalate)
2. Animal origin		1.2. Polylactides	Polyglycolide, Polylactides
2.1. Polysaccharides	Chitin (Chitosan), Hyaluronate	1.3. Polylactones	Poly(ε-caprolactone)
2.2. Proteins	Collagen (Gelatin), Albumin		
3. Microbe origin		2. Polyols	Poly(vinyl alcohol)
3.1. Polyesters	Poly(3-hydroxyalkanoate)	3. Polycarbonates	Poly(ester carbonate)
3.2. Polysaccharides	Hyaluronate	4. Miscellaneous	Polyanhydrides, Poly(α-cyanoacrylate)s, Polyphosphazenes, Poly(orthoesters)

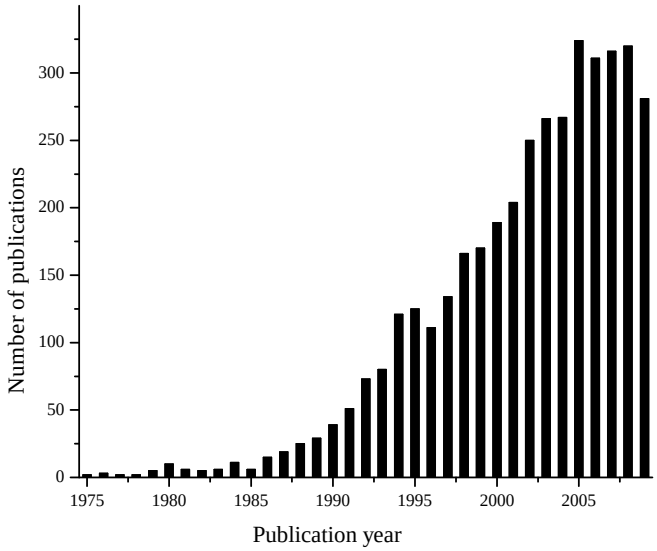

Figure 2. Comparison of the annual number of scientific publications from 1975-2009 for "biodegradable polymers" (data analysis of the publications was done using the SciFinder Scholar search system with the term "biodegradable polymers", on 5 October 2010).

Work on biodegradable polymers has received a lot of attention since the past 10 to 15 years which is evident from the drastic increase in the number of annual publications as shown in **Figure 2.**

2.2.2. Degradation mechanisms

The degradation of a polymer can be chemical, physical, and biological. The non biotic effects include chemical hydrolysis, thermal polymer degradation, oxidation, or scission of the polymer chains by irradiation (photo-degradation). The biotic degradation of a polymer is the attack of the microorganisms on the non water-soluble polymers. These are known as "biodegradable polymers". The biodegradable polymers can be of natural i.e. animal or plant origin or synthetic **(Table 1).**

Because of the lack of water solubility and the size of the polymer molecules, the microorganisms are unable to transport the polymeric materials directly into the cells where all the biochemical processes take place. Hence, it is necessary to reduce the molar mass of the polymer sufficiently to get water soluble intermediates which can be transported into the microorganisms and can undergo the appropriate metabolic

pathway.[34] The end products of these metabolic processes are carbon dioxide, water and methane (in case of anaerobic degradation) along with a new biomass. Thus, a biodegradable polymer has the ability to break down by biological means into raw materials of nature and disappear into nature. Because of the co-existence of both biotic and non-biotic effects, the entire mechanism of polymer degradation can also be known as environmental degradation.

Environmental factors not only help the polymer to degrade, but they also play a major role in influencing the activity of different microorganisms. Parameters such as humidity, temperature, pH, salinity, the presence or absence of oxygen, have important effects on the microbial degradation of polymers.

Another important factor in polymer degradation is the chemical structure and the chemical composition of the polymer. Polymers usually do not consist of one homogeneous component but they can contain different polymers (blends) or low molecular weight additives like plasticizers. The different structures of a polymer, for example copolymers which consist of random, alternate or block copolymers, and branched or crosslinked polymers, can influence the degradation behaviour of that polymer. In addition, the crystallinity and crystal morphology of a polymer depends on the processing parameters and it can change with time. All these above factors are responsible in determining the degradation behaviour of a polymer.

Due to the presence of C-C backbone, most of the synthetic polymers are resistant to various types of degradation. However, polymers containing heteroatomic functional groups in the backbones like polyesters, polyanhydrides, polyacetals, polyamides, polyphosphazenes, or polycarbonates are prone to hydrolysis or attack by the microorganisms and thus confer degradability.

Degradation starts by the enzymatic or non-enzymatic hydrolysis of the polymer to form oligomers or small molecules containing functional groups such as the carbonyl group, or alcohols like in the case of polyesters. Due to a relatively bigger size, the enzyme cannot diffuse into the depth of the solid substrate, therefore enzymatic hydrolysis takes place only on the surface of the substrate and starts from a relatively less ordered region or amorphous region instead of the more rigid crystalline interior. After the hydrolysis of the surface, the small molecules generated at the surface are washed away by water

and the enzyme attacks another new layer. Hence, the molecular weight of the substrate does not change much, only the loss of weight of the solid substrate is observed. Non-enzymatic (basic or acidic) hydrolysis also starts from the surface and prefers the amorphous region but the small basic or acidic reagents are capable of diffusing into the solid substrate to start in-depth degradation. Consequently, the molecular weight decreases but the total weight change of the solid cannot be detected very fast. The second step of degradation is the breakdown of the resulting small molecules by micro-organisms into CO_2, water and biomass.

There are also a few degradable polymers with C-C backbones, one is a naturally occurring polymer, polyisoprene (Natural rubber) **(Figure 3)**.

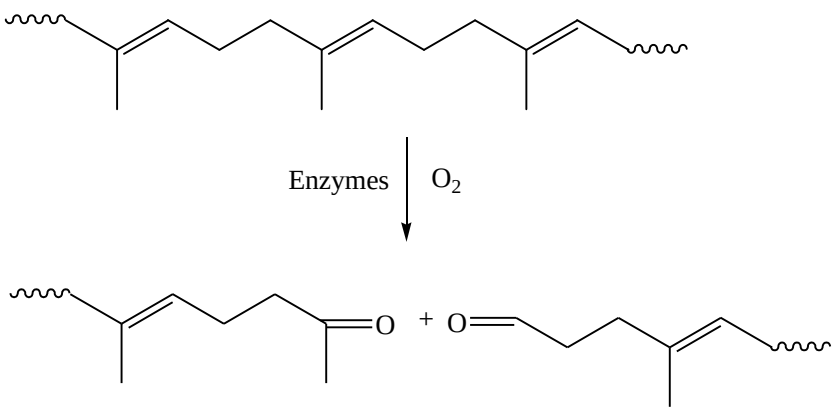

Figure 3. Enzymatic oxidative degradation of polyisoprene.

The others are synthetic vinyl polymers like poly(vinyl alcohol) and poly(vinyl methyl ether). These polymers contain pendent functional groups that undergo photo, thermal or enzymatic oxidative degradation **(Figure 4)**.

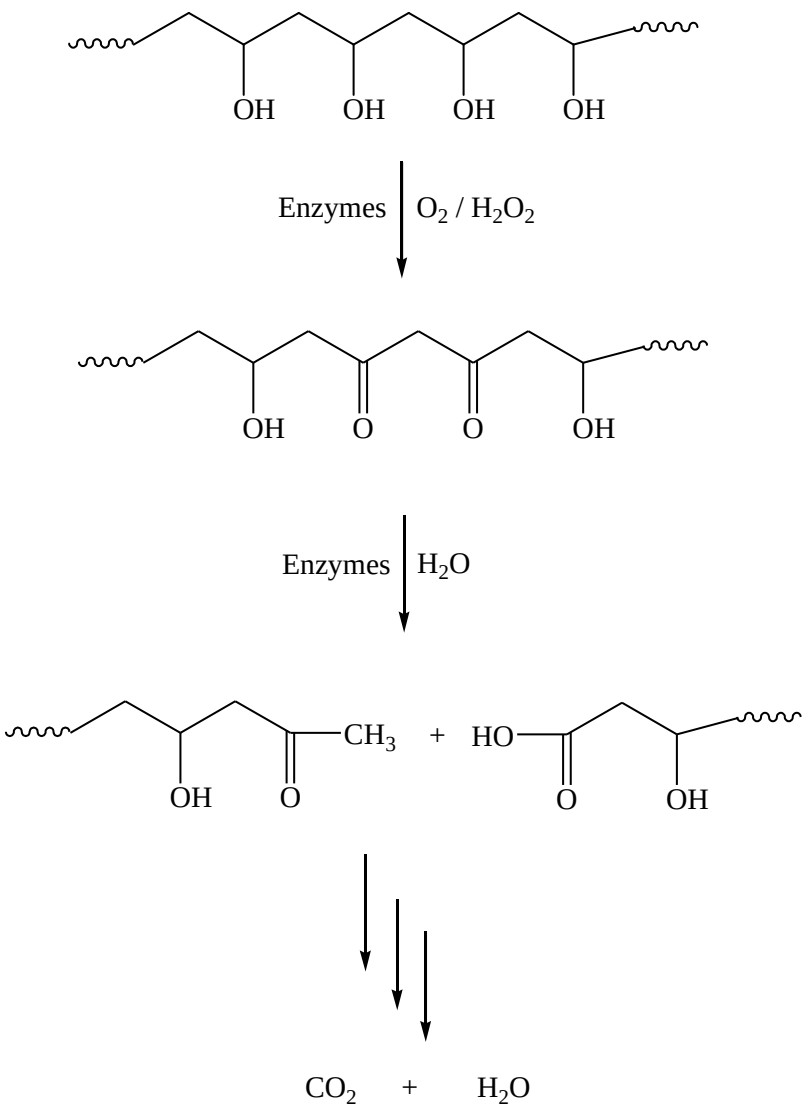

Figure 4. Enzymatic oxidative degradation of poly(vinyl alcohol).

2.2.3. Polymer degradation by erosion

All degradable polymers can undergo surface erosion or bulk erosion. The degradation behaviour depends on the diffusivity of water inside the polymer matrix, the rate of degradation of the polymer's functional groups, and the dimensions of the polymer matrix. In surface erosion, the polymer is eroded from the surface while in case of bulk erosion, degradation takes place throughout the whole of the sample. Surface eroding polymers do not allow water to penetrate into the material and erode layer by layer. Bulk eroding polymers take in water throughout the material and erode inside and on the

surface of the polymer. Typical examples of the polymers undergoing surface erosion are poly(ortho)esters and polyanhydrides. In this case, erosion proceeds at constant velocity at any time during erosion. However, bulk eroding polymers such as polylactides (PLA), polyglycolides (PGA), poly(lactic-*co*-glycolic acid) (PLGA), polycaprolactones (PCL), have no constant erosion velocity. Schematic illustration of surface and bulk erosion is shown in **Figure 5**.

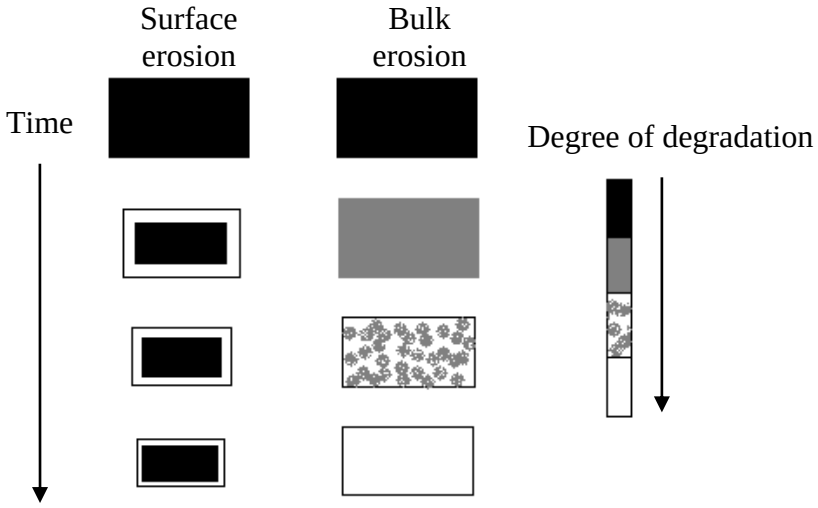

Figure 5. Schematic diagram of surface erosion and bulk erosion in a polymer matrix.

Polymer erosion plays an important role in essential processes such as the release of drugs from polymer implants. By knowing the kind of erosion a polymer undergoes, it can be effectively used for the design of drug delivery systems.[35, 36]

2.2.4. Biodegradable polyesters

A vast majority of the biodegradable polymers have been extensively studied.[37] Among these poly(α-hydroxy acids) like poly(lactic acid) (PLA) and poly(glycolic acid) (PGA), and a range of their copolymers have a long history of use as synthetic biodegradable materials. These polymeric materials have found a lot of use in biomedical applications like suture plates, stents, dialysis media and drug-delivery devices. It is also being evaluated as a material for tissue engineering. A wide range of aliphatic polyesters can be designed by changing the synthesis conditions to meet the specific requirements such

as crystallinity, glass transition temperature, solubility, hydrophobicity, degradability, biocompatibility, melting temperature, and so on. The aliphatic polyesters except for poly(α-hydroxy acids) are degraded by the enzymes excreted from the microorganisms. **Table 2** gives an insight into the degradation rates for various polyesters.

Table 2. Properties of synthetic biodegradable polymers.[33]

Polymer	Structure	M_w / kDa	Degradation rate
Poly(glycolic acid)	Crystalline	-	100% in 2-3 months
Poly(L-lactic acid)	Semi-crystalline	100-300	50% in 1-2 years
Poly(glycolic acid-*co*-L-lactic acid)	Amorphous	40-100	100% in 50-100 days
Poly(ε-caprolactone)	Semi-crystalline	40-80	50% in 4 years
Poly(L-lactic acid-*co*-ε-caprolactone)	Amorphous	100-500	100% in 3-12 months
Poly(orthoester)	Amorphous	100-150	60% in 50 weeks

2.2.5. Classification of degradable polyesters

Based on the constituent monomers, the aliphatic polyesters can be categorized into two kinds. One is polyhydroxyalkanoate, a polymer of hydroxyl acid (HO-R-COOH). The hydroxyl acids can be divided further into α, β, ω-hydroxyl acids based on the position of OH group with respect to the COOH group. The other type is poly(alkylene dicarboxylate), which are produced by condensation reaction between prepolymers having hydroxyl or carboxyl terminal groups using chain extenders such as diisocyanate. Direct polycondensation between low-molecular weight diols and diacids produces only low molecular weight polymers. A detailed classification of the aliphatic polyesters is given in **Table 3.**

Table 3. Classification of aliphatic polyesters.[33]

Polymers	Chemical structure		Examples
Poly(α-hydroxy acid)	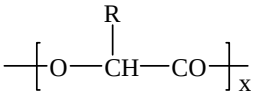	R = H R = CH_3	Poly(glycolic acid) (PGA) Poly(L-lactic acid) (PLLA)
Poly(β-hydroxyalkanoate)	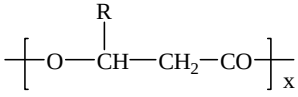	R = CH_3 R = CH_3, C_2H_5	Poly(β-hydroxybutyrate)(PHB) Poly(β-hydroxybutyrate-*co*-β-hydroxyvalerate) (PHBV)
Poly(ω-hydroxyalkanoate)	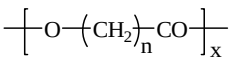	n = 3 n = 4 n = 5	Poly(γ-butyrolactone) Poly(δ-valerolactone) Poly(ε-caprolactone)
Poly(alkylene dicarboxylate)	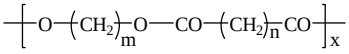	m = 2, n = 2 m = 4, n = 2 m = 4, n = 2,4	Poly(ethylene succinate) (PES) Poly(butylene succinate) (PBS) Poly(butylene succinate-*co*-butylene adipate) (PBSA)

2.2.6. Synthesis of polyesters

One way of synthesizing aliphatic polyesters is by condensation polymerization or step polymerization i.e. the condensation of a hydroxy-acid (HO-R-COOH) or reaction of a diol (HO-R_1-OH) and a diacid (HOOC-R_2-COOH) **(Figure 6)**. However, this method is not suitable for obtaining high molecular weight polyesters. Another drawback is the broad molecular weight distribution obtained due to the failure to accurately control the polymer's molecular weight. Further, the monomers are thermally unstable and side reactions such as dehydration and decarboxylation readily occur.

Figure 6. Synthetic route of poly(ethylene adipate) by condensation polymerization.

Another conventional route is by ring-opening polymerization (ROP) of cyclic esters in the presence of a catalyst such as stannous octoate using an initiator that contains an active hydrogen atom **(Figure 7)**.[38, 39]

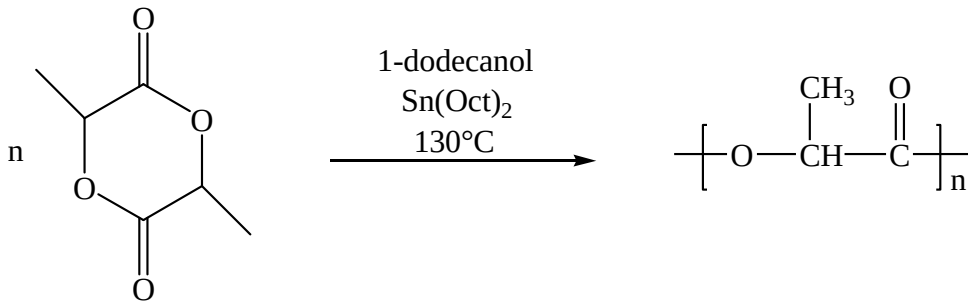

Figure 7. Ring-opening polymerization of cyclic esters to synthesize poly(lactic acid).

The general mechanism to prepare polyesters by ring-opening polymerization involves initiation either by an anionic, a cationic or coordination-insertion mechanism **(Figure 8)**. The coordination-insertion mechanism is commonly used as it is a living polymerization, enables synthesis of high molecular weight polymers. Moreover, it does not epimerize stereocentres such as those found in lactides.

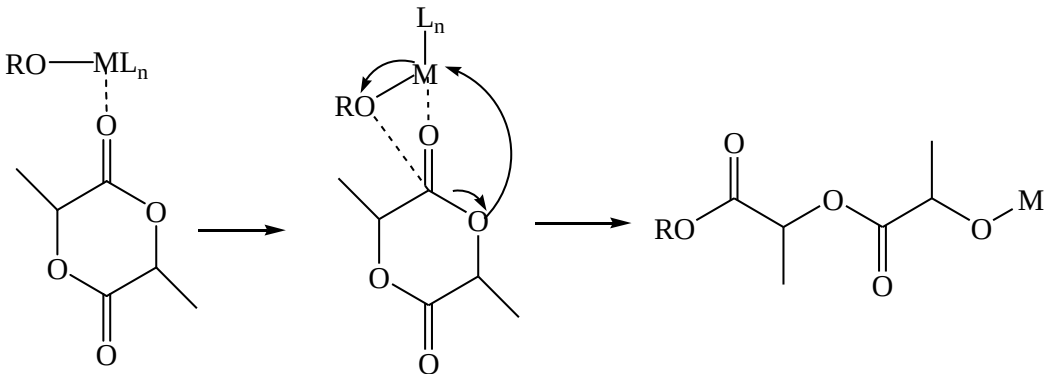

Figure 8. Coordination-insertion mechanism of lactide to obtain poly(lactic acid).

The mechanism involves the coordination of the lactone to a Lewis acidic metal alkoxide complex, which activates and attacks the lactone at the carbonyl carbon. The ring opens due to the cleavage of the acyl bond. There is generation of a new metal alkoxide species and a new cycle begins.

2.3. Microencapsulation

2.3.1. Introduction

Microencapsulation is the process of surrounding tiny droplets or particles of liquid or solid materials by a continuous film of polymeric material acting as a wall. The microcapsules can be less than one micron to several hundred microns in size. The material inside the microcapsule is referred to as the core or the internal phase and the polymeric wall is sometimes referred to as the shell, coating or membrane **(Figure 9)**.

Microencapsulation serves as a good method for isolating the core from the surroundings like in the case of vitamins, which need to be isolated from the deteriorating effects of oxygen. In addition, protecting a reactive core from a chemical attack by isolation and retarding the evaporation of a volatile material acting as a core are also some of the uses of microencapsulation. Hygroscopic properties of a core material can be reduced by microencapsulation. Furthermore, the other objective of microencapsulation is also to bring about controlled release of some materials like drugs and pesticides.

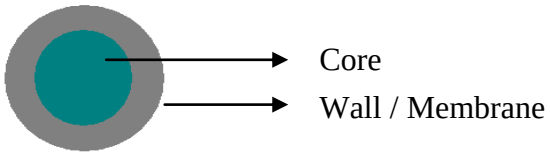

Figure 9. Diagram of microcapsule structure.

In a controlled release system, the bioactive materials like drugs and pesticides are incorporated in the polymeric shell so that they are released slowly in a more effective way.

The release of the core material is regulated by the polymeric membrane acting as a wall. The release rate largely depends on the thickness of the polymeric wall, its chemical structure i.e. its degradability and size of the microcapsule.[40]

In case of microencapsulation of drugs, the particle size is an important factor. Most injectable particles are ideally 20 to 80 μm in diameter. Smaller particle size means greater surface area-to-volume ratio and greater solubility. Hence, they are more easily assimilated by the human body.

Biodegradable polymers have been extensively used for the past few decades to carry out microencapsulation of bioactive materials due to their biodegradability and biocompatibility.

A majority of the biodegradable polymers have been used in the form of microparticles from which the incorporated materials are released in a controlled manner. The biodegradable polymers due to their ability to be cleaved into smaller units by chemical or enzyme - catalyzed hydrolysis, have been used extensively as carriers for the controlled release of drugs. These can be implanted into the human body without a need for any surgical operation for their subsequent removal. In addition, these biodegradable materials can be effectively used for agricultural applications where core materials like pesticides or pheromones can be released into the environment in a controlled manner and the polymeric material gets completely degraded with time.

The biodegradable polymers commonly used for microparticle preparation are polyesters, polyanhydrides, polyorthoesters, polyphosphazenes and polysaccharides shown in **Figure 10**.

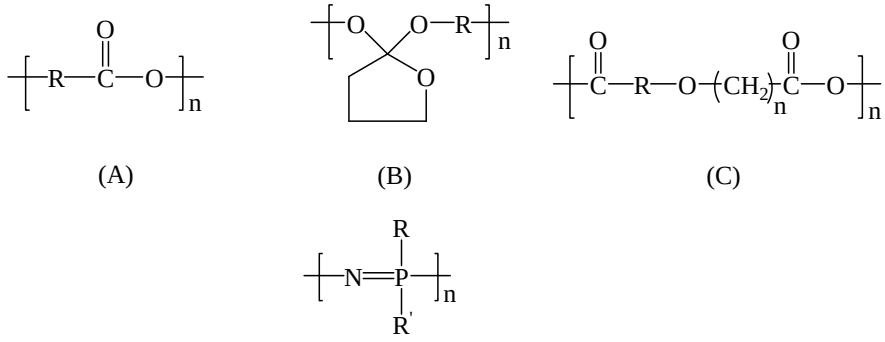

Figure 10. Chemical structures of biodegradable polymers (A) Polyesters (B) Polyorthoesters (C) Polyanhydrides (D) Polyphosphazenes.

2.3.2. General methods of microencapsulation

The various methods used for the preparation of microcapsules can be categorized into two kinds - physical and chemical. The difference lies in the fact that in a chemical method the capsules are produced in a tank or reactor containing liquid while in a physical method, gas phase is employed as part of the encapsulation and they rely mostly on commercially available devices and equipments to generate microcapsules. A few of the chemical methods used for microencapsulation are described below.

2.3.2.1. Chemical methods

2.3.2.1.1. Coacervation

Coacervation is the process in which colloidal polymer aggregates formed upon the separation of a homogeneous aqueous polymer solution are deposited onto the surface of dispersed liquid droplets, thus, resulting in the production of microcapsules. After separation of the remaining water phase, the coated particles may be dried or otherwise treated to form hardened particles. The coacervation of the polymer coating can be induced by different mechanisms. In a simple way, coacervation is induced by changes in temperature or salt concentration, or addition of a non-solvent or an incompatible polymer to the solution. Polysaccharides are well suited to this application due to their water solubility and functional groups that can be exploited for coacervation.

Microencapsulation by coacervation involves three steps:

1) Formation of three immiscible chemical phases: The three immiscible phases are the core material, shell/coating, and continuous aqueous phase. To form the three phases, the core material is dispersed in a solution of the coating polymer dissolved in the continuous aqueous phase. Physical or chemical changes in the coating polymer solution can be brought about to induce phase separation of the polymer. The phase separation of the polymer to form the coating material phase, an immiscible polymer in a liquid state, can be brought about by the following ways:

a) By changing the temperature of the polymer solution
b) By adding a salt
c) By adding a non-solvent
d) By adding incompatible polymer to the polymer solution
e) By inducing a polymer-polymer interaction.

2) Deposition of the liquid polymer coating onto the core material: This occurs if the polymer is adsorbed at the interface formed between the core material and the liquid continuous phase. A reduction in the total free interfacial energy of the system, brought about by the decrease in the surface area of the coating material during coalescence of the liquid polymer droplets promotes the continuous deposition of the coating material.

3) Microcapsule isolation: It involves hardening of the coating thermally, by crosslinking or by desolvation techniques to obtain microcapsules.

Furthermore, monomers can also be dissolved in the liquid continuous phase and subsequently polymerized at the interface.

2.3.2.1.2. Interfacial polymerization (IFP)

In Interfacial polymerization, the microcapsule formation takes place via rapid polymerization of monomers at the surface of the droplets or particles of dispersed core material.[41]

The two reactants in a polycondensation meet at an interface and react rapidly. The basis of this method is the Schotten-Baumann reaction involving an acid chloride and a compound containing an active hydrogen atom, such as an amine or alcohol, polyesters, polyurethane, or polyurea. A solution of the core material and a diacid chloride are emulsified in water and an aqueous solution containing an amine and a polyfunctional isocyanate is added. Base is present to neutralize the acid formed during the reaction. Condensed polymer walls form instantaneously at the interface of the emulsion droplets.

2.3.2.1.3. In-situ polymerization

In situ polymerization is a chemical encapsulation technique very similar to interfacial polymerization. The distinguishing characteristic of in situ polymerization is that no reactants are included in the core material. All polymerization occurs in the continuous phase, rather than on both sides of the interface between the continuous phase and the core material, as in IFP. Examples of this method include urea-formaldehyde (UF) and melamine-formaldehyde (MF) encapsulation systems.

2.3.2.1.4. Solvent evaporation method

In the solvent evaporation method, the microcapsule coating material (polymer) is dissolved in a volatile solvent which is immiscible in the liquid continuous phase. The core material is then dissolved or dispersed in the coating material solution. The core-coating material mixture is then dispersed in the liquid continuous phase via agitation to obtain microcapsules. The system is agitated until the solvent evaporates completely. A propeller style blade attached to a variable speed motor can be used to bring about the dispersion of the oil phase in the continuous phase.[42]

The rate of evaporation of the solvent, temperature cycles and agitation rates play a significant role in determining the microcapsule size in the solvent evaporation method. Moreover, the microcapsule properties largely depend on the choice of solvent for the continuous phase and for preparing the polymer coating solution. The solvent evaporation method is suitable for both water soluble and water insoluble core materials. A variety of film forming polymers can be used as coatings.

2.3.2.1.5. Solvent displacement method

The solvent displacement method is similar to the solvent evaporation method.[43] The only distinguishable factor is that the solvent for the polymer coating material is miscible in the liquid continuous phase. The coating material is dissolved in the solvent to obtain the coating material solution. The core material is then dissolved in the coating solution. The core material is usually water insoluble.

After the injection of the organic phase into the aqueous phase, a rapid interfacial spreading is observed as a result of the mutual diffusion between the solvents, which provides energy for oil droplet formation. Once the solvent diffusion is complete, the polymer aggregates around the oil droplets. Thus the solvent displacement method involves interfacial deposition of the polymer aggregates around an oily core in which the lipid soluble material can be incorporated.

The solvent displacement process is a good method to prepare particles suitable for intravenous administration since by this method monodispersed nanoparticles can be prepared by simple dispersion of the organic phase into the aqueous phase with a high yield of encapsulated lipophilic substances.

In order to obtain a stable dispersion, proper emulsification of the dispersed phase into the continuous phase is necessary. Mechanical energy is required to obtain the dispersed state. This mechanical energy input is provided by a number of devices illustrated in **Figure 11.**

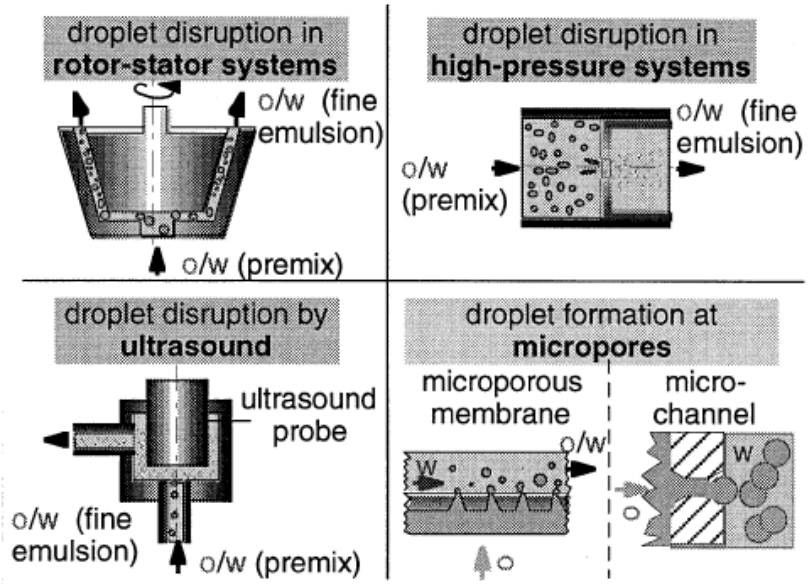

Figure 11. Mechanical emulsification by various devices.[44]

Figure 12 describes the process involved in the continuous mechanical emulsification. In the first step, mechanical energy disrupts the droplets of a pre-mix in the dispersion zone. In the next step, an emulsifier is added to the system to stabilize the newly formed droplets against coalescence.

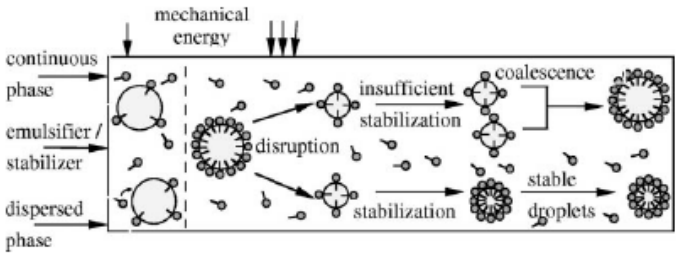

Figure 12. The process of mechanical emulsification.[45]

Out of the various methods of mechanical emulsification, rotor-stator systems and high-pressure homogenizers are the ones that are widely used. In these systems, droplets of the dispersed phase are broken under the action of shear or inertial forces in turbulent or laminar flow.[45]

The rotor-stator systems (Ultra-Turrax, colloid mills, and toothed-ring dispersing machines) consist of a high-speed centrifugal-type rotor mounted within a stationary stator that is held in place by three or four frame arms. During operation, high-speed rotor revolution creates a powerful suction that draws both liquid and solid materials into the center of the workhead assembly. There, they are subjected to intense high shear. Centrifugal force then drives the materials to the periphery of the workhead, where they encounter milling action in the clearance between the rotor blade tips and the stator inner wall. Intense hydraulic shear follows as the materials are forced out though the openings in the stator and are projected radially at great velocity back into the body of the mixture.[46] The disadvantage of these systems is that the production of low viscosity emulsions with droplet sizes less than 1 µm is not possible.

The most common mechanism for homogenization is high pressure homogenization. There, liquid is pressed at high pressure (approx. 2000 bar) though a homogenizing valve. When passing the valve, the liquid undergoes a short (approx.50 µs) high-pressure low-pressure cycle. Due to the strong turbulence, the dispersed phase is crushed by shearing and impact effects.[47] In special high-pressure homogenizers, pressures more than 2000 bar can also be built up. With high pressure homogenizers, a mean droplet diameter of less than 0.2 µm can be achieved. Different types of equipment in this category now exist, for example, Microfluid™ technology, Nanojet™ and emulsiflex from Avestin. This type of equipment can deliver pressures in the order of 1000 bar and as high as 3000-5000 bar.[48]

Ultrasonic homogenization is highly efficient in carrying out mixing, emulsification, dispersing and deagglomeration. The homogenization is based on cavitation. When liquids are exposed to intense ultrasonication, sound waves propagate though the liquid causing alternating high-pressure and low-pressure cycles. During the low-pressure cycle, high-intensity ultrasonic waves create small vacuum bubbles in the liquid, as the liquid vapor pressure is attained. When the bubbles reach a certain volume at which they can no longer absorb energy, they collapse violently during a high-pressure cycle. This phenomenon is referred to as cavitation. Ultrasonic cavitation in liquids causes high speed liquid jets of up to 1000 km/h. The resulting currents and turbulences disrupt particle agglomerates and lead to violent collisions between individual particles. Thus ultrasound is an effective means for dispersing and deagglomeration **(Figure 13).**[49, 50]

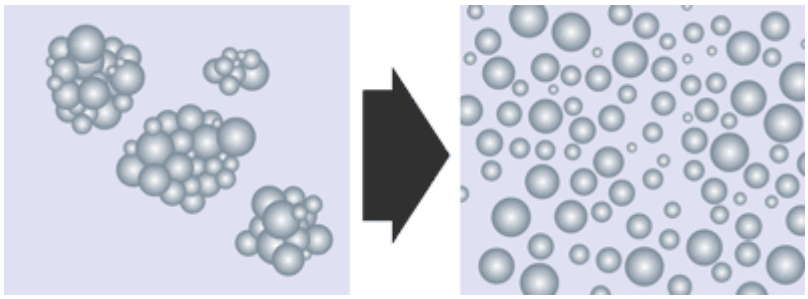

Figure 13. Deagglomeration of particles using high intensity ultrasonication.[51]

In case of membrane emulsification, the dispersed phase is forced though the pores of a microporous membrane (glass or ceramic membrane) to form small droplets at the membrane surface, which are subsequently detached by the flowing continuous phase. The processing parameters such as, membrane type, average pore size and porosity, crossflow velocity, transmembrane pressure and emulsifier, play an important role in the production of emulsions with narrow emulsion droplet size distributions, with average droplet sizes ranging between 2 and 10 times the supposed membrane pore diameter. Interfacial tension and the action of wall shear stress are also found to be important. In comparison to homogenization and rotor-stator systems, less energy is required to produce droplets of a given size using membrane emulsification. However, one of the main limitations is the low level of dispersed phase flux though the membrane, especially for small submicron droplets.[44, 52]

2.3.3. Stability of polymer dispersion

The stability of a dispersion is of great importance in a number of industries such as pharmaceutical, ceramic, paints and pigments. A stable system is one in which there is no sign of a phase separation or the particles resist flocculation or aggregation and exhibit a long shelf-life. If the particles in a dispersion show a tendency to sediment or cream after a period of time, the dispersion is termed “unstable”.

Particles in a dispersion always show Brownian motion and thus are colliding with each other frequently. The stability of the dispersion depends on the interaction between the particles during such a collision. There are two basic interactions: one is attractive (Van der Waals forces) and the other repulsive. The stability of a dispersion depends upon the balance of the repulsive and attractive forces. When the attractive force dominates, the particles adhere to one another and form aggregates. If all the particles have a mutual repulsion then the dispersion remains stable.

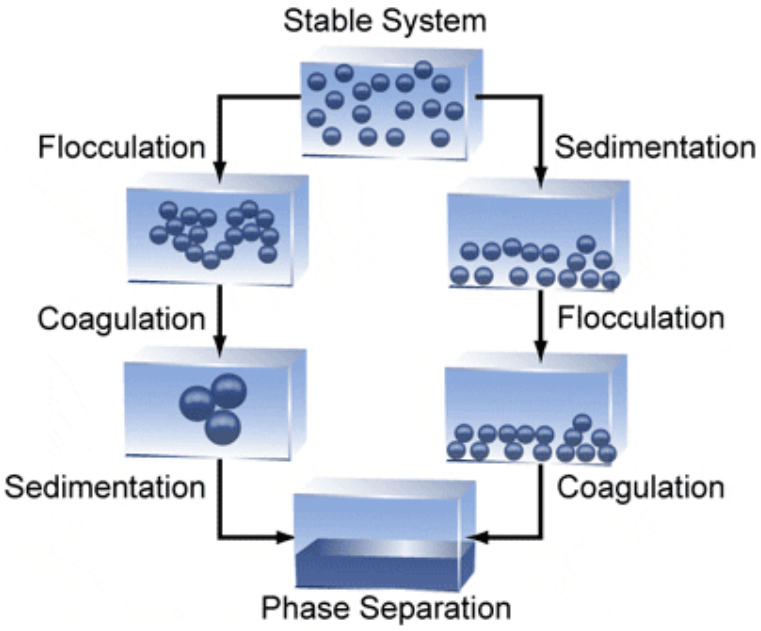

Figure 14. Aggregation of particles in a dispersion.[53]

The aggregation of particles in a dispersion leads to unstability. An initially formed aggregate is called a floc and the process of its formation is termed flocculation. The floc may or may not separate out. If the aggregate changes to a much denser form, it is said to

undergo coagulation. An aggregate usually separates out either by sedimentation (if it is more dense than the medium) or by creaming (if it is less dense than the medium). Usually coagulation is irreversible whereas flocculation can be reversed by the process of deflocculation. Some of these processes are well described in **Figure 14**.[53]

Since there are always strong attractive forces between the particles, it is necessary to provide equally strong repulsive forces between the particles to impart stability.[54] Particles in a dispersion can be stabilized by surrounding them with:
a) an electrical double layer (electrostatic or charge stabilization)
b) adsorbed or chemically attached polymeric molecules (steric stabilization)

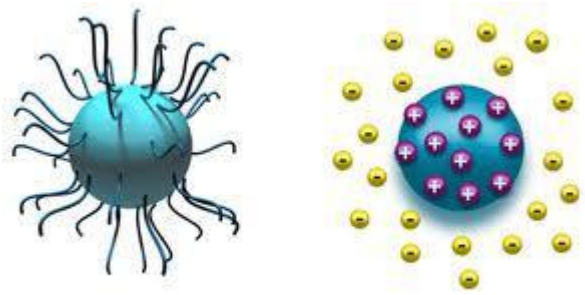

(A) **(**B)

Figure 15. (A) Steric stabilization and (B) electrostatic stabilization of the particles in a dispersion.[55]

2.3.3.1. Electrostatic stabilization

The attractive Van der Waal forces existing between the particles in a dispersion can be counterbalanced by providing the particles with repulsive Coulombic forces. In a liquid dispersion medium, ionic groups can adsorb to the surface of a colloidal particle to form a charged layer. To maintain the electroneutrality, an equal number of oppositely charged ions surround the particles giving rise to a neutral electric double layer. In electrostatic stabilization, the mutual repulsion between these double layers surrounding the particles helps to provide stability **(Figure 15B)**.
This is further proved by the DLVO theory (named after **D**erjaguin, **L**andau, **V**erwey and **O**verbeek) which suggests that the stability of a dispersion depends on both the attractive

Van der Waal forces and electrical double layer repulsive forces that exist between the particles as they approach one another.[55] This theory proposes that an energy barrier resulting from the repulsive force prevents two particles to adhere together **(Figure 16).** But if the particles collide with sufficient energy to overcome that barrier, the attractive force causes them to come into contact where they adhere strongly and irreversibly together. Therefore, if the particles have a sufficiently high repulsion, the dispersion will resist flocculation and the colloidal system will be stable. However, if a repulsion mechanism does not exist then flocculation or coagulation will eventually take place.

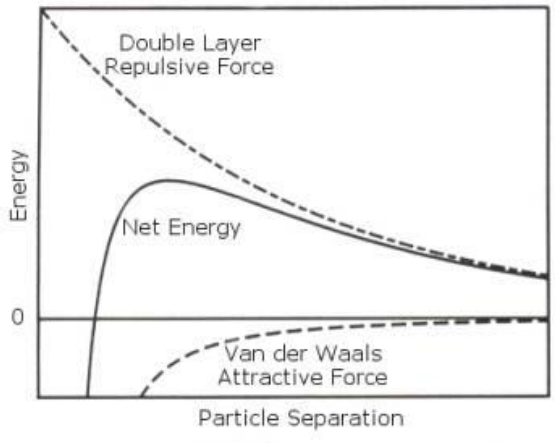

Figure 16. Schematic diagram of the variation of interaction energy between two particles with particle distance according to DLVO theory.[55]

2.3.3.2. Steric stabilization

Polymers with molecular weight more than 10000 Da have chain dimensions comparable to the range of Van der Waal attractive forces. Hence, steric stabilization can be achieved by attaching these macromolecules to the surface of the particles. These polymer molecules form a coating on the surface of the particle creating a repulsive force which separates the particles from one another **(Figure 15A)**.[54]

2.3.4. Role of a surfactant

A surfactant is a substance that when present at low concentrations in a system has the ability of adsorbing onto the surface or interfaces of the system and of altering the

surface or interfacial free energy to a large extent. The term interface means the boundary between any two immiscible liquid phases. The term surface implies an interface where one phase is a gas, usually air.

The interfacial free energy of an interface is the minimum amount of work required to build that interface. The interfacial tension between two phases is defined as the interfacial free energy per unit area. It is the minimum amount of work done to create unit area of an interface or to expand it by unit area. The interfacial tension (or surface tension) is also a measure of the difference in nature of the two phases forming an interface. The more the difference in their nature, the greater will be the interfacial tension between them.

The surface tension of a liquid is therefore the interfacial free energy per unit area of the boundary between the liquid and the air above it.[56] When an interface is expanded, the minimum amount of work done to create the additional interface is the product of the interfacial tension γ and the increase in area of the interface.

$$W_{min} = \gamma \times \Delta \textit{ interfacial area}$$

A surfactant therefore acts by changing the amount of work required to expand the interfaces. Surfactants usually help to reduce the interfacial free energy.

Surfactants have a characteristic molecular structure having a group that has very little attraction for the solvent called the lyophobic group and another group which has a strong attraction for the solvent known as the lyophilic group. Thus a surfactant is amphiphilic in nature. When such a molecule is dissolved in a solvent, the lyophobic group may distort the structure of the solvent, increasing the free energy of the system. When this occurs, the system acts to minimize the contact between the solvent and the lyophobic group. For example, when a surfactant is dissolved in an aqueous medium, the lyophobic group (hydrophobic group) breaks the hydrogen bonds between the water molecules and structures the water lying in the vicinity of the hydrophobic groups. As a result of this distortion, some of the surfactant molecules are expelled to the interface of the system with the hydrophobic groups oriented in such a way that they are away from the water molecules i.e. towards the air. Since the air molecules are non-polar in nature just like the hydrophobic groups, this decrease in the dissimilarity between two phases in contact with each other at the surface results in a decrease in the surface tension of water.

Since the surfactant molecule also possesses a lyophilic group (hydrophilic group), it is not expelled completely from the solvent as a separate phase. Hence there is orientation of the surfactant at the surface in such a way that the hydrophobic group points away from the aqueous phase and the hydrophilic group towards the aqueous phase.

The chemical structures of the groups used as the lyophilic and the lyophobic groups of the surfactant depend on the nature of the solvent and the conditions of use. For a highly polar solvent such as water, the lyophobic group maybe a hydrocarbon or fluorocarbon whereas in a less polar solvent, only some of these may be suitable (e.g. fluorocarbon). In a highly polar solvent like water, some ionic or highly polar groups may act as lyophilic groups whereas the same groups act as lyophobic groups in a non-polar solvent like heptane.

The hydrophobic group is usually a long-chain hydrocarbon residue and the hydrophilic group is mostly an ionic or a highly polar group. Depending on the nature of the hydrophilic group, the surfactants can be classified as follows:

1) *Anionic:* The surface active portion of the molecule bears a negative charge, for example, $RCOO^-$ (Carboxylate), RSO_3^- (Sulfonate), $ROSO_3^-$ (Sulfate), RPO_3^{2-} (Phosphonate).

2) *Cationic:* The surface active portion bears a positive charge, for example, RNH_3^+ (Ammonium salt), $R_2NH_2^+$ (Secondary ammonium salt), $R(C_5H_5N)^+$ (Pyridinium salt).

3) *Zwitterionic:* Both positive and negative charges maybe present in the surface active portion, for example, $R_3N^+O^-$ (Aminoxide), $R_3N^+(CH_2)_nSO_3^-$ (Sulfobetaine), $R_3N^+(CH_2)_nCO_2^-$ (Betaine).

4) *Non-ionic:* The surface active portion bears no ionic charge, for example, most alcohols (-OH), ethers (-O-) or their combination (-O-CH_2-CH_2-OH) like $R(OC_2H_4)_nOH$ (polyoxyethylenated alcohol), $RC_6H_4(OC_2H_4)_nOH$ (polyoxyethylenated alkylphenol).

For a molecule to behave as a surfactant, it must contain a hydrophilic or a polar group and a hydrophobic or a non-polar group.

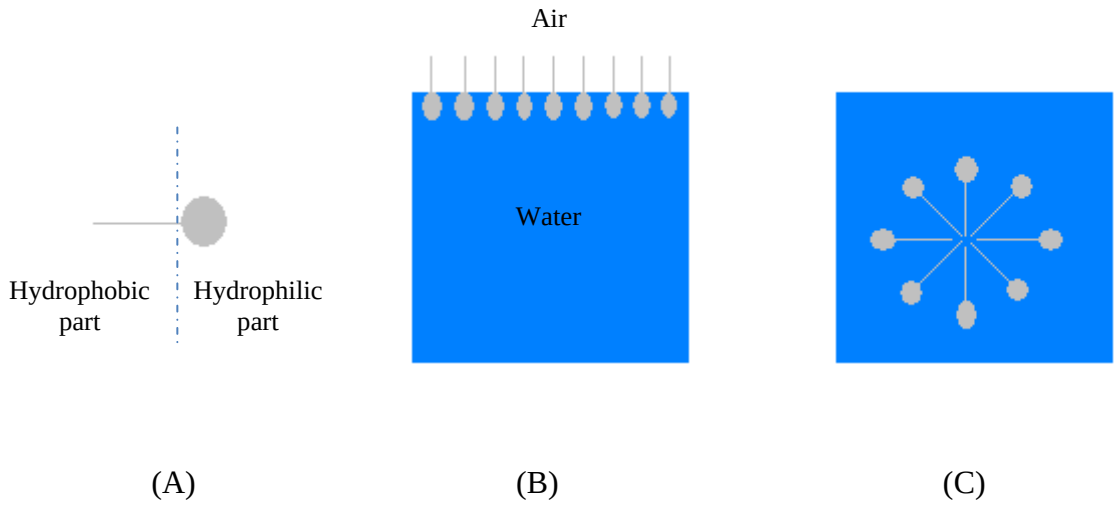

Figure 17. Schematic diagram of the role of a surfactant as a "surface active molecule".

The surfactant having a polar group and a non-polar group as shown in **Figure 17A**, arranges itself at the surface of water in such a way that the polar group interacts with water while the non-polar group is held away from water i.e. towards air or towards a non-polar liquid as shown in **Figure 17B**. The presence of these molecules on the surface disrupts the cohesive energy at the surface and thus lowers the surface tension. Hence, they are also known as "surface active molecules".

Another way in which these molecules can arrange is in the form of aggregates, in which the hydrophobic parts are oriented within the cluster and the hydrophilic parts are exposed to the solvent. Such aggregates are called micelles, as shown in **Figure 17C.**

The amount of the surfactant molecules present at the surface or as micelles in the bulk of the liquid depends on the concentration of the surfactant. At low concentrations, the surfactant molecules prefer to arrange on the surface. As the concentration of the surfactant increases and the surface becomes loaded with the surfactant, more molecules will arrange as micelles. At some concentration, the surface becomes completely loaded and further addition of the surfactant molecules must arrange as micelles. This concentration is known as the Critical Micelle Concentration (CMC) which can be determined using surface tension measurements.

At very low concentrations of the surfactant, there should be only a slight change in surface tension. With increasing concentration, the surface tension should decrease and when the surface becomes fully loaded, there should be no further change in the surface tension.

2.4. Miniemulsions

2.4.1. Introduction

Miniemulsions are dispersions of critically stabilized oil droplets of size ranging from 50 nm – 500 nm obtained by shearing a system consisting of oil, water, a surfactant and a hydrophobe.[57, 58]

In the first step of the miniemulsion process, small and stable droplets are formed by shearing a system consisting of a dispersed phase, a continuous phase, a surfactant and an osmotic pressure agent or a hydrophobe. In the second step, the polymerization of these droplets occur leading to the formation of polymer latexes.[57] The process of miniemulsion is well described in **Figure 18.**

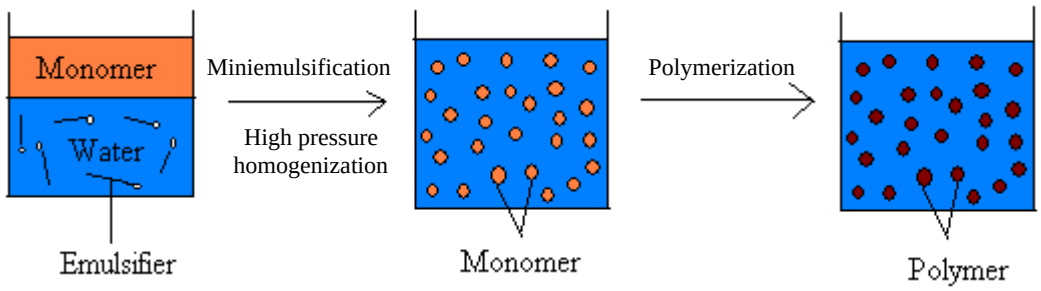

Figure 18. Principle of miniemulsion polymerization.

To create a stable miniemulsion, the droplets must be stabilized against Ostwald ripening and coalescence.

2.4.2. Ostwald ripening and coalescence

Emulsions are defined as systems in which liquid droplets are dispersed in a liquid continuous phase. Stabilization of these emulsions is brought about electrostatically or sterically. Instability and breaking of emulsions is because of two factors - Ostwald ripening and coalescence.

Ostwald ripening, first described by Wilhelm Ostwald, is a phenomenon in which larger particles grow at the expense of the smaller particles **(Figure 19)**. This occurs because the larger particles are more energetically favorable than the smaller ones since the larger

particles have a lower surface to volume ratio and therefore result in a lower energy state (and have a lower surface energy). Since the system tries to lower its overall energy, the molecules on the surface of a small and energetically unfavorable particle tend to detach themselves and diffuse though the solution to attach to the surface of a larger and more energetically favorable particle. Hence, the smaller particle tends to shink and the larger particle continues to grow.

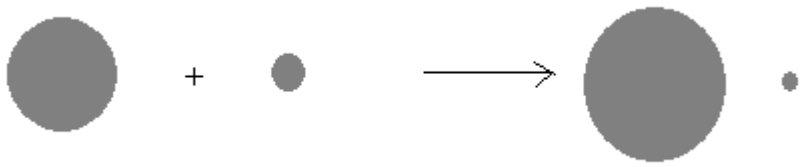

Figure 19. Schematic representation of the Ostwald ripening process.

Ostwald ripening is observed in solid solutions, where when a phase precipitates out of a solid, due to energetic factors, the larger precipitates draw material from the smaller precipitates and continue to grow.

It is also observed in liquid-liquid systems like in oil/water emulsion polymerization, where monomer molecules diffuse from the smaller droplets to larger droplets owing to increased solubility of a single monomer molecule in the larger monomer droplets. The rate of diffusion of these monomer molecules depends on their solubility in the continuous phase of the emulsion. This causes destabilization of the emulsion.

Figure 20. Schematic representation of coalescence.

When a miniemulsion is desired, the coalescence by the collision of the droplets **(Figure 20)** is suppressed by the effective addition of a surfactant. For the stabilization against Ostwald ripening by diffusion processes, a highly water-insoluble agent called a hydrophobe is added to the system.

Ostwald ripening can be effectively suppressed by the use of a hydrophobe which counteracts the Laplace pressure of the droplet. This hydrophobe which is added to the dispersed phase, being extremely water insoluble cannot diffuse from one droplet to the other and remains trapped inside the droplet giving rise to an osmotic pressure inside which counteracts the Laplace pressure. The effectivity of the hydrophobe increases with decrease in solubility in the continuous (water) phase. Ugelstad et al. have shown the role of cetyl alcohol as a hydrophobe in stabilizing a miniemulsion.[59]

The hydrophobe used in a miniemulsion is sometimes referred to as a "co-surfactant". However, this term is misleading since the role of a co-surfactant, in addition to the surfactant, is to further lower the interfacial energy by acting as a surface-active agent, but it is unable to form micellar aggregates itself.

Key factors that govern the formation of a miniemulsion are the type of homogenization and the addition of a hydrophobe. Homogenization can be obtained by the use of ultrasonication or high pressure homogenizer.

3. Preparation of water insoluble Poly(vinyl alcohol) fiber mats

3.1. Introduction

Poly(vinyl alcohol) (PVA) is a water-soluble polymer. The solubility of PVA in water largely depends on its average molecular weight and its degree of hydrolysis. The hydroxyl groups present in PVA are the reason for its high affinity to water.[60-62] However, inter- and intra-molecular hydrogen bonds between the hydroxyl groups hinder its solubility in water. On the other hand, the residual acetate groups present in partially hydrolysed PVA have hydrophobic character and hinder the inter-and intra-molecular hydrogen bonding between the adjacent hydroxyl groups leading to higher solubility in water.

The presence of adequate number of these acetate groups increases the water solubility of PVA. This is the reason that heating at 80 °C or above is required to dissolve a completely hydrolysed grade of PVA while PVA grade that is less than 88% hydrolysed dissolves in water even at 20 °C. The solubility of PVA shows a sharp decrease with increase in hydrolysis.

Complete biodegradability and non-toxicity of PVA makes it a useful polymer in various applications. However, the water solubility of PVA after electrospinning limits it’s applications to a large extent. Hence, crosslinking PVA after electrospinning is a good method to bring about water insolubility.

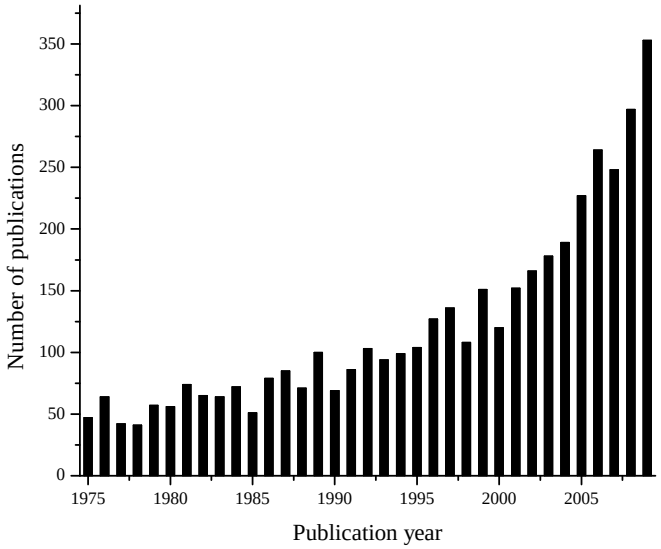

Figure 21. Comparison of the annual number of scientific publications from 1975-2009 for "Polyvinyl alcohol crosslinking" (data analysis of the publications was done using the SciFinder Scholar search system with the term "Polyvinyl alcohol crosslinking", on 6 October 2010).

In recent years, crosslinking PVA for various applications has received a lot of attention as evident from the drastic increase in the number of scientific publications shown in **Figure 21**.

3.2. Motivation

PVA fibers can be insolubilized by crosslinking which enhances its utility to a large extent. Crosslinked PVA[63] has been used for various applications for example mouldings with good oxygen barrier properties have been prepared from a 1:1 mixture of PVA and polyamide followed by treatment with aqueous formaldehyde suitable for food containers.[64] A physical mixture of polyethylene and PVA prepared in inert gas atmosphere at 200 °C with 2.8% crosslinking has been formed into sheets with good oxygen barrier properties.[65] Varma et al. improved the mechanical and crease resistance of PVA fibers by crosslinking with hexamethylene diisocyanate.[66]

PVA crosslinked with oxalic acid has also been used as membrane material for reverse osmosis.[67] PVA has been used as a film-forming polymer in dispersions. PVA capsules in aqueous medium containing a hydrophobic material have been prepared, stabilized by

crosslinking with aldehydes like formaldehyde or glyoxal in the presence of hydrochloric acid.[68-71]

Apart from this, because of its relative inertness and low chemical reactivity, crosslinked PVA has been used for many biological applications for example as an immobilizing site for biologically active substances such as enzymes.

3.3. Concept

In this study, PVA crosslinking was carried out to hinder the dissolution of PVA fibers in aqueous media. When PVA is reacted with aldehydes, the hydrophobic groups present help to decrease the solubility of the fibers in water whereas the reaction with dialdehydes leads to the formation of inter-molecular crosslinkages.

Post polymerization modification techniques were used to crosslink PVA to render insolubility in water. Various techniques like irradiation, chemical and physical methods were carried out to crosslink PVA fibers. The idea was to obtain crosslinked PVA fiber mats insoluble in water both at low temperatures and high temperatures. To achieve this, both pre-treatment and post-treatment of the fibers with the chemical crosslinking agents as well as irradiation was realized.

3.4. General crosslinking methods

Stability of PVA against water by using chemical crosslinking agents has been an intensive topic of research since quite a few years. The general mechanism involves the reaction of the complimentary functional groups of the crosslinking agents with the hydroxyl groups of PVA. Water stable electrospun PVA fiber mats find a lot of applications in the field of tissue engineering, drug-delivery, and filtration. Some of the efforts in literature to crosslink PVA fibers after electrospinning include the use of difunctional aldehydes[72, 73], glyoxal and glutaraldehyde[74, 75] followed by a subsequent heat treatment. Boric acid[76] was also used as a crosslinker apart from some dicarboxylic acids like oxalic acid, maleic acid[77, 78] **(Figure 22)**, succinic acid, diisocyanates[79], dianhydrides[80, 81]. Dicarboxylic acids and dianhydrides induce esterification with PVA, dialdehydes result in acetalization (in the presence of Lewis or Bronsted acids as catalysts) and diisocyanates lead to the formation of carbamates.

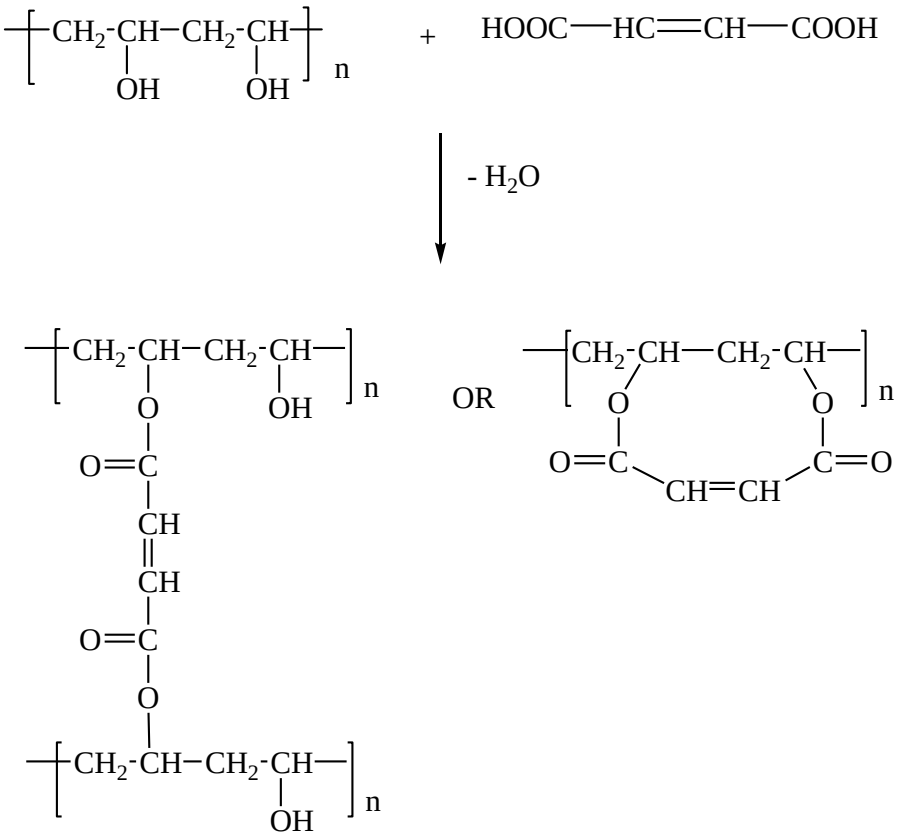

Figure 22. Scheme of the reaction between PVA and maleic acid.

Electrospun PVA fibers treated with methanol also show insolubility in water due to increase in the degree of crystallinity of PVA fibers.[82]

Photo crosslinking of PVA fibers by using chemically modified PVA has also been carried out to improve their water-stability.[83] A chemically derivatized PVA made by polymer analogous reaction with thienyl acryloyl chloride groups, was electrospun and was found to be water stable after UV irradiation **(Figure 23).**[84]

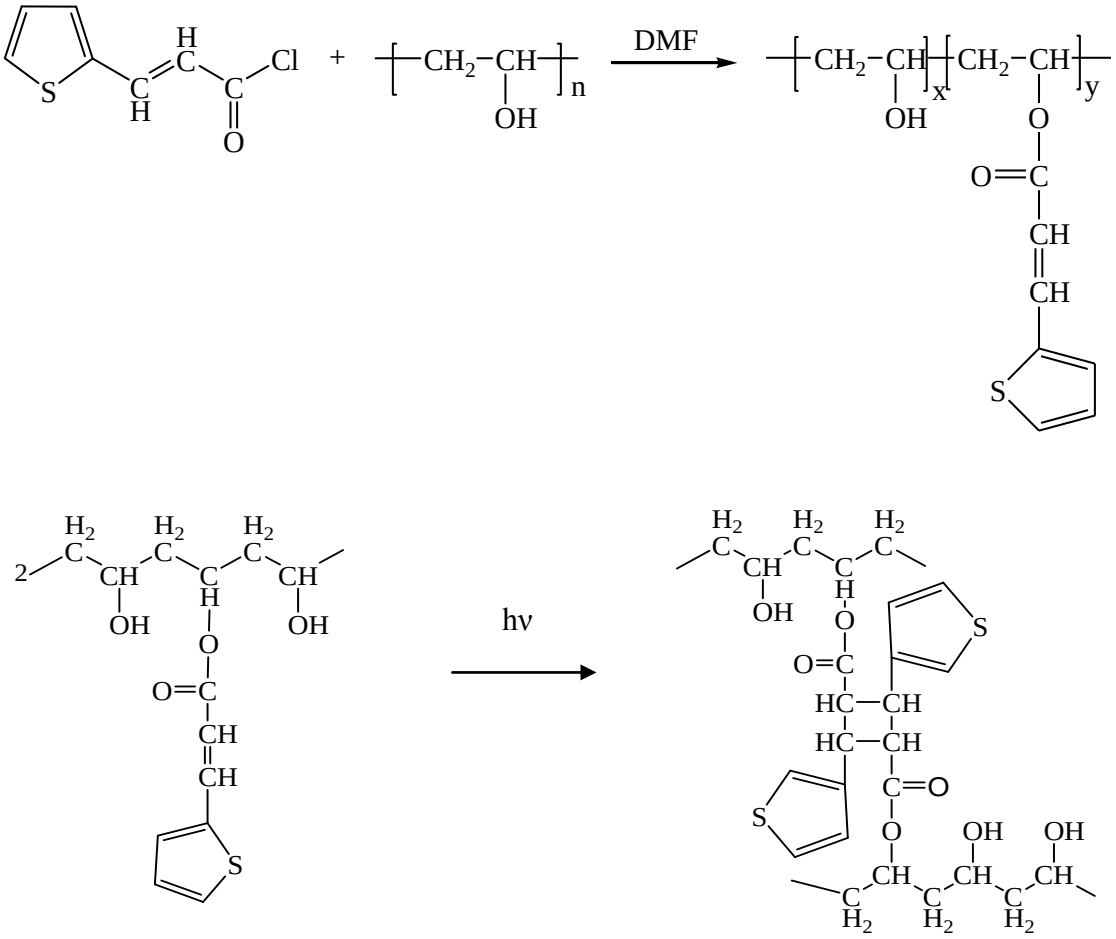

Figure 23. UV-induced crosslinking of PVA-thiol.

Based on a similar concept, McGuinness et al. used another PVA derivative, PVA with pendant styrylpyridinium groups (SbQ), as a photocrosslinkable polymer to prepare water insoluble PVA fibers.[85]

In situ crosslinking of electrospun PVA nanofibers has also been reported by using glutaraldehyde as crosslinking agent in presence of hydrochloric acid as catalyst.[86] The fibers were crosslinked during the electrospinning process in a simple one-step process.

3.5. Results and discussion

Chemical crosslinking of Poly(vinyl alcohol) is an excellent method not only to render the system insoluble but also to confer additional properties to the system like improving the mechanical properties and the thermal stability. On chemical crosslinking, the PVA functional groups are substituted by different pendant chemical groups or the PVA is polymerized into a three-dimensional crosslinked network.

3.5.1. Chemical crosslinking methods

3.5.1.1. Chemical crosslinking using cavasol

An attempt here was made to crosslink Poly(vinyl alcohol) while electrospinning, thereby eliminating the need for any post-treatment. For this purpose, polymer films were made as a model with the crosslinker and the solubility of the films were checked in water at room temperature and at ~ 90 °C.

As a crosslinker initially, Monochlorotriazinyl-β-cyclodextrin (MCT-β-CD) was used.[87] It is the reactive form of β-cyclodextrin which is commercially available with the name Cavasol ® W7 MCT.

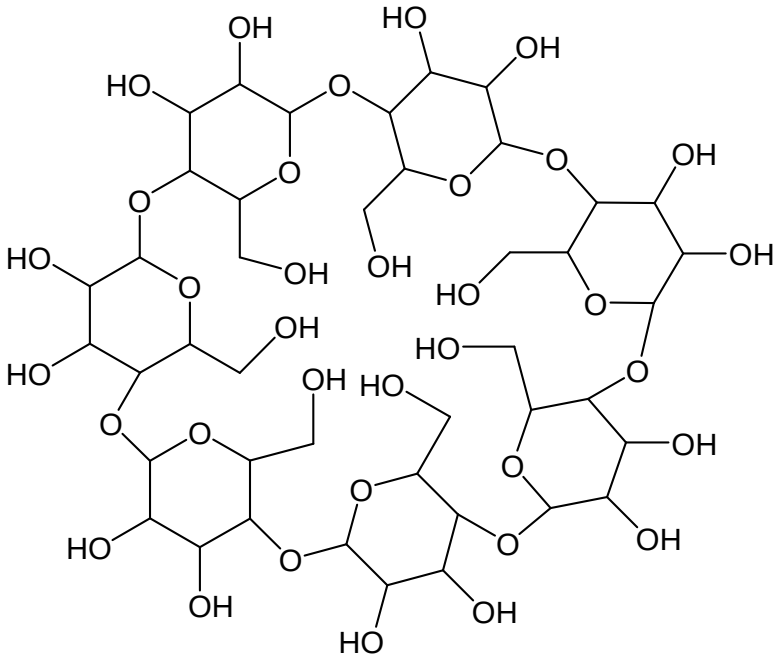

Figure 24. Chemical Structure of β-Cyclodextrin.

Cyclodextrins are cyclic oligosaccharides produced from starch with enzymatic degradation. Typical cyclodextrins are α-, β- and γ-cyclodextrins. β-cyclodextrins are the cyclodextrins containing 7 D-(+)-glucopyranose units **(Figure 24)**. In MCT-β-CD, each β-cyclodextrin molecule contains two or three monochlorotriazinyl groups which can react with the –OH groups of PVA to form a covalent bond **(Figure 25)**.

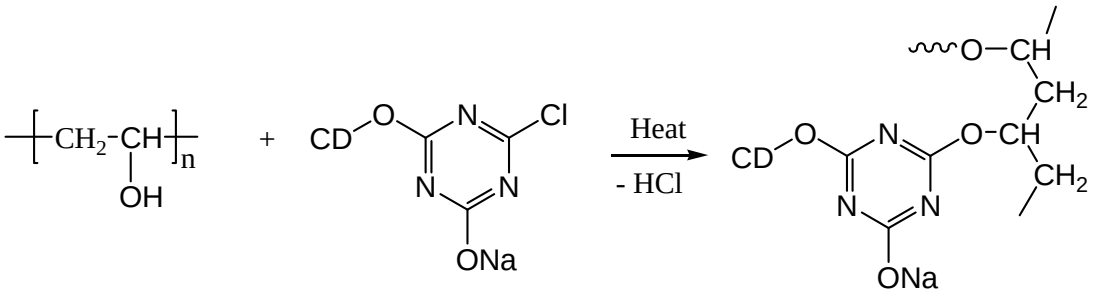

CD = Cyclodextrin

Figure 25. Crosslinking reaction of PVA with monochlorotriazinyl-β-cyclodextrin (cavasol).

3.5.1.1.1. Preparation of PVA / cavasol fibers

A 10 wt% PVA / cavasol aqueous solution was electrospun to obtain nanofibers with diameters ranging from 100 nm to 1 μm. Sodium dodecyl sulphate was added in the electrospinning solution as the surfactant. The fiber morphology was characterized using SEM **(Figure 26)**.

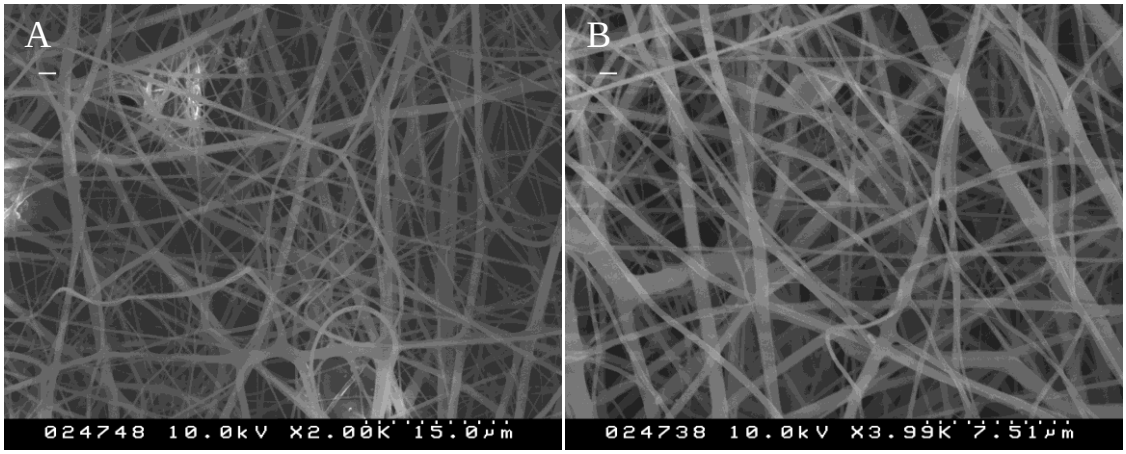

Figure 26. SEM images of (A) 10 wt% PVA / cavasol fiber mat and (B) 10 wt% PVA / cavasol fiber mat after heat treatment.

In a similar way, different weight ratios of PVA to cavasol were tried, starting from 1:0.1 to 1:1. The weight ratio of PVA to the surfactant (SDS) was kept constant (10 wt%) in each of these solutions.

3.5.1.1.2. Water stability measurements of PVA / cavasol fibers

The water stability of the electrospun PVA / cavasol fibers was analyzed by water treatment at 20 °C for 24 h.

Table 4. Solubility behaviour of different PVA / cavasol fiber mats in water at 20 °C for 24 h.

PVA / cavasol	Solubility of PVA / cavasol fiber mats in water
1:0.1	soluble
1:0.2	soluble
1:0.3	soluble
1:0.4	soluble
1:0.5	soluble
1:0.6	soluble
1:0.7	soluble
1:0.8	soluble
1:0.9	soluble
1:1	soluble

As evident from **Table 4**, all the PVA / cavasol fiber mats were soluble when treated with water at 20 °C for 24 h. Hence, a post-treatment - either heat treatment or UV irradiation, was required to initiate the crosslinking reaction between cavasol and PVA in the PVA / cavasol fiber mats.

3.5.1.1.3. Heat treatment of PVA / cavasol fiber mats

In order to have water stable PVA / cavasol fiber mats, a defined piece of the fiber mat was heated in the oven at 180 °C for 3 min. After heat treatment the fibers were again treated with water at 20 °C for 24 h. The solubility behaviour of the PVA / cavasol fiber mats in water is summarized in **Table 5**.

Table 5. Solubility behaviour of cured (180 °C – 3 min) PVA / cavasol fiber mats in water at 20 °C for 24 h.

PVA / cavasol	Solubility of cured PVA / cavasol fiber mats in water
1:0.1	insoluble
1:0.2	insoluble
1:0.3	insoluble
1:0.4	insoluble
1:0.5	insoluble
1:0.6	insoluble
1:0.7	insoluble
1:0.8	insoluble
1:0.9	insoluble
1:1	insoluble

The percentage weight loss of the PVA / cavasol fiber mats after water treatment at 20 °C for 24 h was calculated as follows:

$$\text{Percentage weight loss} = [1 - (W_2 / W_1)] \quad 100 \quad (1)$$

where W_1 is the weight of the PVA / cavasol fiber mats before water treatment and W_2 is the weight after water treatment. The fiber mats after water treatment were dried completely in a vacuum oven at 40 °C for 2 days before the measurement.

The percentage weight change for all the PVA / cavasol fiber mats heated at 180 °C for 3 min was found to be below 2%. The result of water treatment for 24 h clearly indicates the change in solubility behaviour of the PVA / cavasol fiber mats after curing at 180 °C for 3 min. Hence, heating initiates the crosslinking reaction between PVA and cavasol.
The morphological appearance of the PVA / cavasol fiber mats before and after heat treatment was examined using scanning electron microscopy.

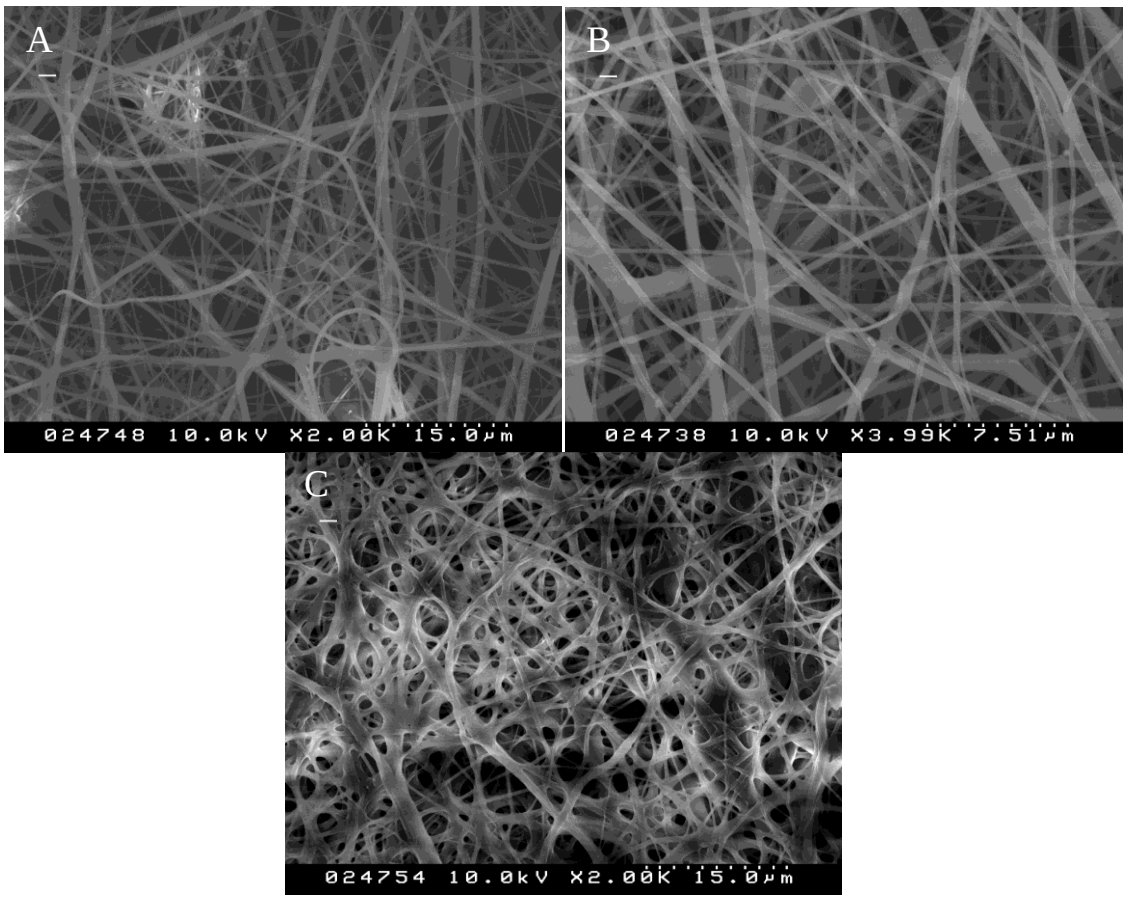

Figure 27. SEM images of (A) 10 wt% PVA / cavasol fiber mat without heat treatment (B) 10 wt% PVA / cavasol fiber mat after heat treatment and (C) cured 10 wt% PVA / cavasol fiber mat after water treatment.

The fiber morphology of the cured and water-treated fiber mat remained almost the same **(Figure 27)**. The fiber diameter of heated PVA / cavasol fiber mats ranged from 100 nm to 1 µm which was similar to that of the non-heated fiber mat. After water treatment, the fiber diameter increased from 200 nm to 2 µm which could be explained by incomplete drying of the fiber mat after water treatment. But the main aim was achieved because the fiber structure was retained.

3.5.1.1.4. Photocrosslinking of PVA / cavasol fiber mats

The water stability of the PVA / cavasol fiber mats was successfully achieved by a short heat treatment. Another way of crosslinking electrospun PVA / cavasol fibers is by UV-irradiation. The fibers were fixed on a rectangular glass slide by an adhesive and then irradiated at 254 nm for different time intervals (5 min, 15 min, 30 min and 1 h). The water stability for each of the samples was tested by dipping them in water at 20 °C for 24 h.

Table 6. Solubility behaviour of UV-irradiated (254 nm) PVA / cavasol fiber mats in water at 20 °C for 24 h.

Irradiation time / min	Solubility of UV-irradiated PVA / cavasol fiber mats in water at 20 °C
5	Soluble
15	Soluble
30	Soluble
60	Soluble

The water solubility of PVA / cavasol fibers did not change after UV-irradiation at 254 nm, as evident from **Table 6**. Even when irradiated for 60 min, the mats remained soluble.

The change in the water solubility was thus brought about only by a heat treatment at 180 °C for 3 min as shown in chapter **3.5.1.1.3.** Post-treatment with UV-irradiation at 254 nm was not successful.

3.5.1.2. Other chemical crosslinking agents

Since our aim was to crosslink PVA during the electrospinning process and completely eliminate the use of any post-treatment procedures like heating or irradiation, other crosslinking agents additionally to MCT-β-CD were examined. These include benzaldehyde, dialdehydes like glyoxal, glutaraldehyde, and borax. Detailed informations are given in the following chapter.

3.5.1.2.1. Borax as the crosslinking agent

The crosslinking reaction between PVA and borax produces a highly viscous oil.[88, 89] This would make electrospinning difficult. Instead of trying to electrospin PVA / borax solution, a post-treatment by dipping the electrospun PVA fiber mat into a borax solution to crosslink it was chosen.

Borax, sodium tetraborate decahydrate [$Na_2B_4O_7.10H_2O$], when dissolved in water, dissociates into sodium ions and tetraborate ions. The tetraborate ion reacts with water to form boric acid and the hydroxide ion

$$B_4O_7^{2-}(aq) + 7\,H_2O \longrightarrow 4\,H_3BO_3(aq) + 2\,OH^-(aq)$$

The boric acid further reacts with water to form the borate ion.

$$H_3BO_3(aq) + 2\,H_2O \longrightarrow B(OH)_4^-(aq) + H_3O^+(aq)$$

When PVA solution and borax solution are mixed together, the borate ions react with the hydroxyl groups of PVA.

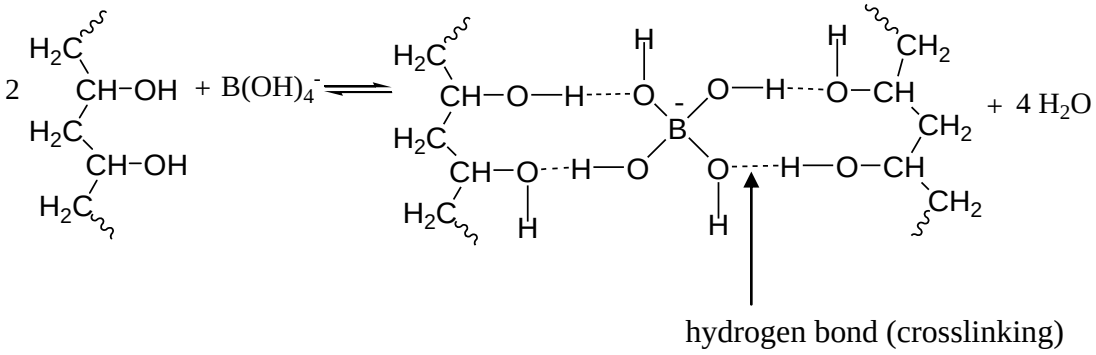

Figure 28. Crosslinking reaction between PVA and the borate ions.

Boron with its four coordination units is able to build up a three dimensional network in a condensation reaction of the borate ion with the hydroxyl groups of PVA as shown in **Figure 28**. But this reaction is an equilibrium reaction and the bonds are not very strong and can be broken and reformed easily. Weak crosslinking within the polymer results in the formation of a viscoelastic gel. Extreme dilution with water may disrupt the hydrogen bonding between hydroxyl groups and borate ions leading to separation of the components so that the gel is not readily reconstituted.

3.5.1.2.1.1. Crosslinked PVA / borax fiber mat

The crosslinked PVA / borax fiber mat was treated with water at 20 °C for 24 h to check solubility in water.

After water treatment for 24 h, the PVA fiber mat dipped with borax solution was found to be soluble in water to a large extent. The dip coating was not effective enough to lead to a stable crosslinking between boron and hydroxyl groups of PVA because the crosslinking was due to weak hydrogen bonds which have the tendency to break easily when dipped into water.

3.5.1.2.2. Benzaldehyde as the crosslinking agent

To be an effective crosslinker, a reactant must have at least two functional groups. Benzaldehyde has only one aldehydic group, so two kinds of reaction mechanisms are possible, which are illustrated in **Figure 29**.[90]

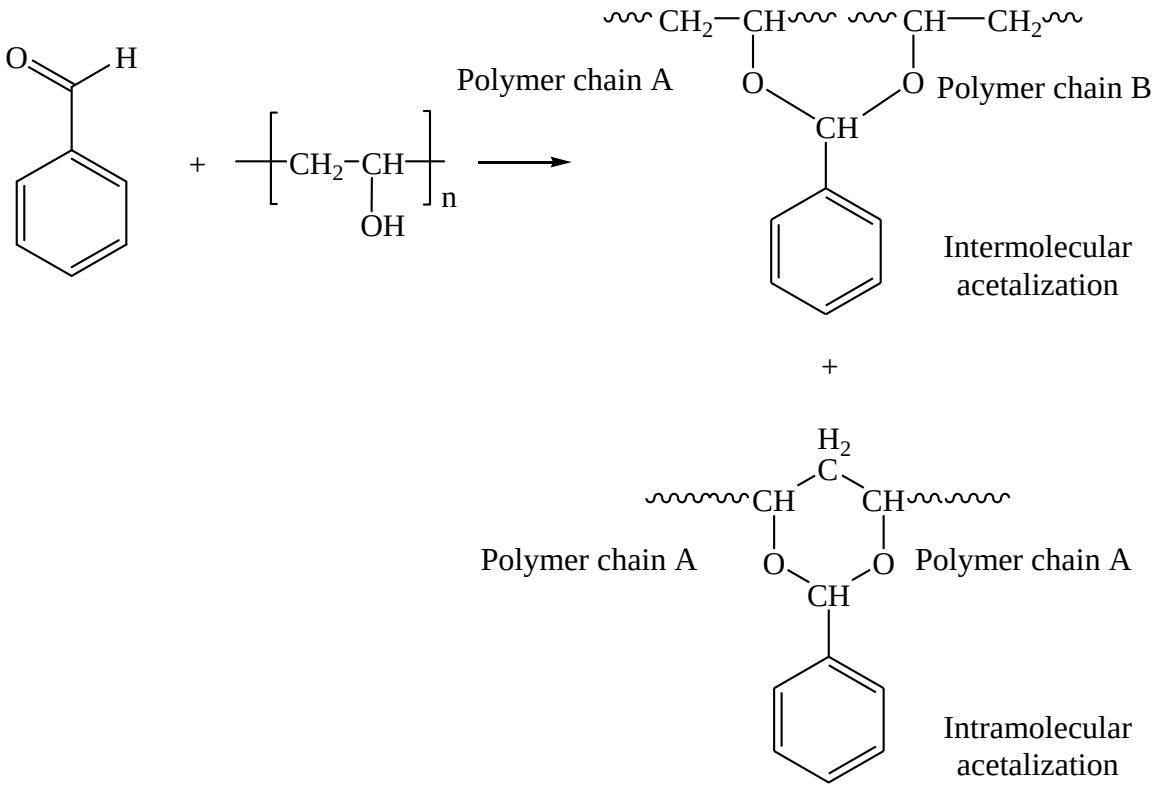

Figure 29. Crosslinking reaction between PVA and benzaldehyde showing two kinds of crosslinking: intermolecular, between two different polymer chains and intramolecular, within the same polymer chain.

Due to the formation of a stable 6-membered ring structure, intramolecular acetalization is more feasible than intermolecular acetalization.

The sample films prepared by solvent casting of the PVA / benzaldehyde solution were tested for water solubility by dipping into water at 20 °C for 24 h. Another sample film was heated in the oven at 80 °C for 1 h and then dipped into water at 20 °C for 24 h. Since our aim was to crosslink PVA so that it was not only insoluble in water at room temperature but also insoluble in water at high temperatures, thus the sample films were also analyzed by dipping them into hot water (~ 90 °C).

The results showed that the films which were dipped in water at room temperature for 24 h were insoluble. But, they were found to be soluble in water at 90 °C. The heated PVA / benzaldehyde films also showed the same results. They were also found to be insoluble in water at room temperature but soluble in water at high temperature.

3.5.1.2.3. Crosslinking of PVA with glutaraldehyde

Glutaraldehyde is a bifunctional compound with two aldehyde groups which can crosslink PVA by forming polymer networks as shown in **Figure 30**.[91]

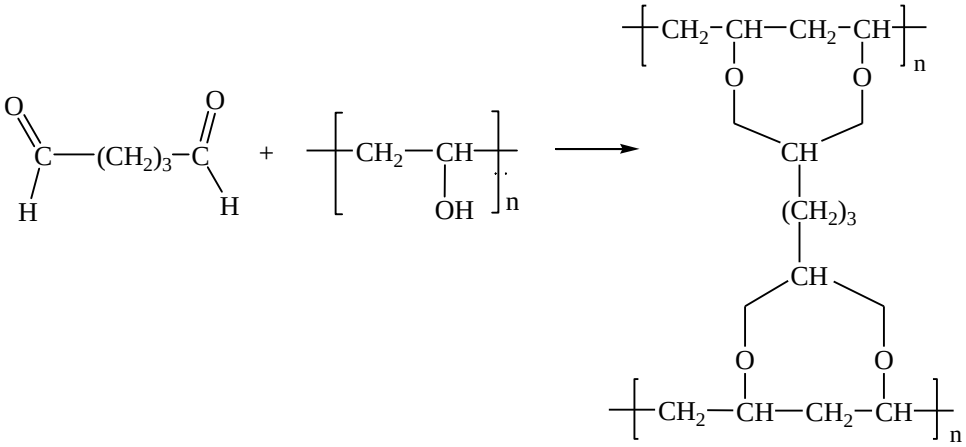

Figure 30. Glutaraldehyde reaction with PVA via acetal mechanism.

Films of PVA / glutaraldehyde solution prepared by solvent casting method were tested for water solubility by dipping in water at 20 °C for 24 h and also in water at 90 °C.

The films dipped in water at 20 °C showed insolubility confirming the formation of three dimensional crosslinks. However, the films that were dipped in water at 90 °C showed solubility after dipping for 1 h, which showed that the crosslinks break when the films are heated to a higher temperature.

Another way of crosslinking PVA with glutaraldehyde was by the addition of concentrated sulphuric acid as a catalyst.[92] In this method, electrospun PVA fiber mat was dipped in acidic glutaradehyde solution.

From the electrospun 10 wt% PVA fiber mat, a defined piece was dipped into the acidic glutaraldehyde solution for 1 min. The fiber mat was then treated with water at room temperature for 24 h and with water at 90 °C.

The PVA fibers mats dipped in the acidic glutaraldehyde solution were found to be insoluble in both water at room temperature and at high temperature. However, the fiber mat lost its morphology and became highly stiff. This occurred because of the crosslinking of the hydroxyl groups present on the surface of the fiber mat.

3.5.1.2.4. Crosslinking of PVA with glyoxal

Glyoxal as another tetrafunctional compound also serves as a good crosslinking agent for PVA. In literature, glyoxal has been used to crosslink PVA in the presence of an acid catalyst followed by heat treatment.[93] The chemical crosslinking reaction between PVA and glyoxal in the presence of acid is shown in **Figure 31.**

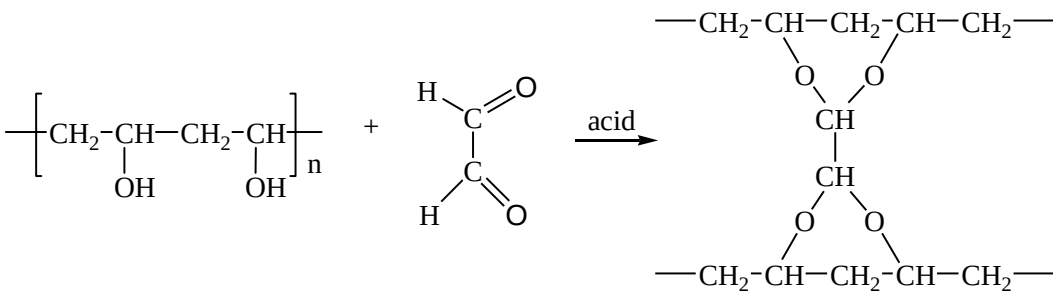

Figure 31. Chemical crosslinking of PVA with glyoxal.

An effort was made to crosslink PVA with glyoxal in the presence of an acid but without any post treatment like heating.

The PVA / glyoxal fiber mat obtained by electrospinning the acidic solution was dipped in water at 20 °C. The mat, however, immediately dissolved in water after dipping which showed that there was no crosslinking between PVA and glyoxal in the presence of acid only. Heating was required to initiate the crosslinking reaction.

The PVA / glyoxal fiber mats were then heated in the oven at two different temperatures: 100 °C for 15 min and 180 °C for 3 min and then again tested by water treatment.

Table 7. Solubility behaviour of non-heated and heated PVA / glyoxal fiber mats in water at 20 °C for 24 h.

Samples	Solubility in water at 20 °C
Non-heated	Soluble
Heated at 100 °C for 15 min	Soluble
Heated at 180 °C for 3 min	Insoluble

As evident from **Table 7**, the fiber mats non-heated and heated (100 °C - 15min) showed no anti-water solubility. However, the mats heated at 180 °C for 3 min were found to be water stable after 24 h. This heating temperature and time was the same as for crosslinked PVA / cavasol fiber mats as discussed earlier.

This brings us to the conclusion that water stable PVA fiber mats crosslinked by using cavasol and glyoxal require the same temperature (180 °C) to activate the crosslinking agent.

3.5.2. Physical methods

The electrospun PVA fiber mats crosslinked by both cavasol and glyoxal showed water stability after curing at the same temperature, 180 °C. The results were compared by testing the water stability of a neat PVA fiber mat annealed at the same temperature (180 °C) and for the same time period (3 min) without any crosslinker.

Since the annealing temperature was quite high which could be a drawback when carrying out large scale productions, PVA fiber mat was heated at different temperatures

starting from 50 °C to 180 °C and the degree of solubility was compared in water at room temperature (20 °C) and water at high temperature (90 °C). It was important that the heated PVA fiber mat showed minimum solubility in water at both these temperatures.

The PVA fiber mat obtained by electrospinning was heated at different temperatures starting from 50 °C to 180 °C in the oven for 3 min. The water solubility was compared for each of the heated fiber mats by dipping them in water at 20 °C for 24 h. The fiber mats after water treatments were dried completely in a vacuum oven at 40 °C for 2 days.

The percentage weight loss of the PVA fiber mats was calculated using equation (1) in chapter **3.5.1.1.3.**

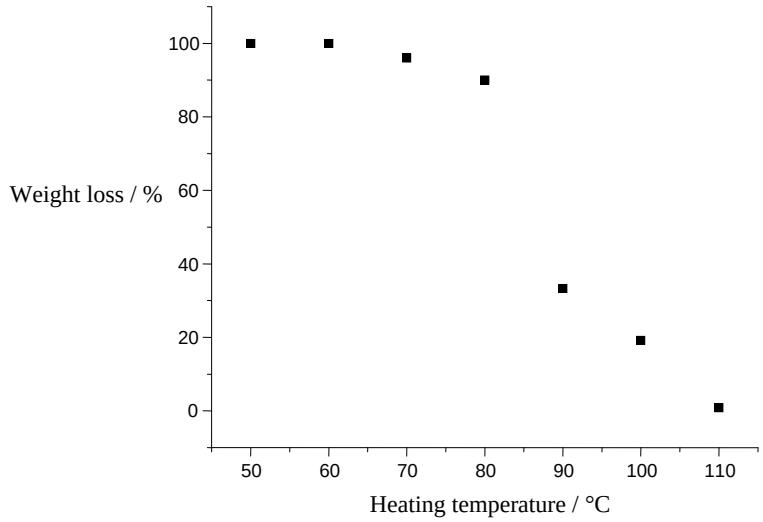

Figure 32. Change in the percentage weight loss of PVA fiber mats after water treatment at 20 °C for 24 h with the heating temperature.

The PVA fiber mats heated at temperatures from 50 °C up to 80 °C show almost complete weight loss after water treatment, while the PVA fiber mats heated above 100 °C show negligible weight loss when heated for 3 min **(Figure 32)**. It was also important for heat treated fiber mats to show minimum solubility in hot water. It was seen that the percentage weight loss of PVA fiber mats in hot water decreased with increase in heating temperature. For the fiber mats heated at 180 °C for 3 min, the weight

loss was minimum when dipped in water at 70 °C for 5 min. Above 70 °C, the fiber mat tend to become soluble.

It can be concluded that the best temperature required to improve the water resistance of PVA fiber mats in both water at lower and higher temperatures was found to be 180 °C.

Apart from the heating temperature, the heating time was also varied. The PVA fiber mats were heated at a constant temperature (180 °C) but for different time intervals starting from 1 min up to 10 min. The percentage weight loss was calculated after dipping the mats in water at 20 °C for 24 h. The plot of percentage weight loss vs. heating time is shown in **Figure 33**.

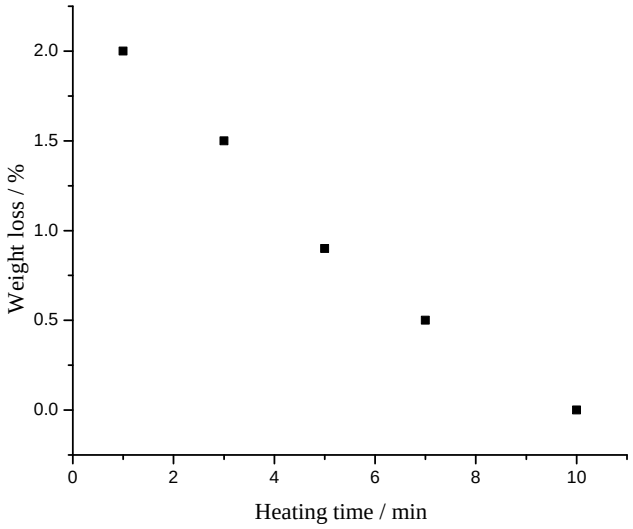

Figure 33. Change in percentage weight loss of PVA fiber mats heated at 180 °C with time.

The PVA fiber mats heated above 3 min at 180 °C turned pale yellow after heating. This may be due to the decomposition of PVA by excessive heat treatment. The heat-treated PVA at 180 °C for 3 min showed a percentage weight loss of only 1.5% after a water treatment for 24 h, calculated by using equation (1).

The insolubility of PVA after heat treatment could be due to two possible reasons: one, due to the condensation reaction between hydroxyl groups leading to the formation of ether linkages and the other could be the change in the crystallinity. Physical methods like heating might increase the degree of crystallinity of PVA. This may occur by

removal of residual water within the fibers by heating, breaking the PVA and water hydrogen bonds, and replacing it by intermolecular hydrogen bonds between the hydroxyl groups, which would increase the number of physical crosslinks in the electrospun PVA fibers resulting in additional crystallization.

The 10 wt% PVA fiber mats and the heated PVA fiber mats were analysed for water treatment. The non-heated PVA fiber mats were immediately soluble in water at room temperature while the heated 10 wt% PVA fiber mats were found to be water resistant at room temperature and up to 70 °C.

3.5.2.1. Wide Angle X-Ray Diffraction (WAXD) Analysis

The change in the crystalline structure of the PVA heated mats was analyzed by Wide angle X-ray diffraction **(Figure 34).**

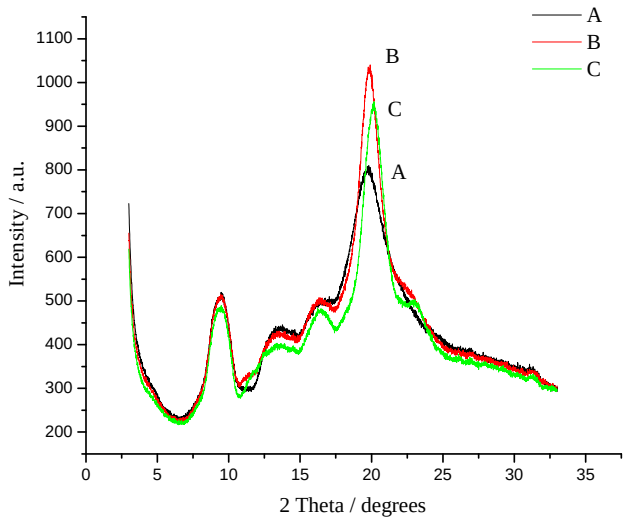

Figure 34. X-ray diffraction patterns of (A) electrospun PVA fiber mat (B) PVA fiber mat heated at 130 °C for 3 min and (C) PVA fiber mat heated at 180 °C for 3 min.

The X-ray diffraction pattern of the non-heated PVA fiber mat was compared with the mats heated at two different temperatures, one at 180 °C and the other at a lower temperature of 130 °C. The WAXD analysis of the PVA non-heated fibers showed a different diffraction pattern as compared to the heated PVA fiber mats. The XRD patterns of the non-heated and heated PVA electrospun fiber mats showed the PVA peak

at 2θ ~ 20°. However, the intensity of the heated PVA fiber mats was found to be higher. Non-heated PVA fiber mat showed an intensity of ~ 800, while PVA fiber mat heated at 130 °C showed an intensity of 1040 **(Figure 34B)** and the mat heated at 180 °C showed an intensity of ~ 950 **(Figure 34C)**. This increase in the peak intensities proves the increase in crystallinity after heat treatment. In addition, the sharpness of the peaks at 2θ ~ 20° also increased after heating. Furthermore, the WAXD pattern for PVA fiber mat heated at a comparatively lower temperature, 130 °C, showed greater increase in peak intensity as compared to the PVA fiber mat heated at 180 °C. This is attributed to the fact that heating removes the residual water within the fibers. As a result, PVA-water hydrogen bonding is replaced by intermolecular hydrogen bonding between the hydroxyl groups resulting in additional crystallization. However, the intensity of the peak decreased as the heating temperature was increased. This is because the crystalline property increases up to a particular temperature on heating after which decomposition of PVA starts, resulting in decrease in crystallinity.[94] This means heating PVA fiber mats at a temperature of 180 °C started the decomposition of PVA due to excessive heat treatment at the onset temperature of the melting of PVA. This resulted in decreased crystallinity as compared to the fiber mats heated at 130 °C.

3.5.2.2. Thermal stability (TGA)

The other reason attributed to the insoluble behaviour of PVA nanoweb in water could be the formation of ether linkages by a crosslinking reaction between hydroxyl groups of two polymer chains. To prove this, isothermal TGA of the electrospun PVA fiber mat was carried out at a temperature of 180 °C for 3 min to observe the effect of heating on weight loss **(Figure 35).**

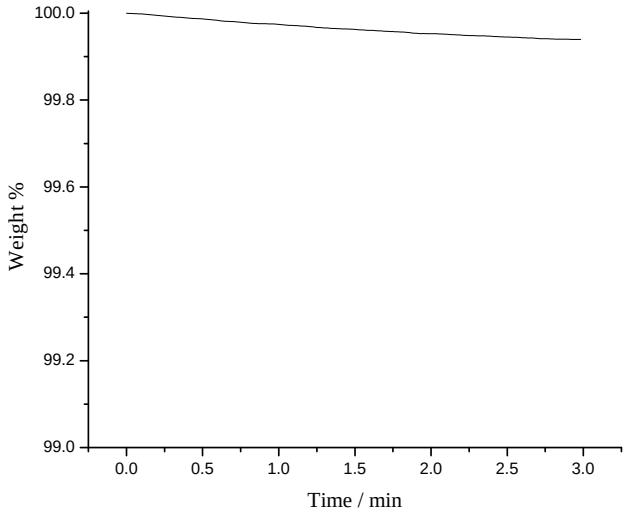

Figure 35. Isothermal TGA of PVA fiber mat at 180 °C for 3 min.

The isothermal TGA of the PVA fiber mat at 180 °C for 3 min showed that the weight loss after heating was around 0.05 wt% which was quite negligible. This proves that there was no condensation reaction between the hydroxyl groups at 180 °C, as otherwise the weight loss would have been much higher. Hence, it is the change in crystallinity, as proved by WAXD analysis, which is responsible for the water insoluble behaviour of the electrospun PVA fiber mats after heat treatment.

3.6. Conclusion

A heat treatment in the oven at 180 °C for 3 min successfully altered the water soluble behaviour of PVA fiber mats into water insolubility. The water stable behaviour of PVA was analyzed by water treatment of the heat treated fiber mats for a period of 24 h at room temperature. The percentage weight loss was found to be 1.5% after water treatment which was negligible. The mats were also found to be stable in water up to 70 °C.

The reason for the insolubility was attributed to a change in the degree of crystallinity of PVA fibers, as proved by X-ray diffraction. The crystallinity increased for the mats heated at a temperature of 130 °C. However, the increase in crystallinity was relatively

lower for the mats heated at 180 °C for the same time interval. Isothermal TGA of the fiber mats at 180 °C showed that the weight loss after heating for 3 min was almost negligible. Hence, there was no crosslinking reaction between the hydroxyl groups of PVA on heating, because a crosslinking reaction at 180 °C would have changed the weight of the mats to a large extent.

4. Modification of wettability of water insoluble Poly(vinyl-alcohol) fiber mats by sol-gel coating.

4.1. Introduction

The sol-gel process, also called chemical solution deposition, is a technique widely used in the fields of materials science and ceramic engineering.[95-98] In general, it is used to prepare glassy and ceramic materials. However, it can also be used to produce thin films which act as protective coatings on metals, glass or other types of substrates.

In the sol-gel process, inorganic networks from silicon or metal alkoxide monomer precursors are formed.[99, 100] A system of colloidal particles in a solution (sol) gradually evolves towards the formation of a macroscopic material (gel) containing both a solid phase and a liquid phase, which consists of either discrete particles or a polymer network. Once the liquid evaporates, a strong glass-like material remains. The basic sol-gel reaction consists of two chemical reactions - one is hydrolysis and the other is the condensation reaction. The hydrolysis reaction produces the sol while the condensation reaction produces a macroscopic gel on the substrate leading to the formation of a thin film. The precursors for synthesizing the colloidal particles consist of a metal or a metalloid surrounded by reactive ligands. A metal alkoxide is used commonly as a precursor because it reacts readily with water. The most widely used metal alkoxides are the alkoxysilanes, such as tetramethoxysilane (TMOS) and tetraethoxysilane (TEOS).

The basic sol-gel reaction starts when the metal alkoxide is mixed with water and a hydrolysis reaction starts. Ethanol is used as a solvent because water and alkoxides are immiscible. The hydrolysis reaction is completed when all the (OCH_2CH_3) groups are replaced by the (OH) groups provided sufficient amount of water is present. This produces a sol which consists of $Si(OH)_4$ (silicic acid) and ethanol.

$$Si(OCH_2CH_3)_4 + 4\,H_2O \longrightarrow Si(OH)_4 + 4\,CH_3CH_2OH$$

In the next step, two partially or completely hydrolyzed molecules react together in a condensation reaction to liberate water.

$$2\ Si(OH)_4 \longrightarrow (OH)_3Si{-}O{-}Si(OH)_3 + H_2O$$

As the reaction proceeds, polycondensation takes place and the number of Si—O—Si bonds increases, which results in a formation of a macroscopic gel.

The addition of a catalyst like HCl increases the rate of the hydrolysis reaction. Under the acidic conditions, the protonation of the alkoxide group becomes more likely. This withdraws the electron density from the silicon atom making it more electrophilic and thus increasing the susceptibility of attack from water.

4.2. Wettability of a solid surface

The wettability of a solid surface is defined as the property of that surface that determines how fast a liquid such as water or any solvent will adhere to the substrate.[101] The ability of the liquid to spread readily and uniformly over the surface of the solid is defined as the wetting ability of that liquid. Liquids with high surface tension like mercury show little or no wetting ability, while those with lower surface tension show high wetting ability. The wettability can be measured by determining the contact angle between the liquid and the solid surface **(Figure 36)**. Wetting or the spreading of a liquid on a solid surface depends on the properties of the solid surface like the chemical composition and the geometrical microstructures of the surface as well as the liquid used. Therefore the wettability of a solid surface can be manipulated by changing the surface properties of that solid or by changing the properties of the liquid of interest. The chemistry and the roughness of the solid surface determine the water contact angle of that surface**.** Therefore, hydrophobicity can be induced on a surface by increasing the roughness of the surface. This is possible by coating it with low-surface-energy materials such as fluoroalkylsilanes or silicone-based compounds.[102-104]

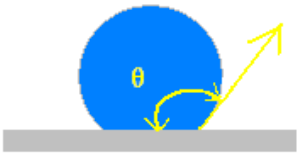

Figure 36. The contact angle "θ" of a liquid on a solid surface.

The molecules of a liquid are subject to a cohesive force which keeps them united to one another, but there is also an adhesive force which is the force with which the molecules of the liquid adhere to the surface of materials that they contact. When the forces of adhesion are greater than the forces of cohesion, the liquid tends to wet the surface, when instead the forces of adhesion are less by comparison to those of cohesion, the liquid tends to "refuse" the surface. The contact angle (θ) is the angle at which the liquid-vapor interface meets the solid-liquid interface. The contact angle is determined by the resultant between adhesive and cohesive forces. The wettability of a solid surface decreases as the contact angle increases. A surface with a contact angle less than 90° indicates high wettability while a surface with a contact angle greater than 90° indicates low wettability and is considered to be “hydrophobic” in case water is the wetting liquid **(Figure 37)**. It is found to be useful in many applications such as textiles, coatings, self-cleaning etc**.** Super hydrophobic surfaces have a contact angle greater than 150° showing almost no contact between the liquid drop and the solid surface.

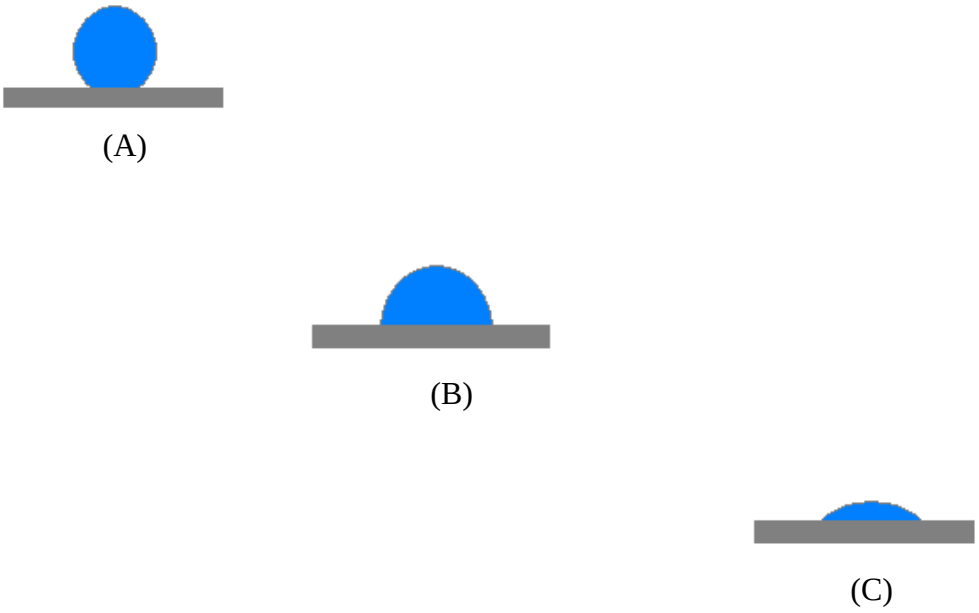

Figure 37. The wetting of a solid surface by a liquid. (A) shows low wettability with high contact angle and (C) shows high wettability with low contact angle.

4.3. Results and discussion

4.3.1. Hydrophobic Poly(vinyl alcohol) by sol-gel process

Crosslinked PVA fiber mats have a relatively low water uptake due to the decrease in the number of hydroxyl groups. The water uptake efficiency decreases as the crosslink density increases. Since the insolubility of PVA in water was not due to crosslinking, hence the hydroxyl groups were freely available for water uptake. Thus, the water insoluble PVA fiber mats were found to have high water absorbancy.

In order to decrease the water uptake efficiency of the water insoluble PVA fiber mats, a simple sol-gel treatment of the fiber mats was brought about.[105] The super-hydrophilicity of the electrospun PVA fiber mats was converted into super-hydrophobicity by the deposition of a hydrophobic sol-gel coating.

4.3.2. Sol-gel coating

The sol-gel solution consisted of tetraethyl orthosilicate (TEOS) and n-decyltrimethoxysilane (DTMS) as the active chemicals. The chemical structures of TEOS and DTMS are shown in **Figure 38.**

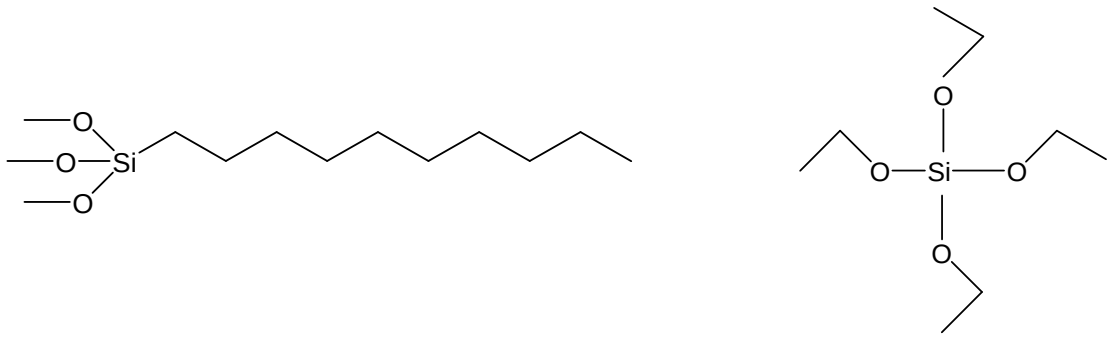

(A) (B)

Figure 38. Chemical structures of (A) n-decyltrimethoxysilane (DTMS) and (B) tetraethyl orthosilicate (TEOS).

The coating solution for the heated PVA fiber mat was prepared with the molar compositions of:

$$TEOS:DTMS:ethanol:H_2O:HCl = 0.5:0.1:20:11:0.008$$

followed by continuous stirring at room temperature for 24 h. The heated PVA samples were dip-coated with this sol-gel solution by immersing the samples into the solution for 10 s. The samples were then dried in air for 24 h. The water contact angle was measured to determine the surface hydrophobicity. To see the effect of dipping time on the hydrophobic behaviour of PVA fiber mats, they were immersed in the sol-gel solution for a longer time i.e. 2 min and the contact angle was measured. The morphology of the fibers before and after coating was analyzed by SEM and the fiber diameter was measured.

Furthermore, to have an insight on the effect of coating on non-heated PVA fibers, post-heat treatment was tried instead of pre-treatment. For this, neat PVA fiber mats were dipped into the sol-gel solution for the same amount of time (2 min), dried in air for 24 h and then the mat was heated at 180 °C for 3 min. However, after the initial sol-gel treatment there was a significant weight loss which may be attributed to the presence of considerable amount of water in the sol-gel solution. Furthermore, the roughness of the fiber mats increased to a large extent and they became highly brittle.

4.3.3. Role of active chemicals in the sol-gel process

4.3.3.1. Role of TEOS

Tetraethyl orthosilicate (TEOS), a metal alkoxide, acts as the metal precursor for the formation of a continuous polymer network (gel). They can readily react with water and undergo various forms of hydrolysis and polycondensation reactions:

Hydrolysis:

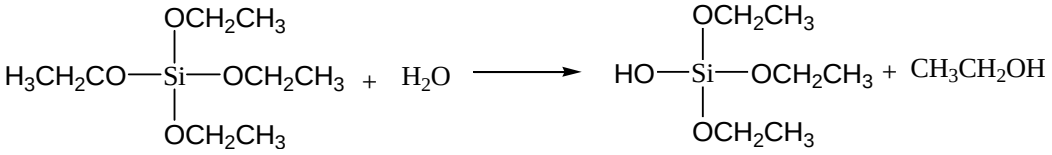

Mechanism of acid catalysed hydrolysis:

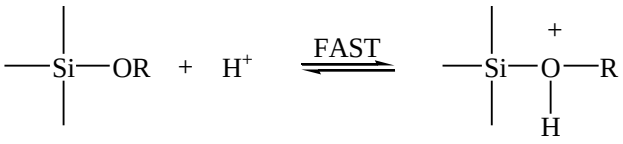

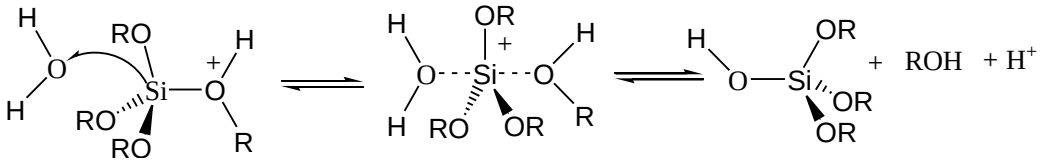

Depending on the amount of water and catalyst present, all the OCH_2CH_3 groups can be converted to OH groups to bring the hydrolysis to completion.

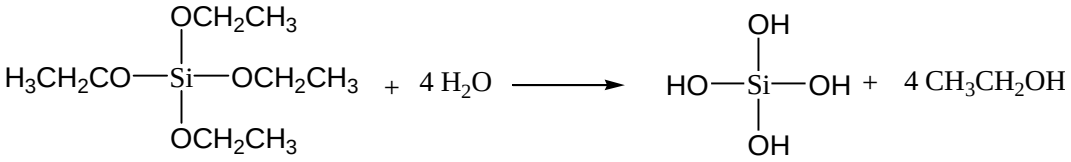

The hydrated silica tetrahedra can interact together though a condensation reaction to form a siloxane [Si-O-Si] bond.

Condensation:

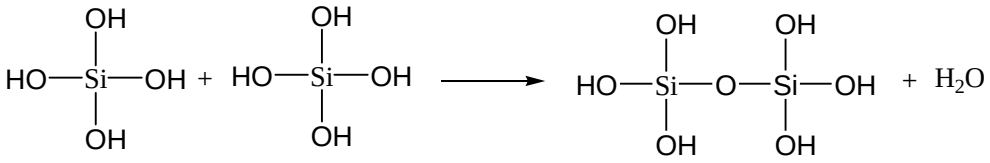

Since fully hydrolyzed $Si(OH)_4$ is tetrafunctional, polymerization can lead to complex branching. Polycondensation can occur to build larger and larger Si-containing molecules leading to the formation of a SiO_2 network.

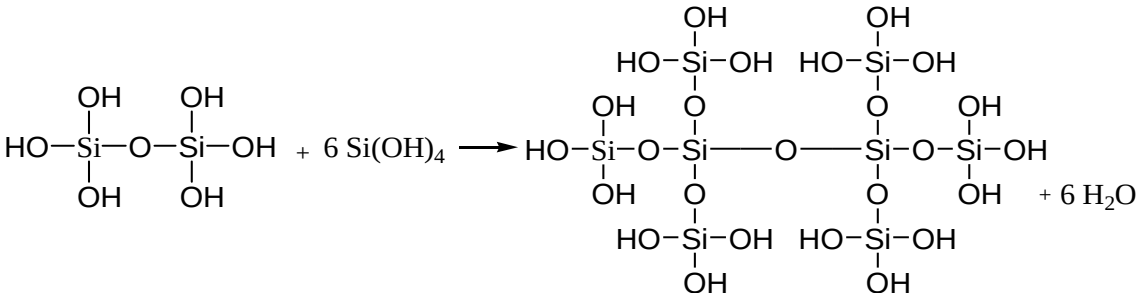

These silane coupling agents react with the surface hydroxyl groups of PVA and form a siloxane network by hydrolysis of the alkoxysilanes tightly bound to the material surface.

4.3.3.2. Role of DTMS

DTMS, n-decyltrimethoxysilane, is a low surface energy compound due to the presence of CH groups. The long aliphatic chain in DTMS acts by making the surface of the fiber mat hydrophobic because it reacts with the silane coupling agent (TEOS) and its function is fixed onto the material surface.

A schematic diagram of the sol-gel reaction on the surface of the cured PVA fiber mats is shown in **Figure 39**.

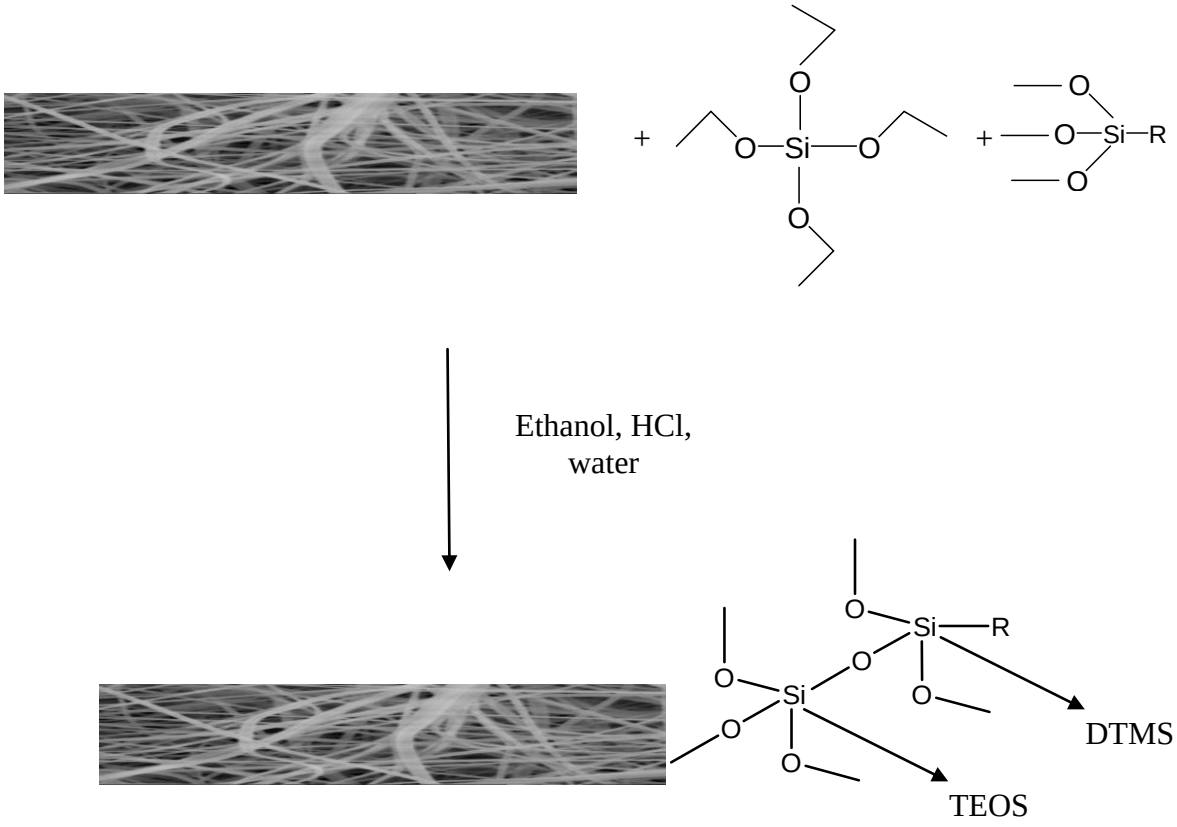

Figure 39. A schematic diagram of sol-gel reaction on the surface of heated PVA fiber mat.

4.3.4. Contact angle measurement of the coated fibers

The contact angle of the heated and coated PVA fiber mats was measured to determine the surface hydrophobicity and was found to be 110° for the samples dipped for 10 s and 144° for the samples dipped for 2 min **(Figure 40)**.

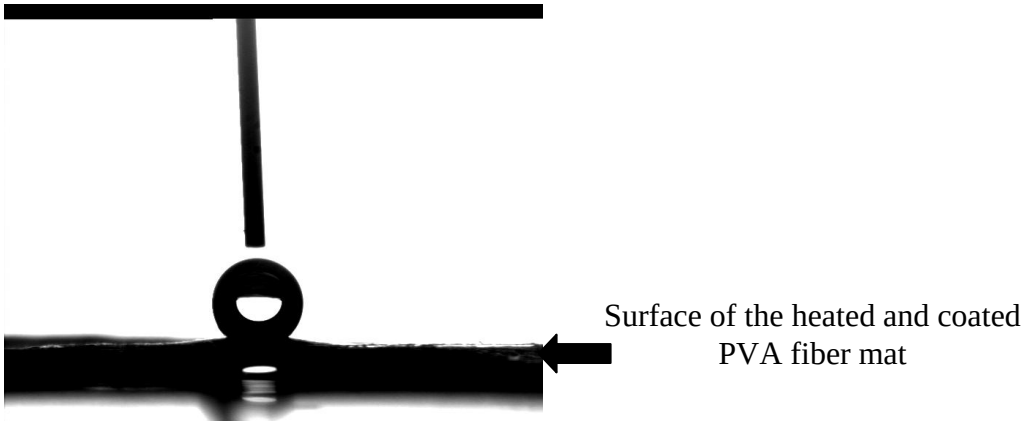

Figure 40. Water contact angle measurement for PVA heated and coated (2 min) fiber mats showed a contact angle of 144°.

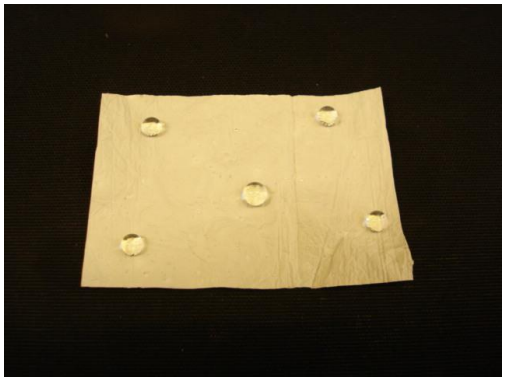

Figure 41. Water droplets placed on the 10 wt% heated and sol-gel (TEOS and DTMS) coated PVA fiber mats showing the hydrophobic behaviour.

It was found that the heated but uncoated PVA fiber mat was hydrophilic with a wetting angle of 0°, it immediately absorbed water due to its porous structure, whereas the heated

and the coated PVA fiber mat was highly hydrophobic showing water contact angle of 144° **(Figure 41)**. This proves that the sol-gel coating was found to be effective to make the fibrous mats hydrophobic. The surface chemistry of the fiber mats was modified by the sol-gel coating.

The morphology of the non-heated, heated and coated PVA fiber mats was measured using the scanning electron microscope. The fiber diameter was measured using the software Image J.

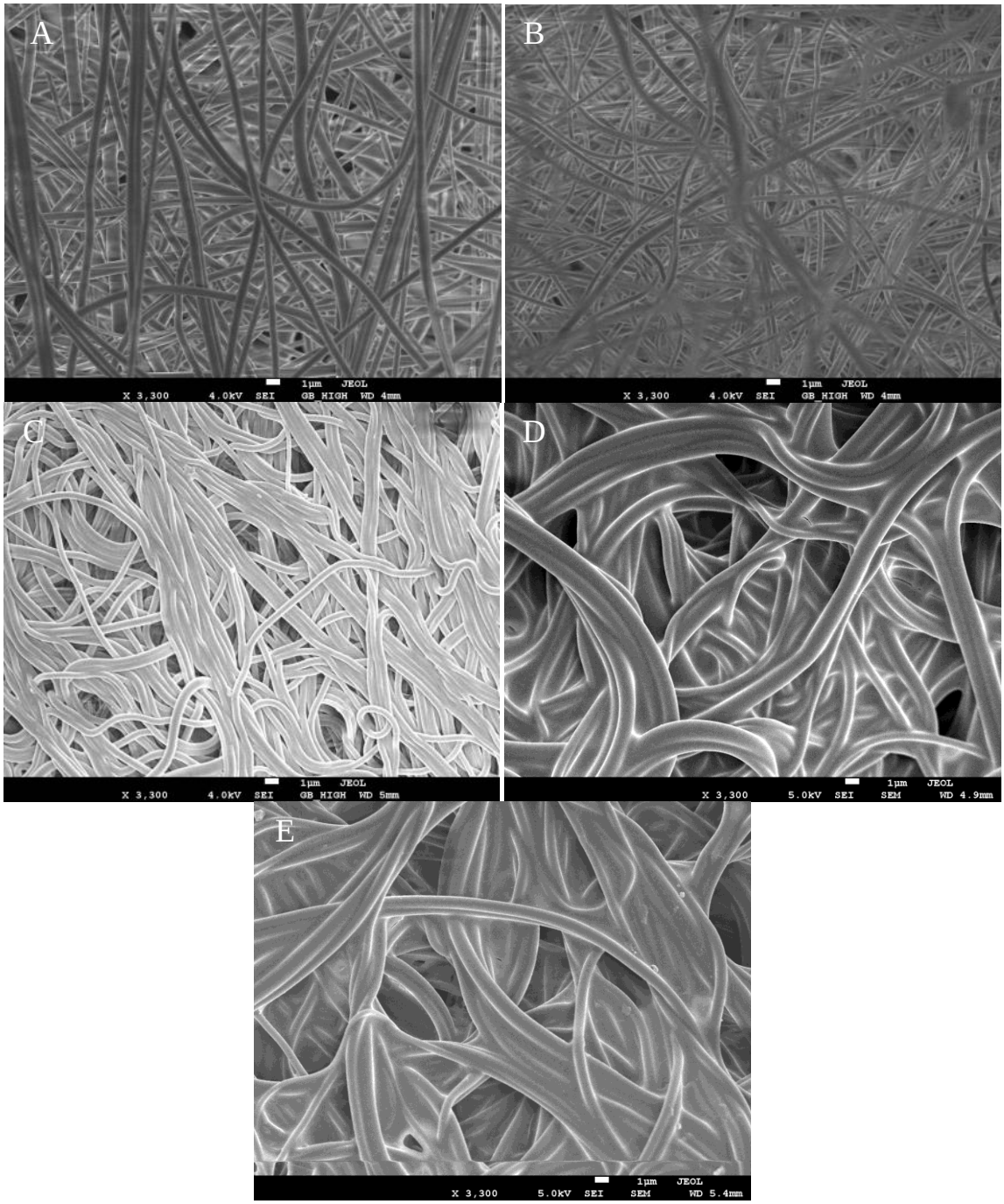

Figure 42. SEM images of (A) 10 wt% PVA fiber mat (B) heated PVA fiber mat, (C) heated PVA fiber after water treatment (24 h), (D) heated as well as coated PVA fiber mat, (E) heated and coated fiber mat after water treatment (24 h).

Figure 42A shows the SEM image of the non-heated and non-coated electrospun 10 wt% PVA fiber mats. The average fiber diameter was found to be 530 nm. The SEM

image of the heated 10 wt% PVA fiber mats is shown in **Figure 42B.** The average fiber diameter was measured as 488 nm. On water treatment (24h), the average fiber diameter of the heated PVA fiber mats increased to 668 nm. The SEM image is shown in **Figure 42C.**

Figure 42D shows the SEM image of the coated 10 wt% PVA fiber mats. As expected, the average diameter of the fibers increased to 780 nm after coating. SEM image of the heated-coated and water-treated (24 h) 10 wt% PVA fibrous mats is shown in **Figure 42E** and the average fiber diameter was calculated to be 810 nm. Hence, after coating and water treatment (24 h), the fiber shape and the fiber structure was retained.

4.3.5. Pore size measurement

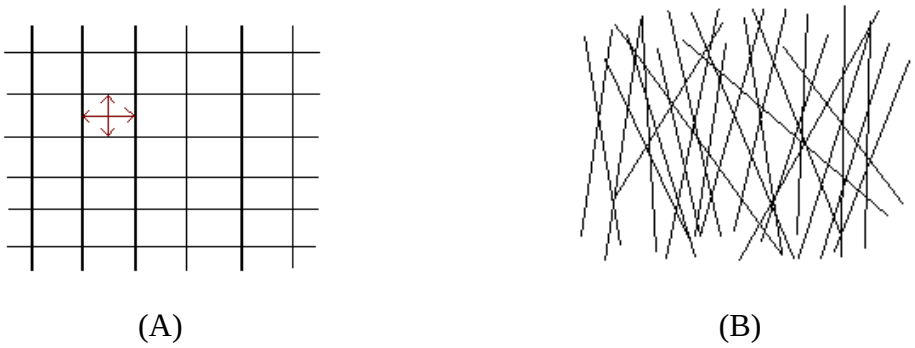

Figure 43. Diagram of (A) plain fiber mats and (B) complex 3D structures.

In plain fiber materials as shown in **Figure 43A**, the pore size can be measured easily under a microscope as the pore structure is very clearly defined. However in complex 3D structures like **Figure 43B**, the pore size distribution is measured using porometry via capillary flow.

The pore size distribution of 10 wt% PVA fiber mats and sol-gel coated PVA fiber mats was compared using the Capillary Flow Porometer.

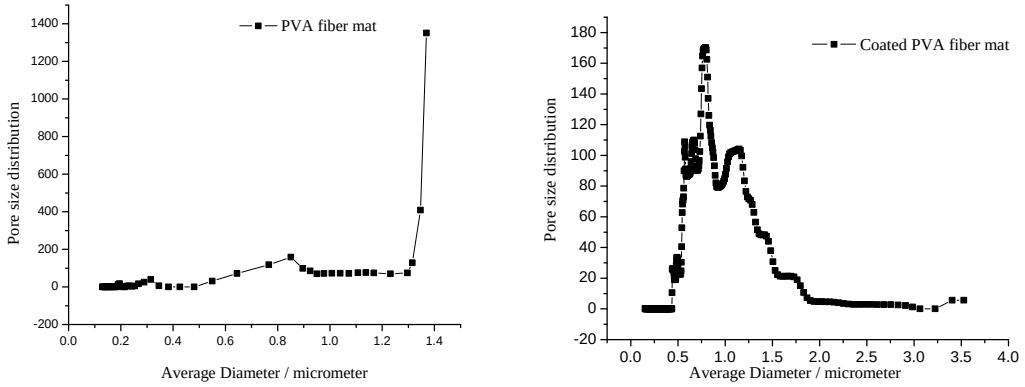

(A) (B)

Figure 44. The pore size distribution and the average diameter of (A) non-coated PVA fiber mat and (B) sol-gel (TEOS and DTMS) coated PVA fiber mat.

As evident from **Figure 44**, the pore size distribution of PVA fiber mat decreased to a large extent after coating. The bubble point (the maximum pore size) for non-coated PVA fiber mat was found to be 1.3 µm (Bubble point pressure = 0.466 bar) while that for the coated PVA fiber mat was 3.6 µm (Bubble point pressure = 0.177 bar). The maximum pore size increased after coating. This can be attributed to the adhesion of fibers after coating thereby increasing the pore diameter. The pressure required to blow open a larger pore is lower than the pressure required to blow open a smaller pore. This is evident from the fact that the pressure required to blow open the largest pore in the non-coated fiber mat (Bubble point pressure) is higher than that in the case of coated fiber mat.

The second parameter measured experimentally was the Mean Flow Pore size (MFP) which is the micron size where 50% of the flow was higher and 50% of the flow was lower. The MFP for non-coated PVA mat was found to be 1.05 µm while that for coated PVA fiber mat was found to be 0.99 µm.

4.3.6. Modification of the sol-gel process

The influence of different parameters on the hydrophobicity of the PVA fiber mats was studied by altering the molar composition of the sol-gel solution and by using a different crosslinker and a different silane in place of TEOS and DTMS.

4.3.6.1. Influence of different silanes on hydrophobicity

The long chain aliphatic groups present in DTMS that get attached on the surface of PVA fiber mats are responsible to bring about hydrophobicity in the mats. Different silanes with increasing carbon chain lengths were used in the sol-gel solution to investigate the effect of the aliphatic groups present in the silanes **(Figure 45)**. The contact angle for each of these heated and coated PVA fiber mats was measured by taking an average of at least five droplets of 3 mg of distilled water.

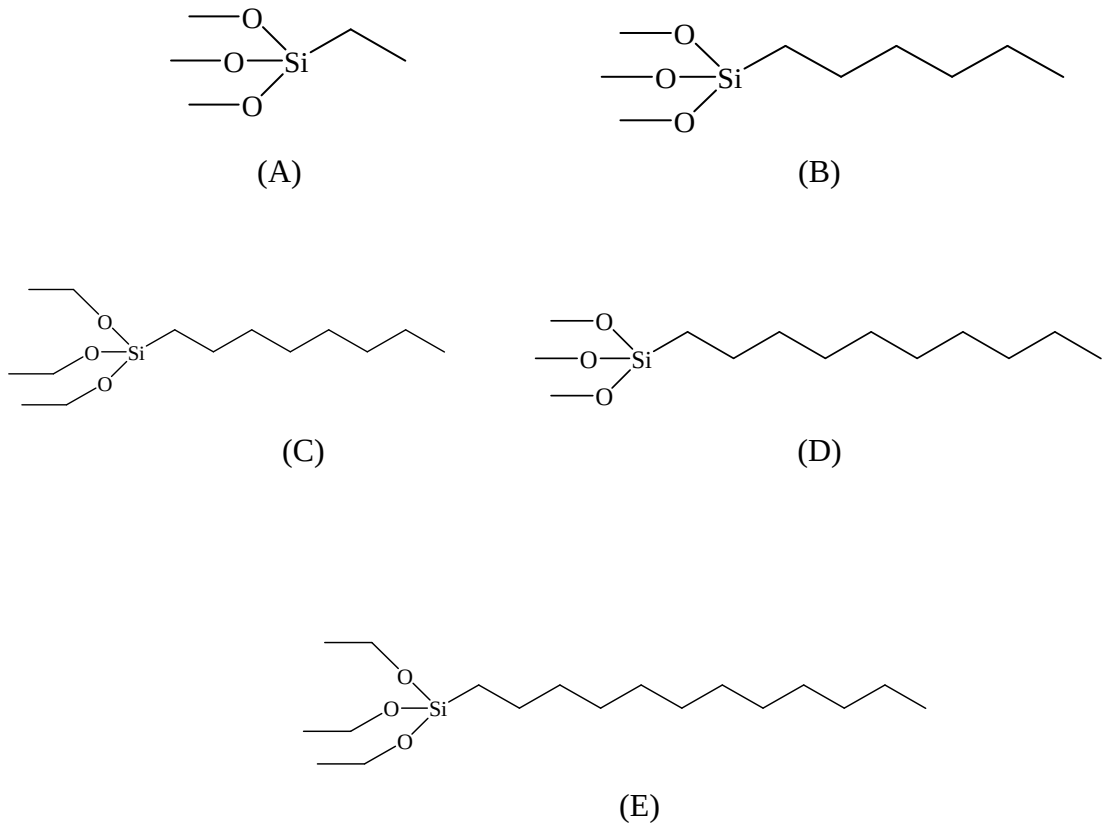

Figure 45. Chemical structure of different silanes (A) ethyltrimethoxysilane, (B) hexyltrimethoxysilane (C) n-octyltriethoxysilane **(**D) n-decyltrimethoxysilane (E) n-dodecyltriethoxysilane used in the sol-gel process.

Table 8. The contact angles measured for silanes with different carbon chain lengths in the sol-gel solution.

Silane	Average contact angle / degrees
Ethyltrimethoxysilane	133
Hexyltrimethoxysilane	141
n-Octyltriethoxysilane	143
n-Decyltrimethoxysilane	144
n-Dodecyltriethoxysilane	145

The contact angle of the heated and coated PVA fiber mats shows an increase with the increase in the carbon chain length of the silanes in the sol-gel solution **(Table 8)**. This shows that the aliphatic groups present in the silanes were responsible to bring about the hydrophobicity on the surface of the PVA fiber mats. Longer the carbon chain length more was the hydrophobicity of the mat.

4.3.6.2. Fluorinated silane in the sol-gel solution

Perfluorooctyltriethoxysilane **(Figure 46)** was used as a fluorinated silane in the sol-gel solution and the effect on the hydrophobicity of the mats was determined.

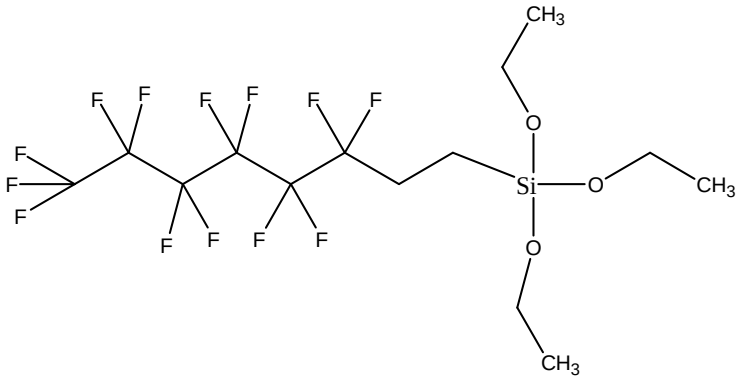

Figure 46. Chemical structure of 1H,1H,2H,2H-Perfluorooctyltriethoxysilane.

When the fluorinated compounds are applied onto a surface, the fluorinated groups like -CF_3 act by reducing the surface energy to a large extent. The interfacial energy is greatly reduced as the fluorinated compounds have the tendency to migrate towards the air/film interface.[106]

The fluorinated silane, perfluorooctyltriethoxysilane, was added in the sol-gel solution along with TEOS in the molar ratio:

TEOS:Perfluorooctyltriethoxysilane:ethanol:H_2O:HCl = 0.5:0.1:20:11:0.008

The heated (180 °C - 3min) PVA fiber mat was dip-coated with this solution containing the fluorinated silane for different time intervals starting from 20 s up to 7 min and the surface hydrophobicity was analyzed by measuring the contact angle.

Table 9. The average contact angle values for PVA fiber mat dip-coated in the sol-gel solution containing the fluorinated silane for different time intervals.

Time for dip-coating	Average contact angle
20 s	131°
2 min	152°
5 min	151°
7 min	150°

Table 9 shows that the average contact angle remains almost constant on increasing the dipping time from 2 min to 5 min, and 7 min. However, there is a large increase in the contact angle on increasing the dipping time from 20 s to 2 min. For the PVA samples coated with the sol-gel solution containing DTMS as the organic compound, the average contact angle was 144° for a dipping time of 2 min as compared to the PVA samples dip-coated with the sol-gel solution containing the fluorinated silane, which showed an average contact angle of 152°. This shows that coating with fluorinated silane containing sol-gel solution decreases the surface energy to a larger extent as compared to coating with a non-fluorinated silane.

4.3.6.3. Influence of Bayresit VPLS 2331 on hydrophobicity

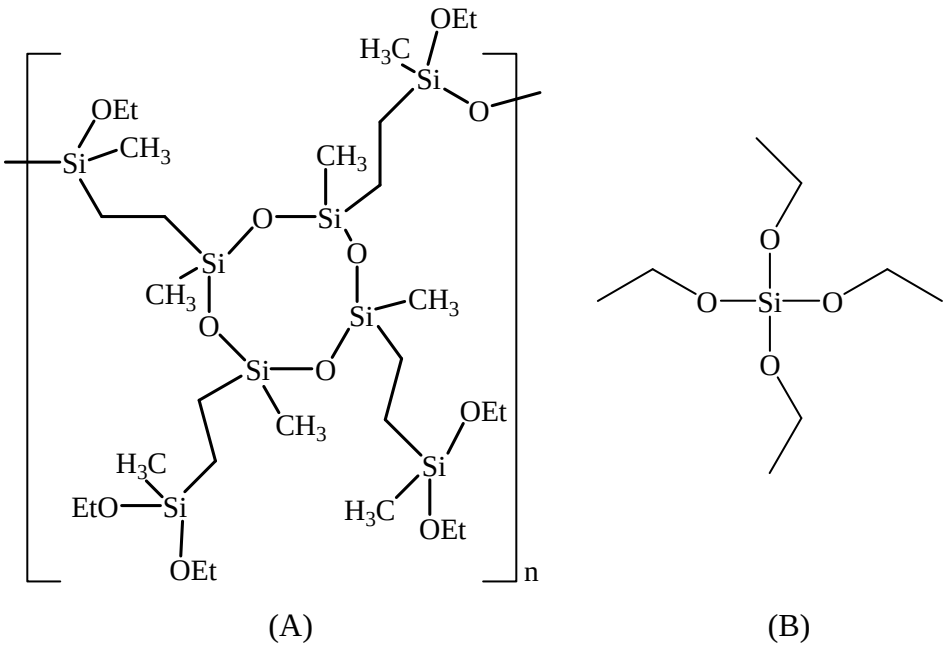

Figure 47. Chemical structures of (A) Bayresit VPLS 2331 (B) TEOS.

In order to have an insight on the role of TEOS as a metal precursor for sol-gel coating systems, a multifunctional ethoxycarbosiloxane, Bayresit VPLS 2331 **(Figure 47A)** was used as a crosslinker in place of TEOS.[107] Bayresit VPLS 2331 is a product of Bayer MaterialScience. The presence of higher functionality renders a higher crosslink density in Bayresit as compared to TEOS which ensures more hardness or scratch resistance in sol-gel coating systems. Apart from that, its flexible ring structure ensures a high level of elasticity. An added advantage of the highly crosslinked inorganic coatings is their significant resistance to solvents and acids. High reactivity of the crosslinker ensures higher hydrophobicity as well. Compared to other sol-gel systems, curing can be performed at lower or moderate temperatures and for a shorter timeframe. Moreover, a faster sol-gel reaction takes place due to its high condensation reactivity.

Bayresit was used in the sol-gel solution with DTMS in the same molar ratio as TEOS. One sample was prepared by dipping the non-heated PVA fiber mat in the sol-gel solution containing Bayresit for 2 min. Two other samples were prepared by heating the

PVA fiber mat at two different temperatures - one at a moderate temperature of 100 °C for 15 min and the other at the usual heating temperature of 180 °C for 3 min and thereafter dip-coating with the sol-gel solution for 2 min. All the 3 samples were then dried in air for 24 h. The non-heated PVA fiber mat **(Sample 1)** and the PVA fiber mat heated at 100 °C for 15 min **(Sample 2)** showed a considerable amount of weight loss after the dip-treatment. The other sample heated at 180 °C for 3 min **(Sample 3)** showed lower percentage weight loss and a contact angle which was comparable to the one obtained in case of TEOS (144°).

Table 10. The percentage weight loss and the contact angle values for the non-heated and heated PVA fiber mats dipped in the sol-gel solution containing Bayresit VPLS 2331.

Sample	Weight loss / %	Average contact angle / degrees
1	24	95
2	20	109
3	1.2	140

As evident from **Table 10**, the sol-gel solution containing Bayresit and DTMS did not show a drastic change in the hydrophobicity of the PVA fiber mats as compared to the mats dipped in TEOS and DTMS solution. Moreover, the presence of water (essential for hydrolysis) in the sol-gel solution completely eliminates the possibility of obtaining water repelling PVA fiber mats without any weight loss or shinkage after the dip-treatment. It can be concluded that heat treatment at 180 °C is an important step in order to obtain water resistant hydrophobic PVA fiber mats.

4.3.6.4. Influence of different molar compositions on hydrophobicity

The molar compositions of the active chemicals were varied to see the effect on the hydrophobicity of the PVA mats. The ratio between TEOS and DTMS was changed from

$$TEOS:DTMS:ethanol:H_2O:HCl = 0.5:0.1:20:11:0.008$$

to

$$TEOS:DTMS:ethanol:H_2O:HCl = 0.1:0.05:20:11:0.008$$

The amounts of DTMS and TEOS were decreased to see the effect on the PVA fiber mats. The solvents and the acid were added in the same molar ratio.

The contact angle for the heated PVA fiber mats dip coated in the sol gel solution containing lower concentrations of TEOS and DTMS was found to be around 90°. Hence with the decrease in the concentrations of TEOS and DTMS, the wetting ability increased or the hydrophobicity decreased. This proves that DTMS acts as a low surface energy material since in higher concentrations it decreases the wettability of a solid surface.

Furthermore, since the hydrophobicity was induced by the presence of DTMS in the sol-gel solution, the amount of this silane was varied to see the effect on the wettability of the heated PVA fiber mats. For this, five sol-gel solutions were prepared with varying amounts of n-decyltrimethoxysilane (DTMS) and the contact angles were measured.

Table 11. The average contact angles of heated (180 °C – 3 min) PVA fiber mats dip-coated in different sol-gel solutions for 2 min.

Percentage decrease in amount of DTMS	Average contact angle
25%	137°
50%	142°
75%	138°
90%	140°
99%	139°

As seen from **Table 11**, the average contact angle of the PVA fiber mats coated with sol gel solutions containing reduced amounts of DTMS remained almost constant. The presence of aliphatic groups in DTMS was one of the reasons for the hydrophobicity of the PVA fiber mats, therefore it was expected that the contact angles would decrease after the amount of DTMS in the sol-gel solutions was reduced. However, an increase in the surface roughness was seen after dip-coating the PVA fiber mats. The morphology of the dip-coated PVA fiber mats was compared by the scanning electron microscope.

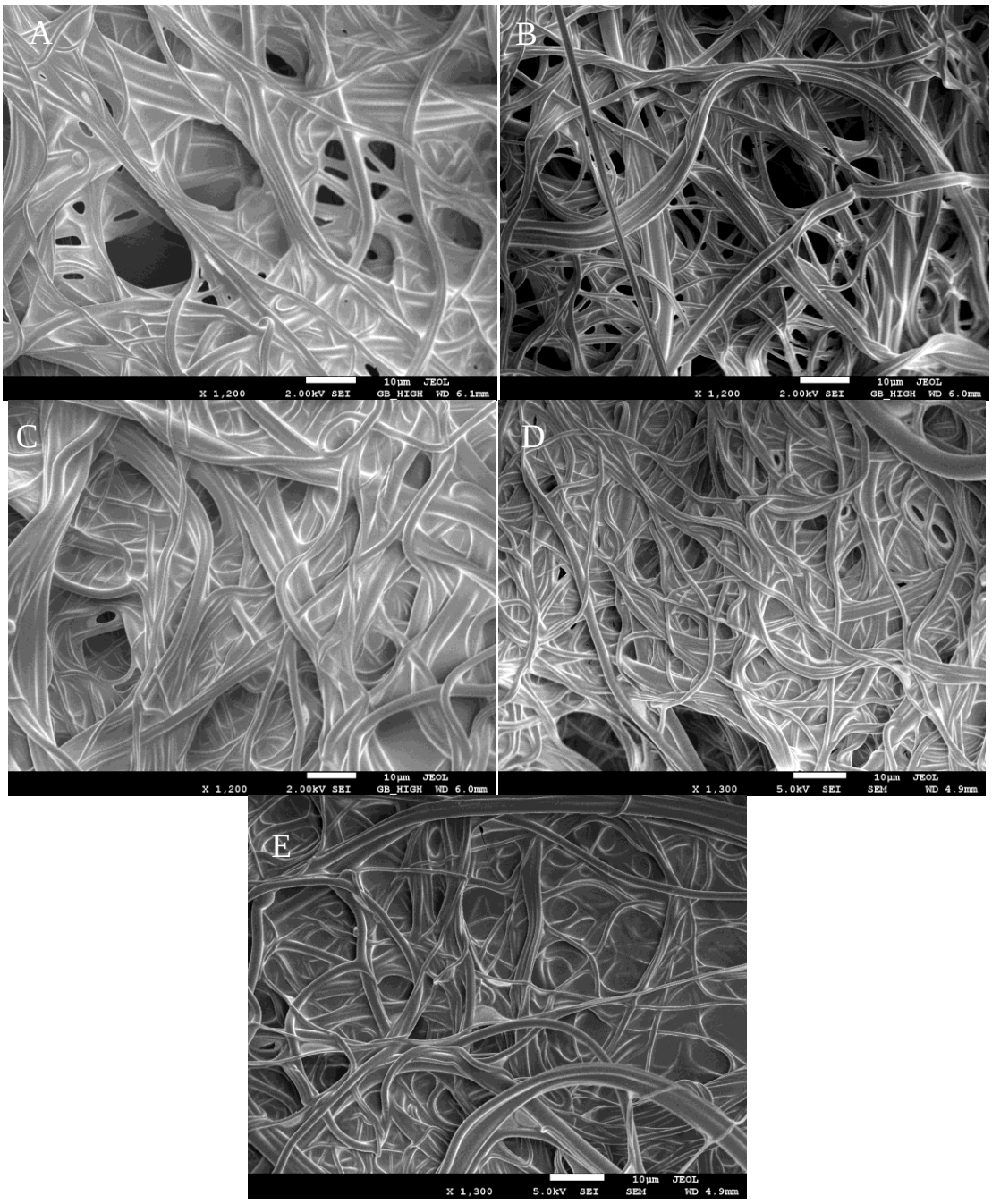

Figure 48. SEM images of heated PVA fiber mats dip-coated in sol-gel solution with (A) 25% reduction, (B) 50% reduction, (C) 75% reduction, (D) 90% reduction (E) 99% reduction in the amount of DTMS.

The SEM images of the sol-gel coated fibers show that the fiber morphology was retained after the sol-gel treatment in all concentrations of DTMS **(Figure 48)**.

4.3.6.4.1. Mechanical properties

The increase in the surface roughness after dip-coating with different sol-gel solutions was analyzed by the tensile strength measurement. The mechanical properties were investigated for each of the samples dip-coated in the sol-gel solutions with different DTMS concentration and the standard force-strain curves **(Figure 49A-F)** were compared. An average of at least five measurements for each sample was taken for final results.

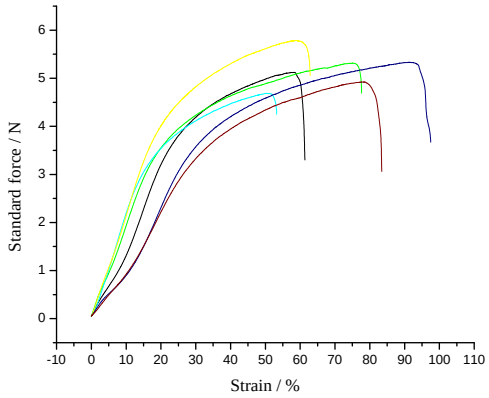

(A) Standard force vs. Strain curve for PVA samples coated in the sol-gel solution with no reduction in the amount of DTMS.

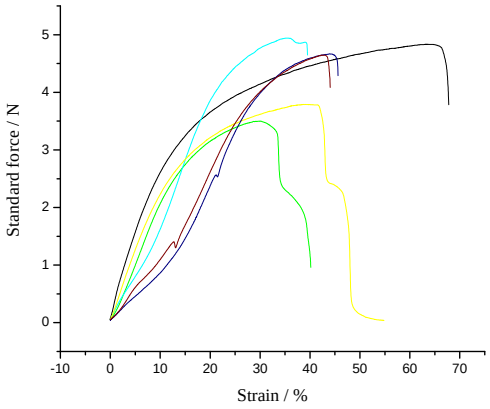

(B) Standard force vs. Strain curve for PVA samples coated in the sol-gel solution with 25% decrease in the amount of DTMS.

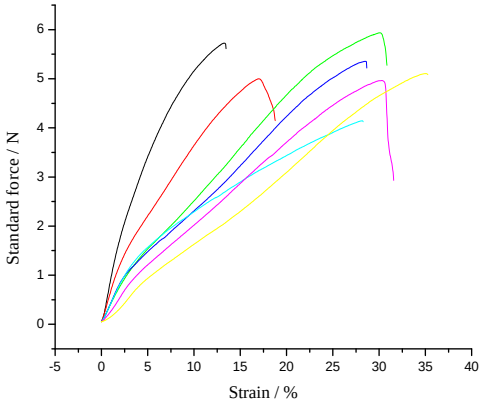

(C) Standard force vs. Strain curve for PVA samples coated in the sol-gel solution with 50% decrease in the amount of DTMS.

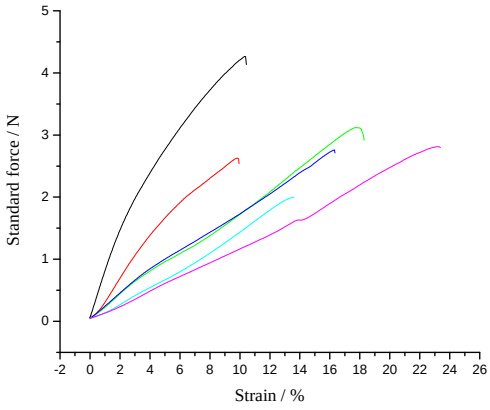

(D) Standard force vs. Strain curve for PVA samples coated in the sol-gel solution with 75% decrease in the amount of DTMS.

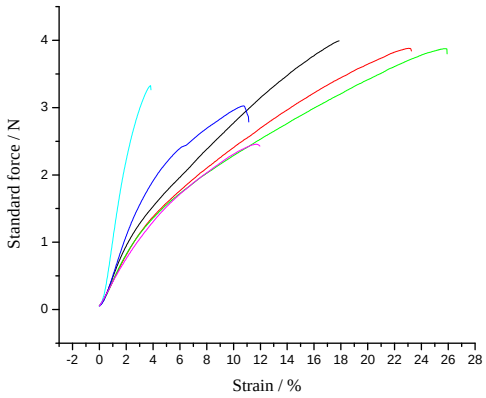

(E) Standard force vs. Strain curve for PVA samples coated in the sol-gel solution with 90% decrease in the amount of DTMS.

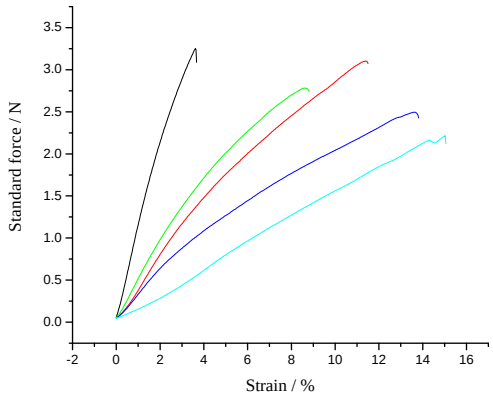

(F) Standard force vs. Strain curve for PVA samples coated in the sol-gel solution with 99% decrease in the amount of DTMS.

Figure 49(A)-(F). Mechanical strength of heated PVA samples after dip-coating in the sol-gel solutions for 2 min.

Table 12. Mechanical properties of heated 10 wt% PVA fiber mats coated with the different sol-gel solutions.

Percentage decrease in the amount of DTMS	F_{max} / N	Modulus / GPa	Elongation at break / %
-	5.19	0.052	72.7
25%	4.39	0.077	47.5
50%	5.18	0.125	26.7
75%	2.93	0.099	15.3
90%	3.43	0.121	15.7
99%	2.77	0.171	10.6

The tensile strength decreases as the concentration of DTMS is lowered in the sol-gel solutions. The elongation at break decreases from 72.7% to 10.6%. From the tensile strength measurements illustrated in **Table 12**, it is quite evident that the roughness of the dip-coated PVA mats increases as the concentration of DTMS decreases. This is the reason why the contact angles of the mats remain almost constant and do not show a rapid decrease even after 99% reduction in the amount of DTMS in the sol-gel solution. This can be attributed to the presence of the rough TEOS-derived surface since the amount of DTMS was lowered, but the TEOS concentration remained constant. In

addition, the excess of DTMS is far too high and leads to film formation between the fibers.

4.3.7. Sol-Gel coating on ceramic surfaces

One of the main applications of the sol-gel process is that it can be used to produce protective coatings on a substrate by spin-coating or dip-coating. Substrates like glass, metals or ceramics can be used for this application. With further drying or a subsequent heat treatment, novel properties can be introduced to glassy substances or ceramic materials.

An effort here was made to introduce some new properties like hydrophobicity, anti-fingerprint, anti-sticking or self-cleaning to ceramic materials by using the sol-gel method.

The sol-gel solution was prepared using TEOS and DTMS in the same molar composition:

$$TEOS:DTMS:ethanol:H_2O:HCl = 0.5:0.1:20:11:0.008$$

One-half of the ceramic material was then dip-coated with this sol-gel solution for 2 min followed by drying in air for 24 h. The other half was left uncoated. The wettability of both the uncoated and the coated parts was compared by measuring the contact angle.

The uncoated part of the ceramic surface showed high wettability as the water contact angle was found to be much below 90° **(Figure 50A)**. However, the coated part showed less wettability and the average contact angle was found to be 102° **(Figure 50B)**.

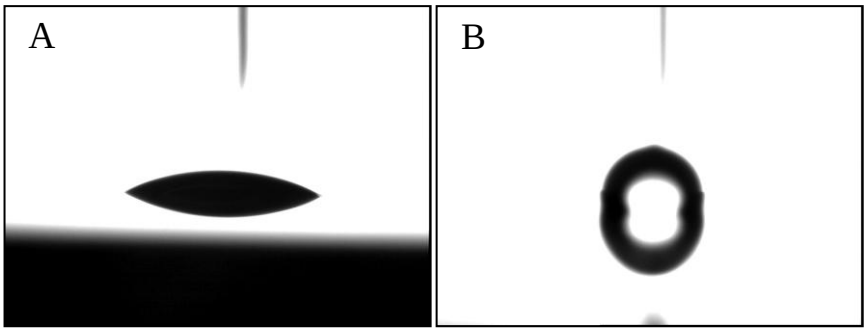

Figure 50. Contact angle measurement of (A) uncoated ceramic surface (B) sol-gel coated ceramic surface. The contact angle measured for the uncoated part was 29° and for the DTMS coated part was 102°.

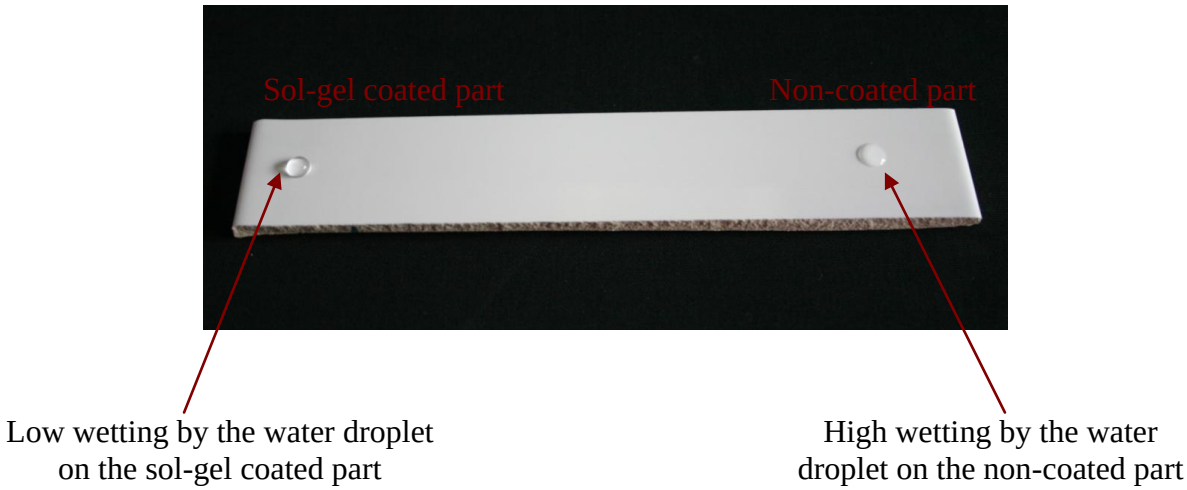

Figure 51. A ceramic surface showing low wetting on the sol-gel coated part and relatively high wetting on the non-coated part.

Figure 51 shows the difference in hydrophobicity on a ceramic surface half coated with the sol-gel solution. Sol-gel coating can also be used to protect the metal surfaces from oxidation, thermal and chemical corrosion and also to improve their strength. Hydrophobicity can be induced in such materials by increasing their surface roughness, which can be achieved either by anodic oxidation of the metal surfaces or by coating them with low-surface-energy materials like silicone based compounds.

4.4. Conclusion

Hydrophobicity was successfully induced in the water insoluble but hydrophilic fiber mats by dipping them into a sol-gel solution containing tetraethyl orthosilicate (TEOS) and n-decyltrimethoxysilane (DTMS) as the active chemicals for 2 min. The contact angle measured for the coated PVA fiber mats was found to be 144° showing low surface wetting. The fiber morphology of the PVA fibers was retained after heating as well as coating which was evident from the SEM images.

The pore size for the non-coated and the coated fiber mats was measured using the Capillary Flow Porometer. The largest pore size for the non-coated PVA mats was found to be 1.3 µm while that for the coated PVA fiber mats was 3.6 µm. This was attributed to the adhesion of the fibers after coating leading to increase in the pore diameter. As expected, the pressure required to blow open the largest pore in non-coated fiber mats was higher than the pressure required in the coated fiber mats owing to the smaller pore diameters in the non-coated samples.

Using silanes with different carbon chain lengths in the sol-gel solution, it was proved that the aliphatic groups in the silanes were responsible to bring about the hydrophobicity, as the contact angle increased with the increase in the carbon chain length.

The mats became super-hydrophobic, with a contact angle greater than 150° on coating with a sol-gel solution containing perfluorooctyltriethoxysilane as the organic functional group along with TEOS. Hence, the heated PVA fiber mats which showed perfect wetting with a contact angle of 0° were successfully converted into super-hydrophobic materials with a contact angle of 152°.

The influence of different molar compositions of the active chemicals was also studied and the hydrophobicity of the PVA fiber mat was measured. The contact angle of the PVA fiber mats dip-coated with the sol-gel solutions containing reduced amounts of DTMS was found to be quite similar. This was attributed to the fact that even though the DTMS concentration was changed in the sol-gel solution, the amount of TEOS remained constant and it was the rough TEOS-derived surface which contributed to the hydrophobicity. The mechanical properties of each of these fiber mats was measured

which showed a decrease in the tensile strength as the concentration of DTMS was lowered.

Moreover, the influence of a different metal precursor on the hydrophobic nature of the PVA mats was also studied. Bayresit VPLS 2331 was used as a metal precursor in place of TEOS in the sol-gel solution owing to its higher functionality and flexible ring structure. Bayresit along with DTMS in the sol-gel solution did not show a drastic change in the hydrophobicity of the heated PVA mats. Furthermore, Bayresit and DTMS sol-gel solution applied to a non-heated PVA mat showed large amount of shinkage thereby eliminating the chance of obtaining water-repelling PVA fiber mats without heating.

Sol-gel coating was also carried out on ceramic surfaces. The wettability of the surface decreased to a large extent after coating as proved by the contact angle measurements. Therefore, sol-gel coating was found to be an effective method to introduce novel properties into electrospinnable materials and ceramic surfaces.

5. Electrospinning of Poly(vinyl alcohol) and polyurethane dispersions in water to obtain crosslinked fiber mats

5.1. Introduction

Polyurethane (PU) dispersions in water are being extensively used in industries as coatings and adhesives. With increasing restrictions on the amount of volatile organic compounds that can be emitted into the atmosphere, PU dispersions are increasingly being used in many commercial applications and industries as an improved and more environmental-friendly solution.[108]

Polyurethane dispersions can be electrospun from water by using PVA as the template polymer. It can also be used to crosslink PVA.[109] It consists of a carbonyl group (from the diisocyanate) as the end group in a polymer chain. This carbonyl reacts with hydroxyl groups of PVA leading to crosslinking.

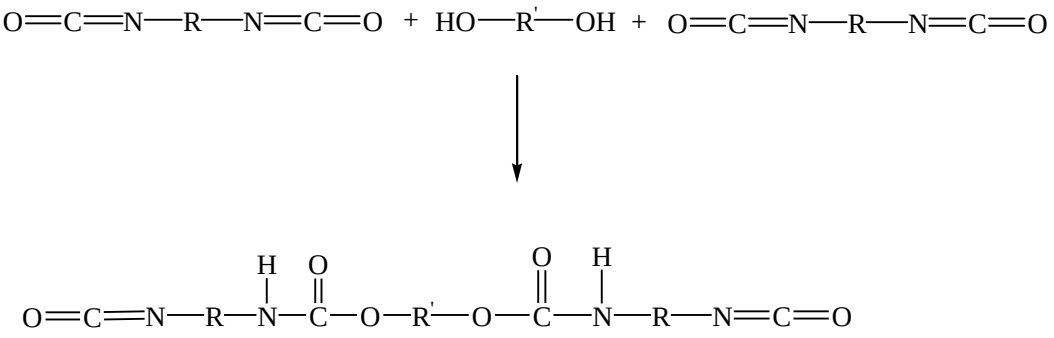

Figure 52. Polyurethane synthesis by reaction between a diisocyanate and a diol.

Polyurethane can be prepared though step-growth polymerization by reacting a monomer containing at least two isocyanate groups and another monomer containing at least two hydroxyl groups **(Figure 52)**. This means that the bifunctional monomers react to form first dimers, then trimers, then longer oligomers and finally long chain polymers. The reaction product is a polyurethane containing the urethane linkage (–NH-COO–). Polyurethanes are produced by a polyaddition reaction of a polyol with a polyisocyanate.

Unlike polycondensation, there is no elimination of a small molecule in a polyaddition reaction.

The diisocyanates used can be aromatic, like methylene diphenyl diisocyanate (MDI), toluene diisocyanate (TDI), or aliphatic, like hexamethylene diisocyanate (HDI), or isophorone diisocyanate (IPDI) as shown in **Figure 53**. However, the aromatic diisocyanates are preferred for the production of polyurethanes over the aliphatic ones. This is because the reactivity of the aromatic diisocyanates is higher than the aliphatic diisocyanates.

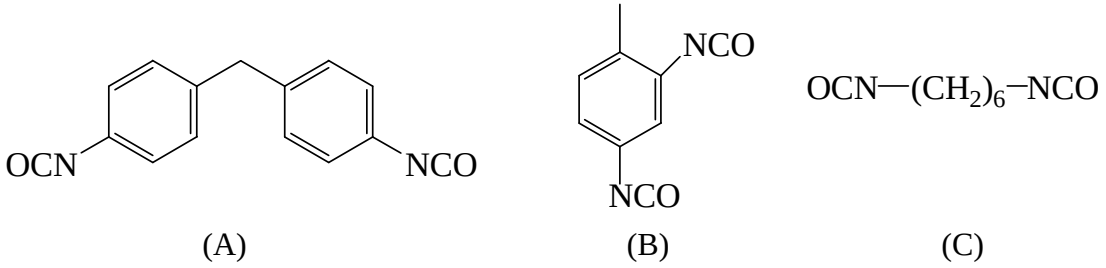

Figure 53. Chemical structures of (A) methylene diphenyl diisocyanate (MDI), (B) toluene diisocyanate (TDI), (C) hexamethylene diisocyanate (HDI).

The isocyanate groups are capable of reacting together and form polymeric isocyanates containing three or more isocyanate groups. An example of polymeric isocyanate is polymeric methylene diphenyl diisocyanate **(Figure 54)**.

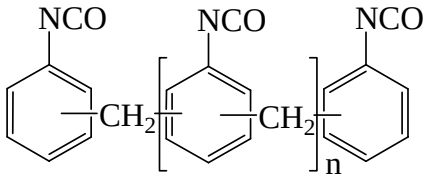

Figure 54. Chemical structure of polymeric methylene diphenyl diisocyanate (MDI).

The functional group reactivity and the number of functional isocyanate groups play an important role in determining the properties of the polyurethane. The functionality and the molecular shape determine the mechanical properties of the polyurethane. The stability of the polyurethane upon exposure to light depends on the choice of the

diisocyanate. Polyurethanes made from aromatic diisocyanates turn yellow on exposure to light, whereas those made from aliphatic diisocyanates are stable. This is because the aromatic diisocyanates contain chomophores which interact with light.

The diols used generally are ethylene glycol, 1,4-butanediol, diethylene glycol etc. The properties of the polyurethane are determined mainly by the choice of polyol. For example, when linear difunctional polyols like polyethylene glycols are used, they result in the formation of softer, more flexible and elastic polyurethanes. When polyfunctional polyols are used, they result in the formation of more rigid structures due to the formation of a three-dimensional crosslinked type of arrangement **(Figure 55)**.

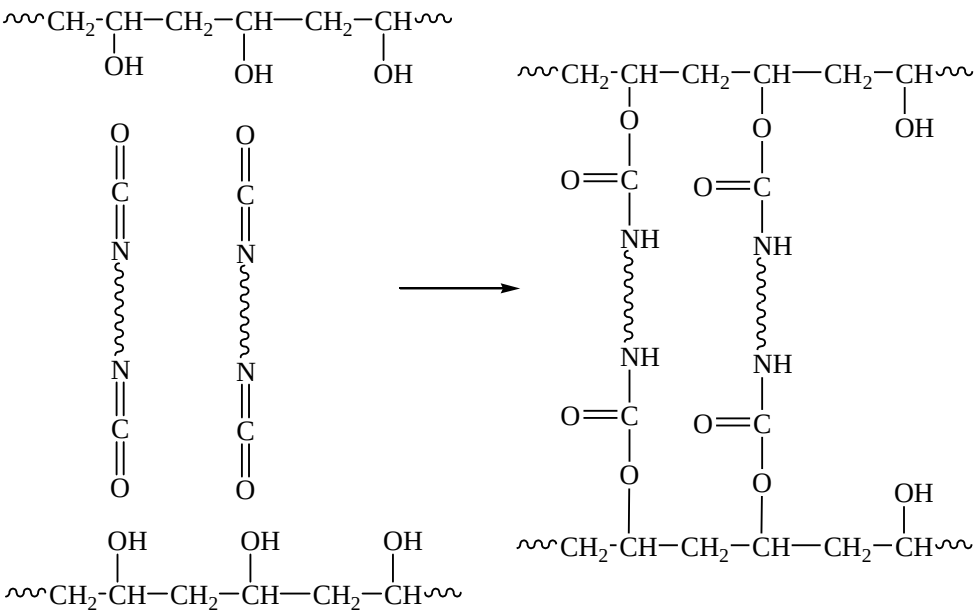

Figure 55. Crosslinking mechanism between poly(vinyl alcohol) and polyurethane.

5.2. Blocked diisocyanates

The isocyanate groups are highly sensitive. They react with water to form carbon dioxide and amine as shown in **Figure 56**.

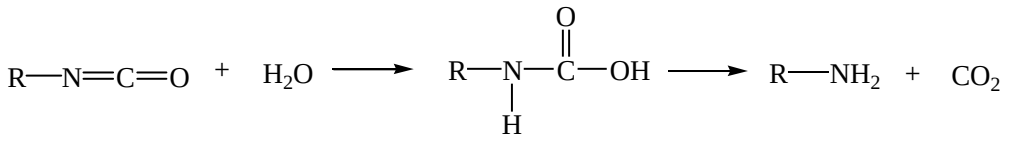

Figure 56. Reaction of isocyanate with water to form amine and carbon dioxide.

Water reacts with the isocyanate group to form carbamic acid which is highly unstable and decomposes to give carbon dioxide and an amine. Consequently, there arises a need for blocking the isocyanates. Moreover, when the isocyanate and the polyol are mixed together, they immediately begin to react with one another. Shelf life is generally very small. At room temperature these blocked isocyanates do not react with the polyol, thus providing longer shelf life.

A common type of a blocked isocyanate is one in which the isocyanate group is reacted with an active hydrogen compound or methylene compound such e-caprolactam, butanone oxime, phenol, or malonic ester. These blocked isocyanates when heated decompose to free the active isocyanate. Increasing temperature moves the equilibrium to the left, releasing isocyanate groups, which then react with active hydrogen species to generate urethane bonds **(Figure 57)**.

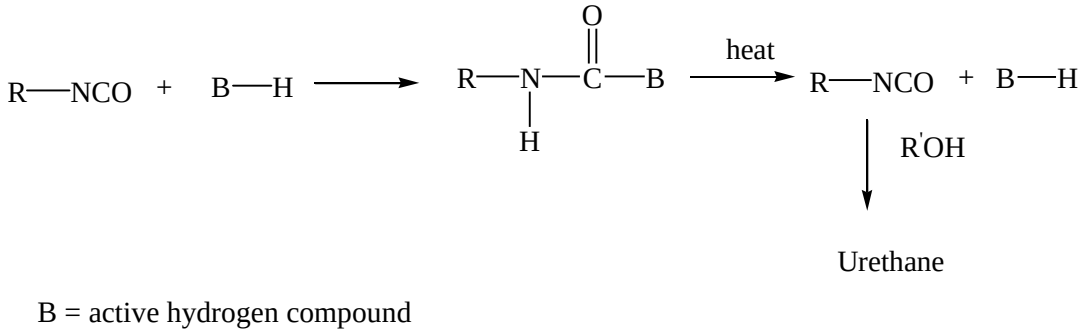

Figure 57. Reaction mechanism for a blocked isocyanate.

Common commercial blocking agents are methylethylketoxime, diethyl malonate, and 3,5-dimethylpyrazole.

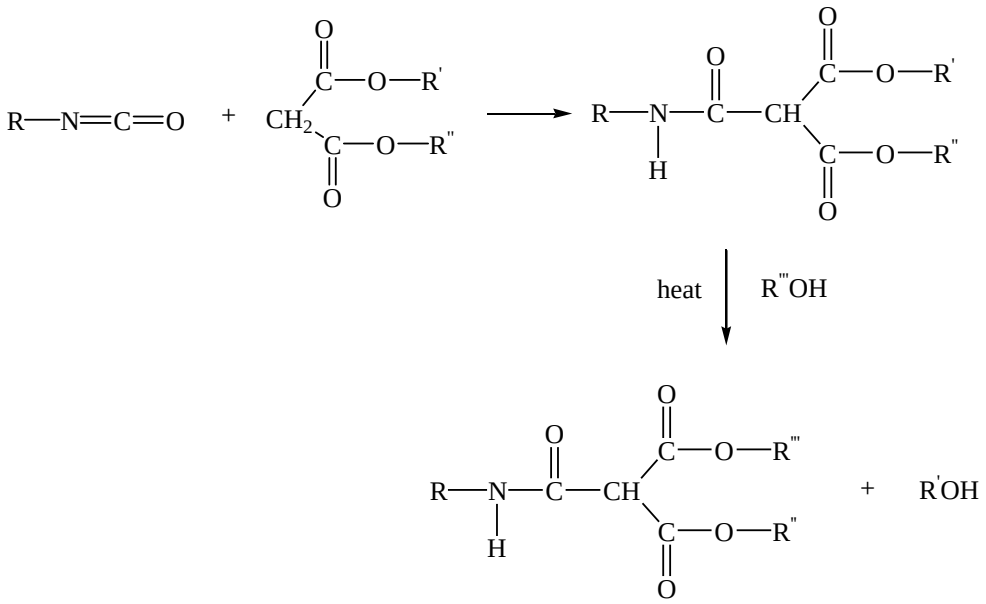

Figure 58. Transesterification reaction of a blocked isocyanate with a hydroxyl functional polyol to form an ester linkage in the malonate blocked isocyanate.

When these blocked isocyanates are heated in the presence of a hydroxyl functional polyol, two types of reactions can take place. Apart from the formation of a normal urethane linkage, transesterification can also take place like in the case of malonate blocked isocyanates **(Figure 58).**

Therefore by using a blocked isocyanate, moisture sensitivity is considerably reduced. Blocked urethanes do not react with residual moisture in solvents at ambient temperatures. Thus, isocyanate grade solvents can be used for prolonged storage periods. Blocked urethanes also reduce or eliminate the toxic hazard associated with the presence of isocyanates.

5.3. Results and discussion

5.3.1. PVA / polyurethane crosslinking

Polyurethane was prepared from a polyisocyanate and a polyol from the Bayer MaterialScience. The isocyanate used was Bayhydur XP 2655, a hydrophilic aliphatic polyisocyanate based on hexamethylene diisocyanate (HDI). The polyol was Bayhydrol A242, a polyacrylic resin containing hydroxyl groups. The PVA / PU fiber mat with an average diameter of 746 nm was obtained after electrospinning of the PVA / PU dispersion in water. The fiber morphology was characterized by scanning electron microscope.

The crosslinking between PVA and PU was carried out by heating the fiber mat in the oven at 60 °C for 2 h. To investigate the degree of the crosslinking reaction, the PVA / PU mat was treated with water at room temperature (20 °C) for different time intervals.

The weight change before and after water treatment was taken and the percentage weight loss was calculated using the following equation:

$$\text{Percentage weight loss} = [1 - (W_2 / W_1)] \quad 100$$

, where W_1 is the weight of the PVA / PU fiber mat before water treatment and W_2 is the weight of the PVA / PU fiber mat after water treatment.

The cured PVA / PU fiber mat was also dipped in water at higher temperature for different time intervals and the weight loss was calculated using the above equation and the results are summarized in **Table 13.**

Table 13. The percentage weight loss of PVA / PU fiber mat after treatment with water at different temperatures for different time intervals.

Temperature / °C	Time / h	Percentage weight loss / %
20	2	8
20	24	11
90	1	12
90	3	13
90	9	14

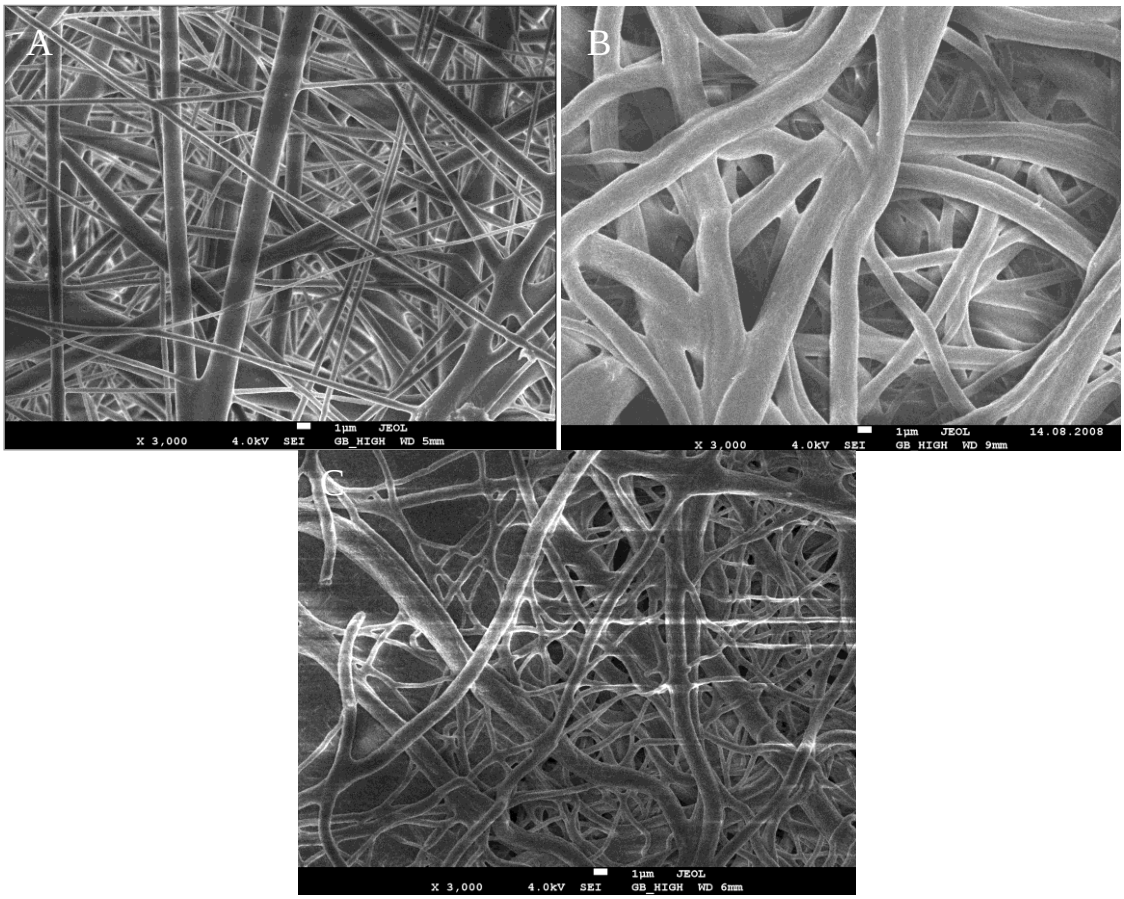

Figure 59. SEM Images of (A) PVA / PU fiber mat (B) PVA / PU fiber mat after water-treatment at 20 °C for 24 h (C) PVA / PU fiber mat after water-treatment at 90 °C for 3 h.

The fiber morphology of the water-treated fiber mats was analyzed using the scanning electron microscope and the fiber diameter was compared with the non-water-treated PVA / PU fiber mats. **Figure 59A** shows the SEM image of the PVA / PU fiber mat without any water-treatment. The average diameter of the fiber mats was found to be 700 nm. The SEM image of the water-treated fiber mats at room temperature for 24 h is shown in **Figure 59B**. The average diameter was calculated and was found to remain unchanged i.e.700 nm. The average diameter, analyzed from **Figure 59C**, of the PVA / PU fiber mats water-treated at 90 °C for 3 h was also found to remain unaffected i.e. 800 nm.

Therefore, by crosslinking PVA and PU, it was possible to obtain fiber mats stable in water both at room temperature and at high temperatures.

5.3.2. Mechanical properties

The change in the mechanical properties of PVA was compared with PVA fiber mats crosslinked with PU **(Figure 60)**. An average of at least five measurements for each sample was taken for final results.

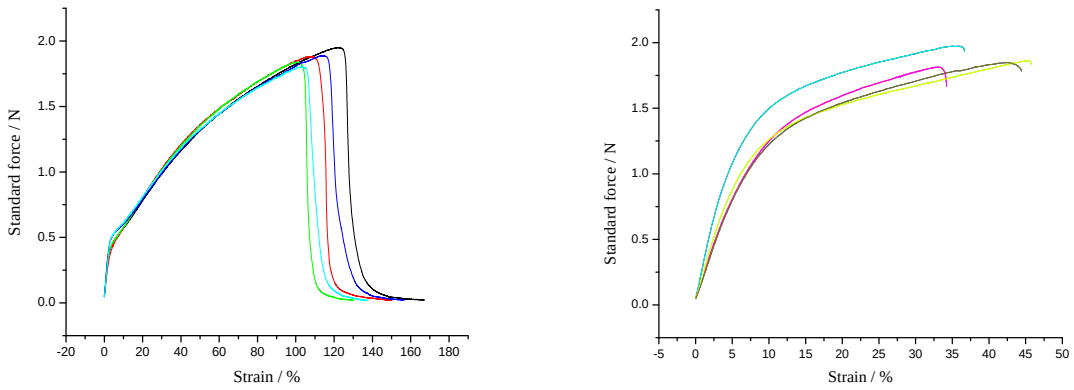

(A) Standard force vs. Strain curves for electrospun PVA fiber mats.

(B) Standard force vs. Strain curves for electrospun PVA / PU fiber mats.

Figure 60. Standard force vs. Strain curves for (A) PVA fiber mats and (B) PVA / PU fiber mats.

Table 14. Comparison of mechanical properties of PVA fiber mat, and PU crosslinked PVA fiber mat.

Sample	F_{max} / N	Modulus / GPa	Elongation at break / %
PVA fiber mat	1.87	0.193	148.3
PVA / PU fiber mat	1.80	0.139	40.3

As evident from **Table 14**, the tensile strength of the electrospun PVA fiber mat decreases after crosslinking with polyurethane. The elongation at break for PVA fiber mat is 148.3% which decreases to 40.3% in PVA / PU crosslinked fibers. This can be attributed to the decrease in the number of OH groups on crosslinking, which decreases the inter-molecular hydrogen bonding between the hydroxyl groups leading to reduction in the mechanical strength.

5.3.3. Pore size determination

The Pore sizes of the electrospun PVA / PU fiber mat were determined by using the Capillary Flow Porometer. The diameter of the pores was compared with those of the electrospun 10 wt% PVA fiber mats.

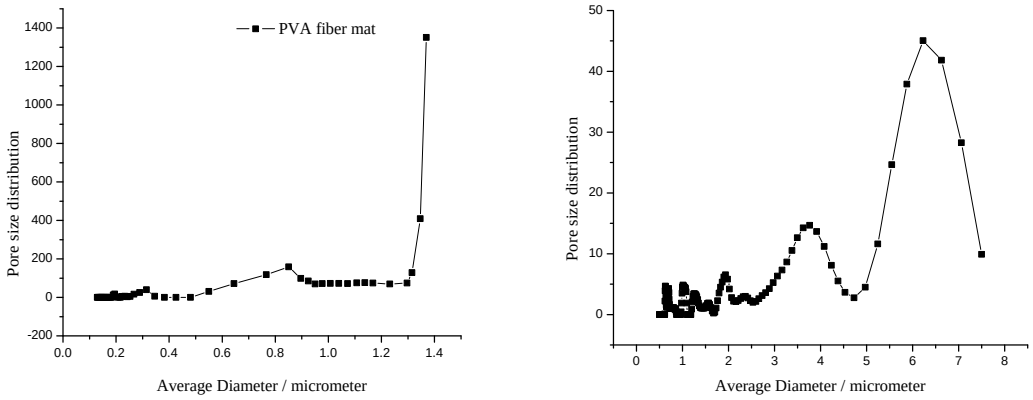

(A) (B)

Figure 61. Pore size distribution vs. average diameter curves for (A) 10 wt% PVA fiber mat and (B) PVA / PU fiber mats.

The bubble point (the maximum Pore size) for PVA fiber mats was found to be 1.3 µm (Bubble point pressure = 0.466 bar) while that for the PVA / PU fiber mats was 7.72 µm (Bubble point pressure = 0.082 bar). The Bubble point pressure is also comparatively lower owing to a larger bubble point diameter in case of PVA / PU crosslinked fiber mats. As seen from **Figure 61,** the pore diameters of the PVA / PU fiber mats are quite high as compared to the electrospun PVA fiber mats. This could be attributed to the shrinkage of the water swellable fibers after heating at 60°C for 2 h.

The second parameter measured experimentally was the Mean Flow Pore size (MFP) which is the micron size where 50% of the flow was higher and 50% of the flow was lower. The MFP for PVA fiber mats was found to be 1.05 µm while that for PVA / PU fiber mats was found to be 0.99 µm.

5.4. Conclusion

Crosslinking of PVA was brought about by reaction with PU, which was synthesized using a polyisocyanate and a polyol from the Bayer MaterialScience. The crosslinking was brought about by heating the obtained PVA / PU fiber mats at 60 °C for 2 h.

The percentage weight loss after water treatment for 24 h at room temperature was around 11% and in water at 90 °C for 9 h was around 14%. The fiber morphology and diameter remained unchanged after water treatment as evident from the SEM images. The tensile strength of the PVA / PU mats decreased in comparison to PVA mats, owing to reduction in the number of hydroxyl groups after crosslinking, thereby decreasing the inter-molecular hydrogen bonding. Furthermore, the pore diameters of PVA / PU mats were found to be higher than PVA fiber mats due to shrinkage of the fibers after heat treatment.

6. Microencapsulation of pheromone using biodegradable polymers for mating disruption of *Lobesia Botrana*

6.1. Introduction

Pheromones have been used extensively for controlling insect pests by disruption of communication without any side-effects. This disruption helps to prevent mating since the male inst is unable to locate the female inst leading to collapse of the mating cycle. However, this approach poses a problem in maintaining a high concentration of the pheromone in the field for a longer period of time say for weeks or even for months. To overcome this problem, two methods are being extensively employed. One is to place large dispensers filled with the pheromone at fixed points in the treatment areas. The other way is by microencapsulating the pheromone which is then directly applied to the crop by conventional methods.

For controlling the species, mating disruption techniques, as a kind of biotechnical plant protection, have been found to be most effective.[110] It is proven to be most useful when applied to large areas and when the populations of the grapevine moth are low. When the moth population is high, supplemental insticide applications might be needed. In the mating disruption technique, dispensers loaded with the synthetic pheromone are deployed thoughout the vineyard. This causes the air to be saturated with the pheromone, such that the male moths are unable to locate the female moths, thereby helping to prevent or delay mating. In the absence of mating or if the female moths are too old when mated, viable eggs are not laid and no larvae are produced to damage grape clusters.

Slow evaporation of the pheromone using evaporators or dispensers has been widely used, for example, for the cabbage looper, *Trichoplusia ni* [111, 112] and for the oriental fruit moth, *Grapholitha molsta* in Australia[113]. Similar experiments have been carried out in Switzerland on the plum fruit moth, *Grapholitha funebran.*[114] Different kinds of dispensers have been used for the slow release of pheromone from a trap, for example, filter papers [115, 116], sand, polythene vials or caps [117] and nylon mesh [111, 118].

Microencapsulation of the pheromone has been brought about by coacervation or interfacial polymerization techniques. The wall membranes in the case of pheromone

have been made of gelatin, polyurea, polyamide, or polyurea crosslinked with polyamide. The release rate of the pheromone in case of microencapsulation depends on the permeability of the polymer membrane. The sizes of the microcapsules prepared have ranged from 1-400 μm.[119]

Sustained release of a pheromone-analogue into the atmosphere has been successfully carried out by encapsulation using coacervation of a gelatin-gum arabic system.[120] Disruption experiments have also been carried out with microencapsulated anti-pheromones against *Adoxophyes Orana*, the summer fruit tortrix moth.[121]

Microencapsulation has also been carried out for the pheromone of the gypsy moth, *Porthetria dispar*.[122, 123] Moreover, use of the sex-pheromone by microencapsulation to disrupt mating by the American dog tick, *Dermacentor variabilis,* has also been successfully carried out.[124]

In this study, microcapsules loaded with the pheromone of the European Grapevine Moth, *Lobesia Botrana*, were prepared using a biodegradable polymer to ensure controlled release of the pheromone into the environment for mating disruption.

6.2. Motivation

Lobesia botrana, the European Grapevine Moth **(Figure 62)**, native to Southern Italy, was first described from Austria, and is now found thoughout Europe, North and West Africa, the Middle East, and Eastern Russia. It belongs to the family Tortricidae, sub-family Oletheutinae. In Europe, some of the common names are *Eudemis* (France), *Tignolleta della vite* (Italy), *Bekreuzter Traubenwickler* (Germany), *Polilla del racimo* (Spain).

Figure 62. The adult female European Grapevine Moth.[125]

It is the most damaging pest of grapevine in Europe, Asia and Africa. Up to four generations can occur thoughout the growing season. The first generation larvae web and feed on the flower clusters. The second generation larvae feed on the green berries. Young larvae penetrate the berry and hollow them out, leaving the skin and the seeds **(Figure 63).** Third generation larvae cause the greatest damage by webbing and feeding inside berries and within bunches.

Bacteria and fungi, especially grey mould *Botrytis cinerea*, develop rapidly on the grapes damaged by the larvae and deteriorate the entire grape bunches. Secondary pests such as raisin moth (*Cadra figulilella*), fruit flies, and ants may also be attracted to the damaged berries. The presence of larvae and rotten fruits lowers the quality of the crop, moulds render vine making difficult and may require the crop to be harvested prematurely.

Figure 63. European grapevine moth *(Lobesia Botrana)* caterpillar on a damaged grape.[126]

The pheromone of the European Grapevine Moth has been identified as (E,Z)-7,9-dodecadien-1-yl acetate **(Figure 64)** by Roelofs et al. (1973).[127] It has since been used as a bait to monitor traps for the pests in vineyards and for the direct control of the moth by mass trapping and mating disruption techniques.

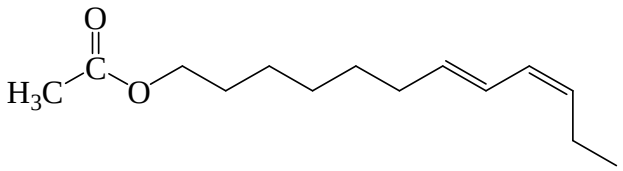

Figure 64. Chemical structure of the pheromone of the European Grapevine Moth, *Lobesia Botrana*.

6.3. Concept

A significant number of microencapsulation techniques were carried out for the confinement and controlled release of the sex-pheromone of the European Grapevine Moth from the microcapsules. Microcapsules loaded with the pheromone were prepared using different methods of microencapsulation like coacervation, emulsion/crosslinking method and solvent evaporation method. Production of microcapsules loaded nanofibers by electrospinning was intended in future. The presence of biodegradable polymer as the wall material of the microcapsules and water as the non-toxic solvent ensures that the method is completely environmental friendly.

6.4. Microencapsulation of pheromone by coacervation

Biodegradable microcapsules loaded with the pheromone of the European Grapevine Moth were prepared by using the coacervation method.[128] A crosslinked hydrophilic and biodegradable polymer, PVA was used as a protective wall material for confining the pheromone and for controlling the release rate of the pheromone through the wall.

In the coacervation method, as discussed earlier, deposition of colloidal polymer aggregates, formed by the separation of the homogeneous aqueous polymer solution, onto the dispersed liquid droplets results in the formation of microcapsules. The separation of the aqueous polymer solution can be brought about by the addition of a salt

which results in the formation of two phases, one rich and one poor in colloidal polymer aggregates.

PVA was used as the wall-forming material because of its ability to coacervate upon a change in temperature. Many inorganic compounds, especially salts, are also known to induce phase separation of aqueous PVA solutions. PVA crosslinked membrane has been extensively used for microencapsulation processes mostly in which a coacervation method is employed.[129] Owing to the swelling behaviour of the polymer network, PVA in its crosslinked form has also been used as drug-delivery device.[130, 131]

The rate of release of the active ingredient from the microcapsules depends mainly on the size of the microcapsules, concentration and the degree of crosslinking of the polymer. Therefore, the size of the microcapsules, the amount of pheromone encapsulated, and the morphology of the microcapsules was analyzed.

PVA with a weight average molecular weight (M_w = 16000 Da) and a degree of hydrolysis of 96% was used as the wall-forming material. Sodium sulfate was utilized as the coacervating agent. The pheromone (E7, Z9-dodecadienyl-1-acetate) was used as the liquid core material. An acidified (e.g. sulphuric acid, anhydrous methanol, acetic acid, 100%) glutaraldehyde solution was used for the crosslinking of PVA.

6.4.1. Phase separation of PVA

To bring about the phase separation of PVA aqueous solution, sodium sulfate was added as the phase separation inducer. The cloud point temperature of the solution i.e. the temperature at which a homogeneous solution separates into two phases was determined. At the cloud point temperature two separate phases are formed - a polymer rich phase and a polymer dilute phase.

The size and concentration of the colloidal polymer aggregates formed in the polymer-rich phase play an important role in determining the nature of the polymer wall that gets adsorbed onto the hydrophobic oil phase. Consequently, the concentration of PVA, the molecular weight and the degree of hydrolysis of PVA, the concentration of the electrolyte and the rate at which the temperature is increased are significant variables which affect the size and concentration of adsorbed colloidal polymer aggregates and, thus, the thickness and morphology of the polymer wall membrane.

Before starting the preparation of the microcapsules, it was important to determine the cloud point temperature of the PVA solution on addition of the electrolyte.

Table 15. Cloud point observations for determining the phase behaviour of the system PVA/sodium sulfate/water.

PVA : salt mass ratio	Cloud point temperature
1:2.5	25 °C
1:5	30 °C
1:6	35 °C

Table 15 shows the results of the phase separation experiments. The result of the addition of the electrolyte to the PVA aqueous solution shows that as the mass ratio of PVA to salt decreases, the cloud point temperature also decreases.

6.4.2. Microencapsulation procedure

Pheromone-loaded microcapsules were prepared by the coacervation method which consists of the following steps: (i) Dispersion of the oil phase (pheromone) into the PVA solution, (ii) addition of the phase separation inducer (sodium sulfate), (iii) crosslinking of the coacervated membrane with glutaraldehyde **(Figure 65)**.

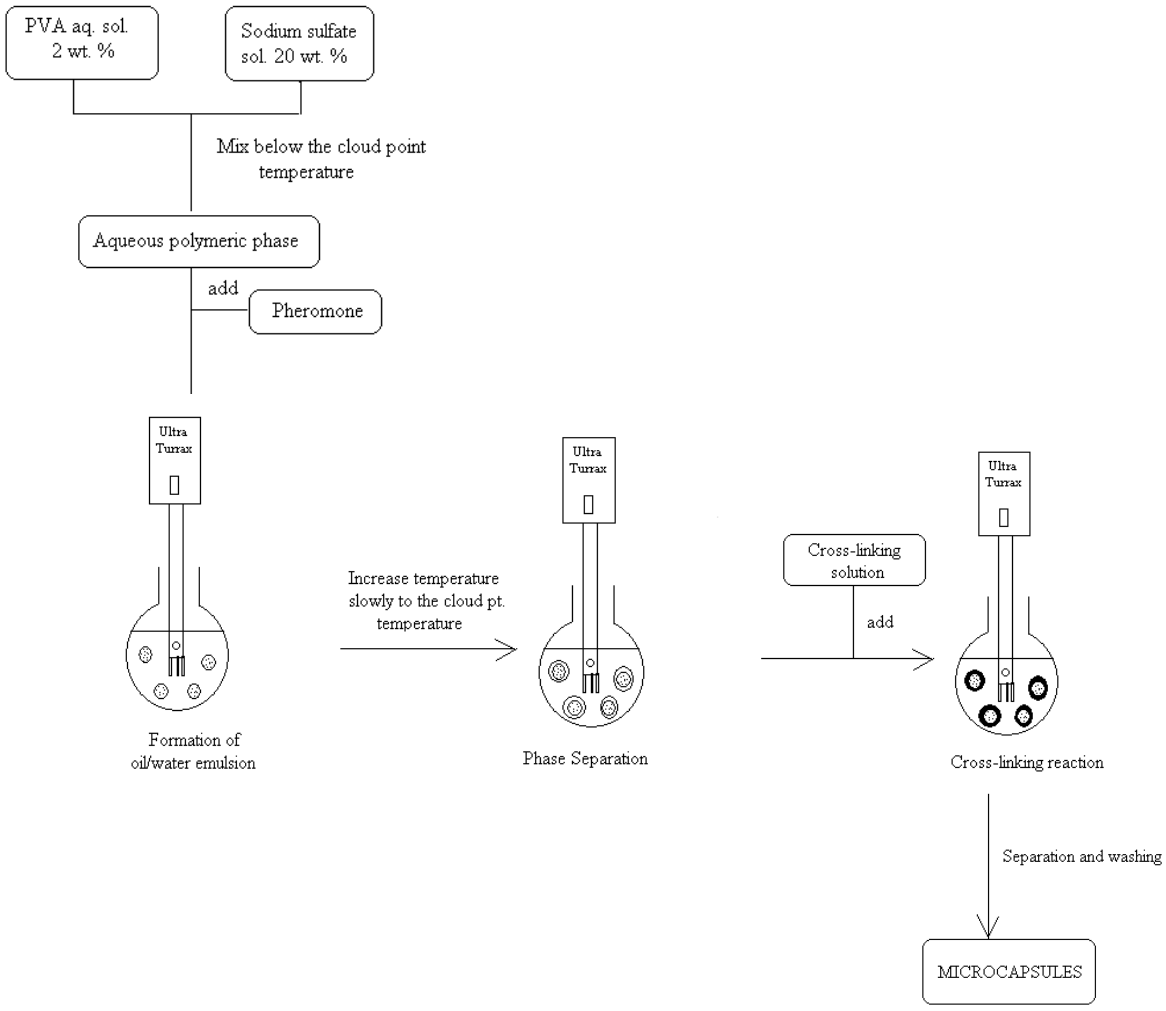

Figure 65. Schematic representation of the coacervation method for the preparation of PVA crosslinked microcapsules.

The particle size of the obtained microcapsules was analyzed using the scanning electron microscope as shown in **Figure 66**.

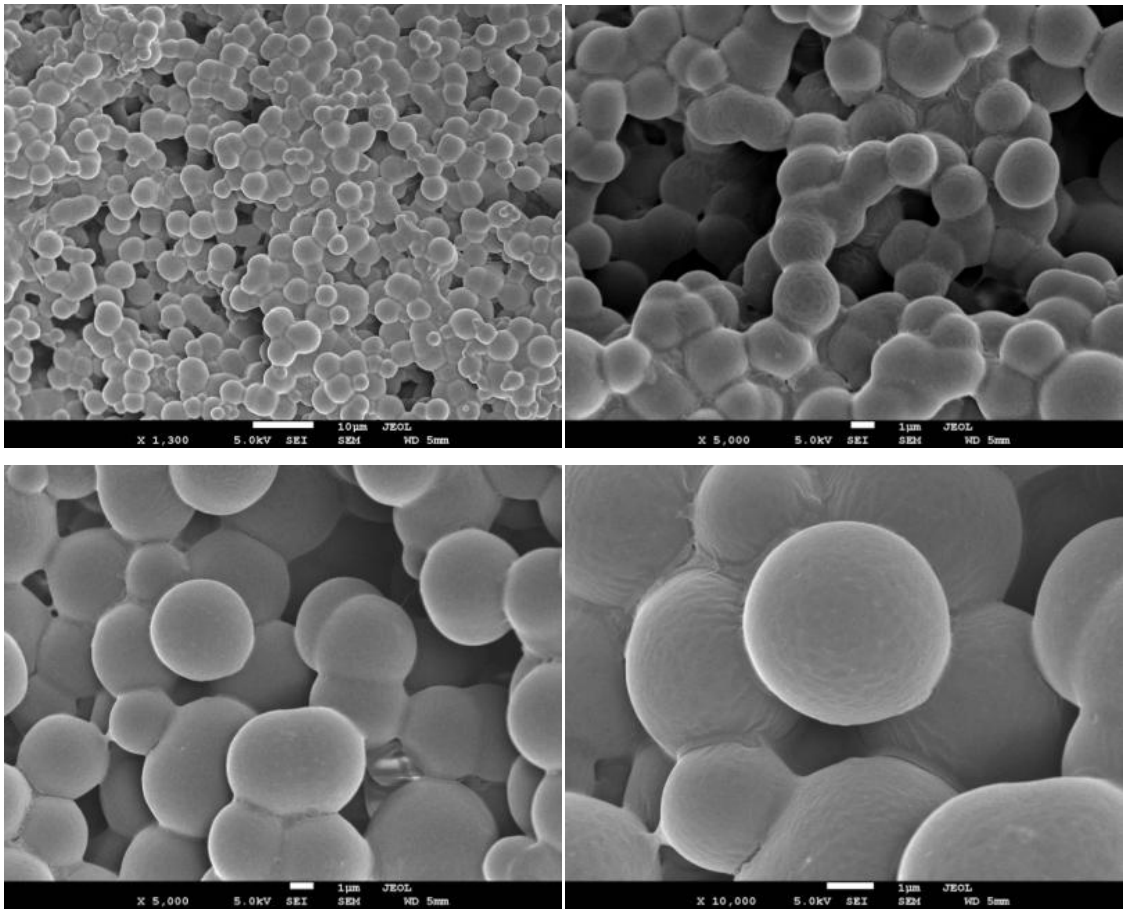

Figure 66. SEM images of pheromone-loaded PVA microcapsules prepared by the coacervation method. The average particle size was found to be 2-4 µm.

The average particle size of the microcapsules was found to be 2 - 4 µm calculated by using the software Image J.

6.4.3. Thermogravimetric analysis

Thermogravimetric analyser was used to determine the amount of pheromone encapsulated in the PVA microcapsules. For this, the TGA analysis of the pheromone was carried out from a temperature of 25 °C to 600 °C at a heating rate of 10 °C/min.

Subsequently, the thermal stability of the PVA microcapsules was analyzed and the amount of encapsulated pheromone was determined.

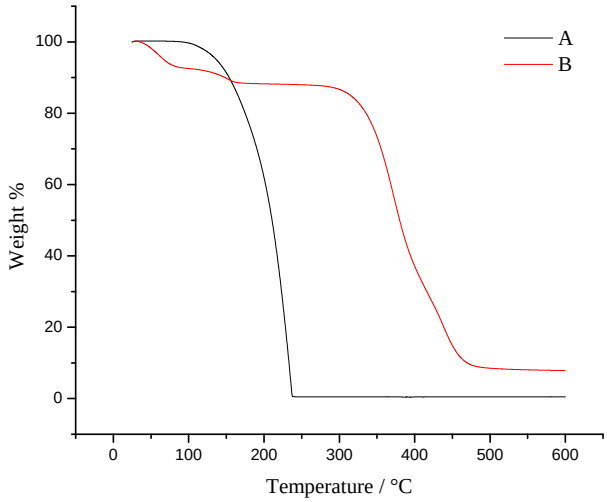

Figure 67. Thermogravimetric analysis (TGA) of (A) pheromone (B) pheromone encapsulated PVA microcapsules prepared by coacervation.

From the thermogram in **Figure 67,** it is evident that the first two degradation steps for PVA microcapsules correspond to the encapsulated pheromone and crosslinked PVA respectively. The pheromone degradation peak is at a temperature of 155 °C and crosslinked PVA shows a degradation peak at a temperature of 376 °C, which is higher as compared to non crosslinked PVA which shows degradation at a temperature of around 300 °C. This proves that crosslinking PVA with glutaraldehyde enhanced its stability. However, the amount of the pheromone encapsulated in the microcapsules was found to be even less than 10 wt%.

A model substance was used as the core material to analyze the effect of encapsulation by the coacervation method. Ethyl caprate **(Figure 68A)** having a chemical structure similar to that of the pheromone was used for this purpose.

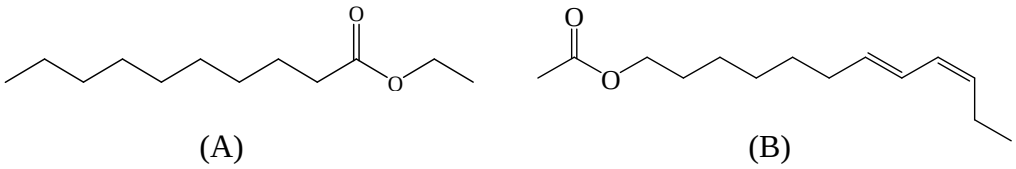

Figure 68. Chemical structures of (A) ethyl caprate (ethyl decanoate) and (B) pheromone (E7, Z9-dodecadien-1-yl acetate).

6.4.4. Microcapsule preparation using ethyl caprate as the core material

Ethyl caprate loaded PVA microcapsules were prepared using the same procedure. After drying, thermogravimetric analysis of the microcapsules was performed to determine the amount of ethyl caprate encapsulated from a temperature of 25 °C to 800 °C at a heating rate of 10 °C/min

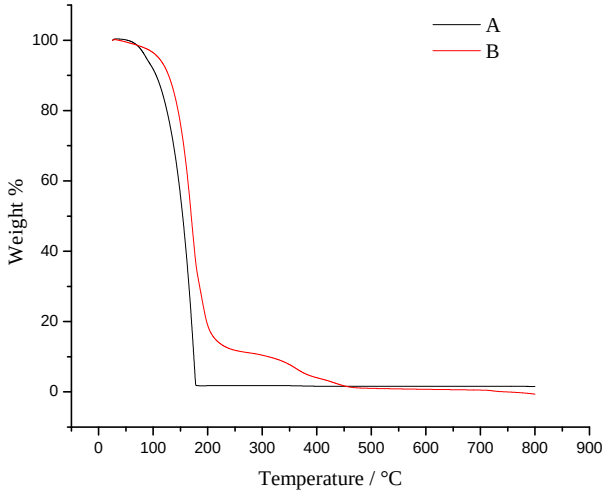

Figure 69. Thermogravimetric analysis (TGA) of (A) ethyl caprate (B) ethyl caprate loaded PVA microcapsules prepared by coacervation.

The TGA curve in **Figure 69** shows 2-step degradation for the PVA microcapsules. One at 170 °C corresponds to that of the encapsulated material, ethyl caprate and the other at 350 °C that of crosslinked poly(vinyl alcohol). In contrast to the amount of encapsulated pheromone, the amount of ethyl caprate encapsulated is more than 80 percent. Consequently, it can be said that the decyl group present in ethyl caprate makes it less

hydrophobic as compared to the pheromone which has a dodecyl group. Hence, ethyl caprate has a better affinity to poly(vinyl alcohol) in comparison to the pheromone.

6.5. Microencapsulation of pheromone by emulsion / crosslinking method

A slightly different method was tried to prepare PVA microcapsules containing pheromone as the core material since coacervation produced microcapsules containing lesser amount of pheromone than required.

A combined emulsion/polymer crosslinking technique was again used to prepare PVA microcapsules containing the pheromone, a lipophilic substance, as the core material.[90] However in this method, curing of the PVA wall was done using benzaldehyde, an oil-soluble aldehyde than glutaraldehyde used in the earlier process. In addition surfactants were used for the emulsification of pheromone in the PVA solution.

PVA with a weight average molecular weight, M_w = 61000 Da and degree of hydrolysis = 98% was used. Tween® 85 (polyethylene glycol sorbitan trioleate) was used as the surfactant. Pheromone was used as the core material. Benzaldehyde and conc. HCl were used for crosslinking of PVA wall.

The microcapsules prepared by emulsion / crosslinking method were analyzed under the digital microscope. The stability of the dispersion increased due to the addition of the surfactant as the particle size decreased. The dispersion prepared by the emulsion/crosslinking method is shown in **Figure 70**. The particle size distribution was found to be 2-10 µm.

Figure 70. Dispersion containing pheromone-loaded PVA microcapsules prepared by the emulsion/crosslinking method.

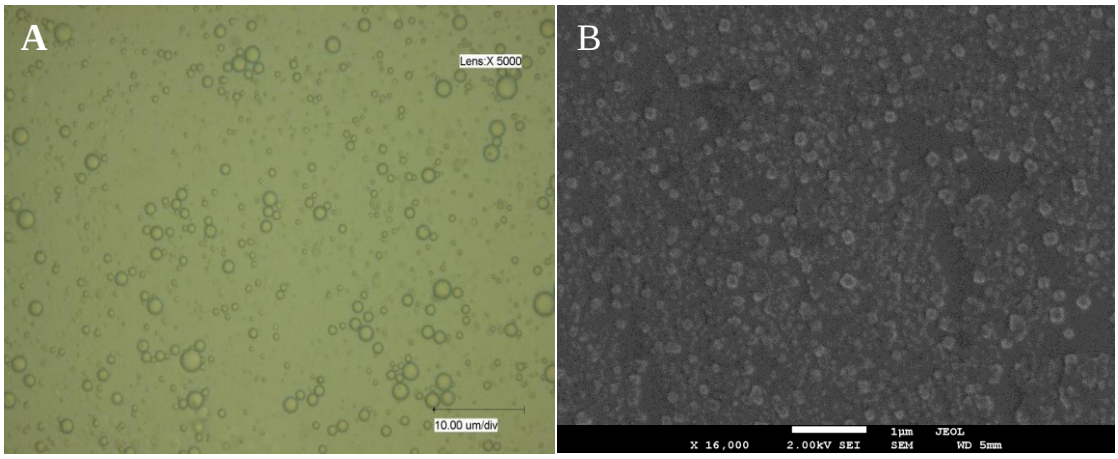

Figure 71. The image of PVA microcapsules obtained by the emulsion/crosslinking method as seen (A) under the digital microscope (B) by the scanning electron microscope (SEM).

The SEM image **(Figure 71B)** was unable to show the presence of microcapsules since they were found to be highly unstable under high vacuum used in the scanning electron microscopy.

Since benzaldehyde was used to crosslink PVA, two kinds of mechanisms took place: intermolecular acetalization and intramolecular acetalization. The presence of the benzal group was indicated by the IR spectrum.

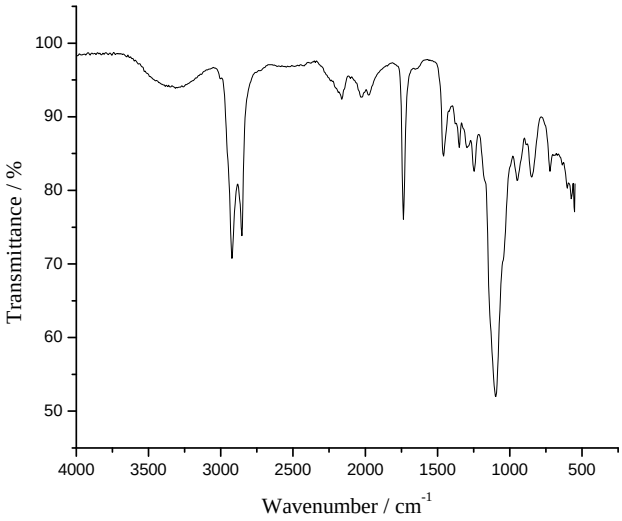

Figure 72. Infra-red spectrum of PVA microcapsules prepared by emulsion / crosslinking method.

The IR spectrum of PVA microcapsules **(Figure 72)** showed the following absorption bands: the O-H stretching at 3302 cm^{-1}, the C-O stretching at 1097 cm^{-1}. The acetate groups of PVA showed an absorption band at 1736 cm^{-1}, and the crosslinked PVA showed phenyl group absorption peak at 1454 cm^{-1}. No carbonyl stretch at 1700 cm^{-1} was seen which showed that all the carbonyl groups of benzaldehyde were utilized in acetal bond formation with the hydroxyl groups of PVA.

In order to have an insight into the amount of pheromone contained in the PVA microcapsules, thermogravimetric analysis of the prepared microcapsules was performed.

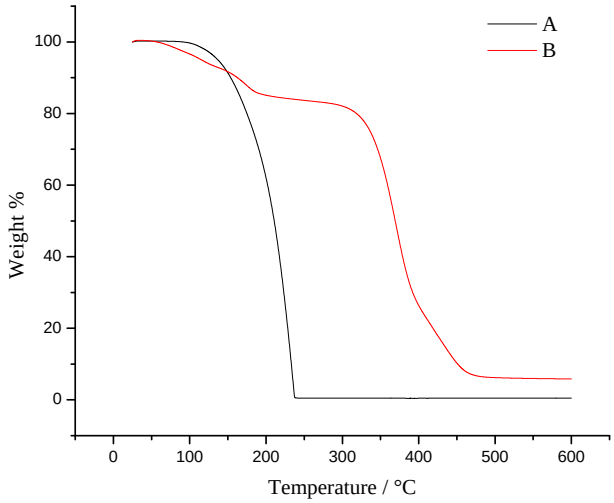

Figure 73. TGA of (A) pheromone (B) pheromone encapsulated PVA microcapsules prepared by the emulsion/crosslinking technique.

The TGA curve of the PVA microcapsules **(Figure 73)** from a temperature of 25 °C to 600 °C showed that the first degradation step at 170 °C corresponds to that of the pheromone and the second degradation step at 372 °C corresponds to that of crosslinked PVA. Again, as seen in the coacervation process, the amount of the pheromone encapsulated in the microcapsules was found to be less than 10 wt%.

The possible reasons for the low amount of the pheromone encapsulated in the PVA microcapsules could be: the presence of long chain dodecyl group in the pheromone decreases its affinity for PVA to a large extent.

In order to increase the affinity of the pheromone for PVA, two methods were applied. In the first method, a different grade of PVA with low degree of hydrolysis was chosen for carrying out the microencapsulation process. This meant that fewer hydrophilic hydroxyl groups were present and more number of hydrophobic acetate groups were present in PVA. This would increase the hydrophobicity of PVA to some extent.

The microencapsulation process was repeated with this PVA (M_w = 14000 Da and degree of hydrolysis = 85%) keeping all other reaction conditions same. The microcapsules obtained by this method were again analyzed by TGA immediately after drying from a temperature of 25 °C to 600 °C at a heating rate of 10 °C/min.

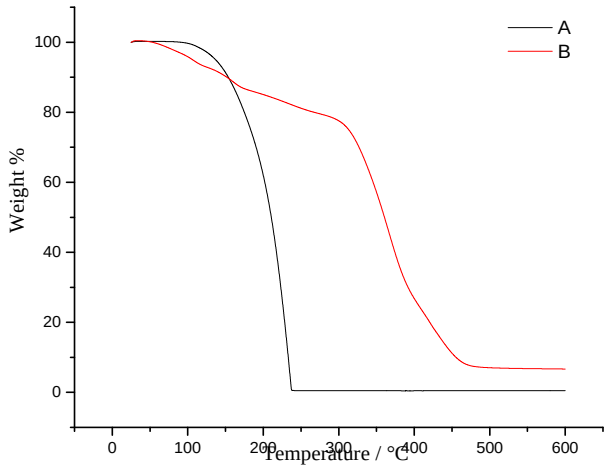

Figure 74. TGA of (A) pheromone and (B) pheromone-loaded PVA microcapsules using PVA with low degree of hydrolysis.

The TGA curve **(Figure 74)** of the microcapsules prepared by using PVA with low degree of hydrolysis showed that there was no change in the amount of pheromone encapsulated inside the microcapsules. The TGA thermogram showed similar degradation steps as in **Figure 73** i.e. for the pheromone at 169 °C and for crosslinked PVA at 367 °C. The amount of encapsulated pheromone was also found to be the same – less than 10 wt%.

After the failure of the first method, the second method applied for increasing the affinity between PVA and the pheromone was the use of 1-decanol **(Figure 75)** as a solvent for dissolving the pheromone in the microencapsulation process.

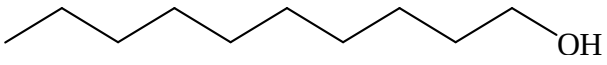

Figure 75. Chemical structure of 1-decanol used as a solvent for dissolution of pheromone to improve its affinity for PVA.

PVA microcapsules were prepared by dissolving pheromone in 1-decanol which contains hydroxyl groups that might increase the affinity for PVA. The obtained microcapsules were again analyzed by thermogravimetric analysis to determine the amount of encapsulated pheromone. The TGA was performed from a temperature of 25 °C to 600 °C at a heating rate of 10 °C/min.

The thermogravimetric analysis (Figure 62) of the prepared microcapsules, however, did not show much change in the amount of encapsulated pheromone as evident from **Figure 76**.

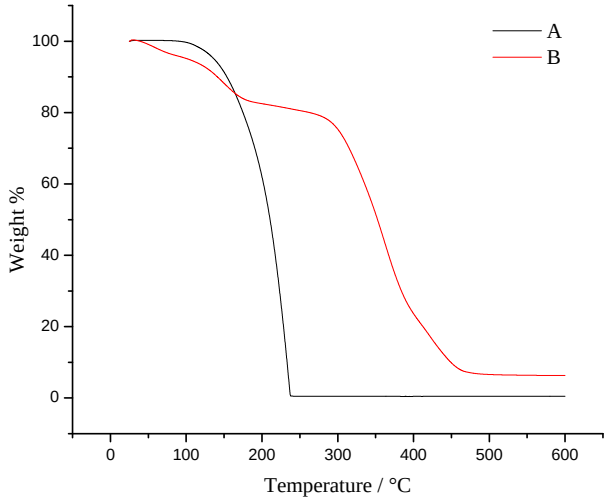

Figure 76. TGA of (A) pheromone and (B) pheromone-loaded PVA microcapsules with pheromone dissolved in 1–decanol.

Therefore none of the methods above succeeded in encapsulating sufficient amount of pheromone inside the PVA microcapsules.

The second reason for reduced quantity of encapsulated pheromone could be that the microparticles obtained were not actually microcapsules but microspheres. This would

mean that the pheromone was not present in the form of a core material surrounded by a polymeric membrane, but instead it was dispersed in the polymer matrix or absorbed at the surface. This was proved by using Cryo SEM.

Cryo SEM is a low temperature scanning electron microscopy technique. In this, aqueous dispersion was rapidly cooled by plunging it into liquid nitrogen. The sample was then fractured to obtain a cross-sectional view.

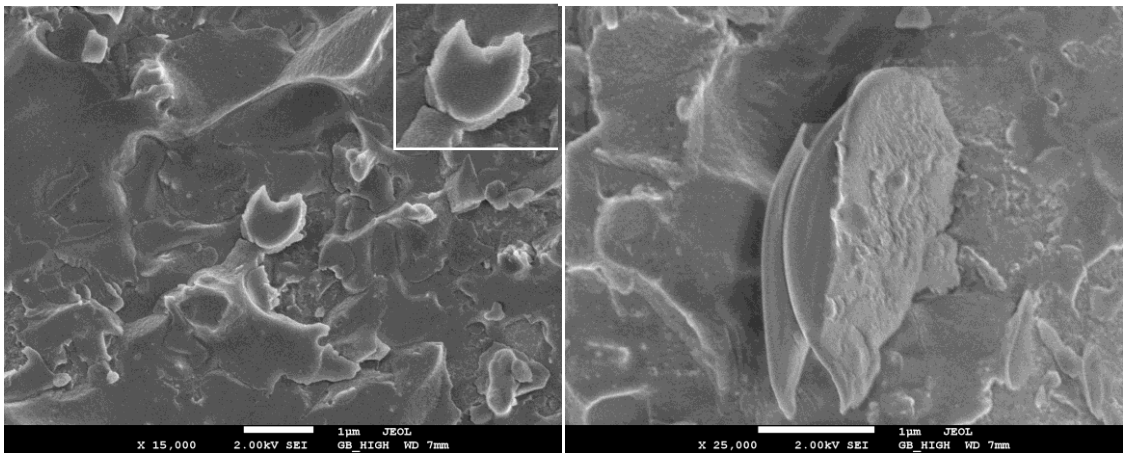

Figure 77. Cryo SEM image of PVA microcapsules obtained by the emulsion/crosslinking method.

From the Cryo SEM image **(Figure 77)**, the microparticles prepared by the emulsion/crosslinking method were found to be microspheres rather than microcapsules. This was sighted as the reason for insufficient amount of pheromone present inside.

Hence, the limitation of this method was that it resulted in the formation of microspheres rather than microcapsules. In addition, the pheromone present inside the microcapsules leached out very fast on drying. This showed that the crosslinking of the polymer wall was not strong enough. This was attributed to the fact that in the reaction between PVA and benzaldehyde, it's the intramolecular acetalization that predominates over the intermolecular acetalization owing to the formation of a stable 6-membered ring structure. Hence, crosslinking between the polymer chains is not hundred percent.
Crosslinking of the microcapsule walls was also carried out by using water-soluble glutaraldehyde (25 wt%) but it resulted in the formation of gel instead of microcapsules.

In this case, the crosslinking of PVA was accomplished by diffusion of the aldehyde from water.

6.6. Microencapsulation of pheromone by solvent evaporation method

Another biodegradable polymer, Polylactide (PLA), was used to encapsulate the pheromone using the solvent evaporation method.[132] PLA, owing to its biodegradable behaviour has been widely used in the microencapsulation processes in agricultural, pharmaceutical fields.

PLA, being a lipophilic polymer, completely eliminates the need for curing of the polymer wall.

6.6.1. Microencapsulation process

The microencapsulation of the pheromone was brought about by oil/water-emulsion solvent evaporation method. The particles obtained were observed under the digital microscope and the SEM **(Figure 78)**.

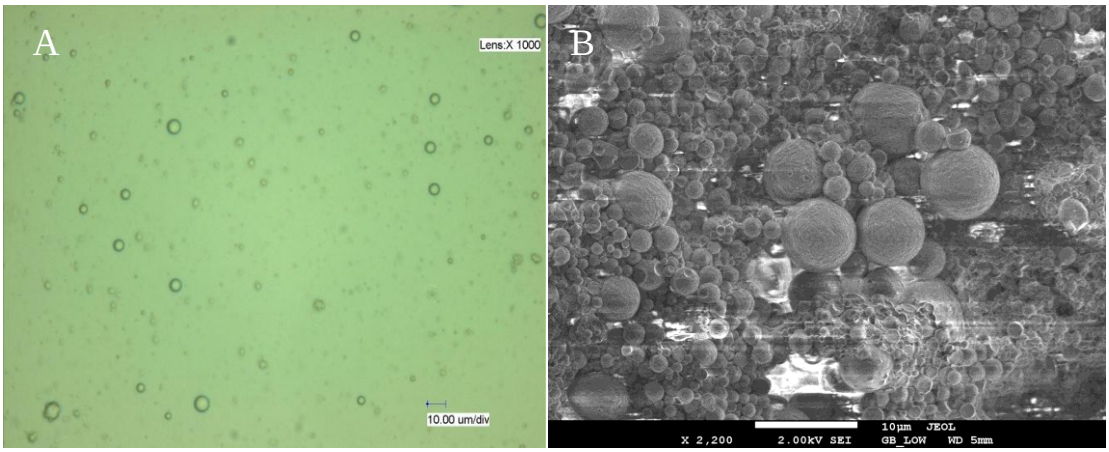

Figure 78. Pheromone containing PLA microcapsules as seen under (A) the digital microscope and (B) the scanning electron microscope.

The particle size distribution varied from 0.5 to 10 µm and the average particle size was 2-3 µm. The microencapsulation process was repeated with different mass ratios of pheromone with respect to PLA for example 1:2, 1:3 and 1:5.

To investigate the amount of encapsulated pheromone, thermogravimetric analysis of the PLA microparticles was carried out. The temperature of heating was from 25°C to 600 °C at a rate of 10 °C/min.

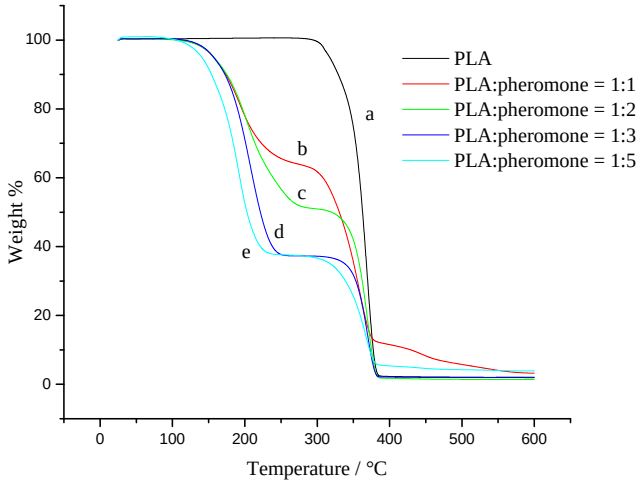

Figure 79. Thermogravimetric analysis (TGA) of (a) PLA, and PLA microparticles containing pheromone in different mass ratios, (b) 1:1 (c) 1:2 (d) 1:3 (e) 1:5.

The thermogram of the PLA microparticles, as shown in **Figure 79,** clearly indicated 2 degradation steps: one corresponding to that of pheromone and the other corresponding to PLA. Furthermore, the peak for pheromone degradation increased with the increase in the amount of pheromone with respect to PLA. The amount of encapsulated pheromone increases from 40% in the case of PLA:pheromone = 1:1 to 60% in the case of PLA:pheromone = 1:5. The maximum amount of the encapsulated pheromone was found to be around 60% as evident from the TGA curves for PLA:pheromone = 1:3 and 1:5.

After establishing the presence of pheromone in the PLA microparticles, it was important to analyze whether the microparticles were microspheres or microcapsules. This was carried out by using Cryo SEM for which PLA microparticles without the addition of pheromone were prepared using the same procedure.The images are shown in **Figure 80.**

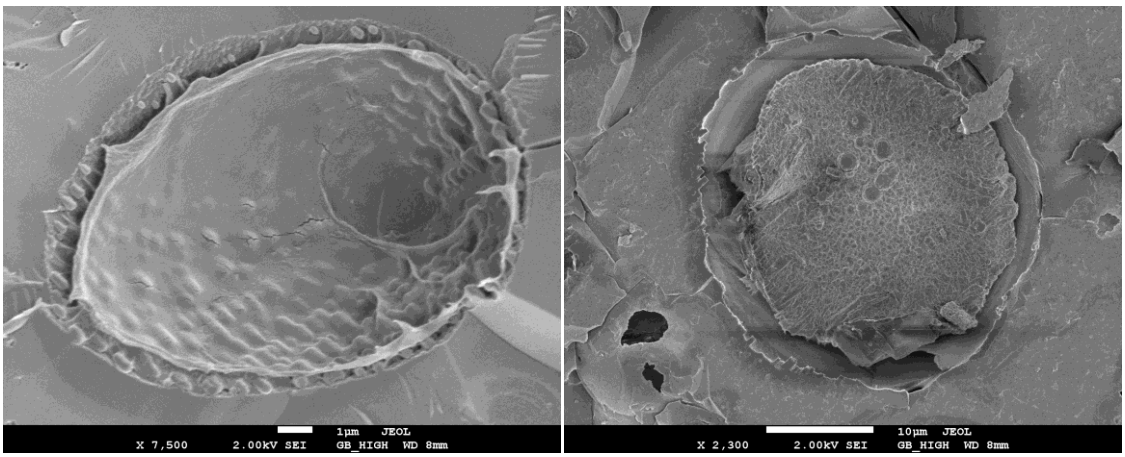

Figure 80. Cryo SEM images of PLA microcapsules prepared by solvent displacement method.

As calculated above, the particle size distribution of these microparticles varied from 1 to 10 µm. This shows that the Cryo SEM images shown above must correspond to that of the microparticles. The obtained images rule out the possibility of the formation of microspheres since they confirm the presence of hollow structures. Thus, the solvent evaporation method led to the formation of PLA microcapsules and not microspheres.

Furthermore, a release study of the encapsulated pheromone in the PLA microcapsules was analyzed by comparing the release rate of free pheromone with the encapsulated pheromone at room temperature using isothermal TGA.

Pheromone containing PLA microcapsules were prepared using the solvent evaporation method in which the mass ratio between PLA and pheromone was 1:3. The microcapsules were analyzed by isothermal TGA at a temperature of 30 °C for 14 h in air. The rate of evaporation of the encapsulated pheromone was studied with time. Similarly, the isothermal TGA of free pheromone was carried out at the same temperature for the same time period in air and the rate of evaporation was compared with that of the encapsulated pheromone.

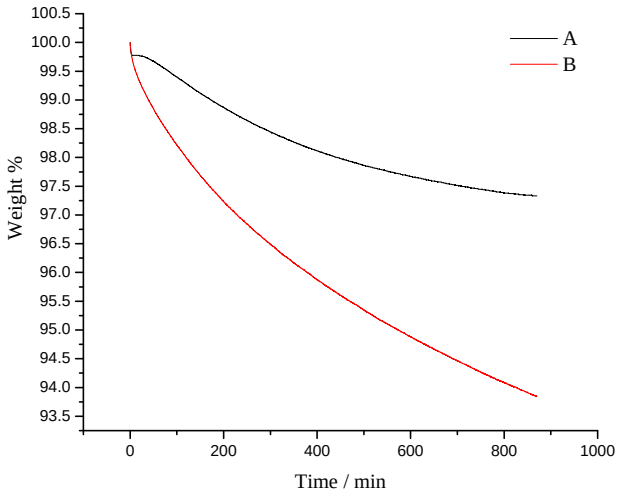

Figure 81. Comparison of release rate of (A) encapsulated pheromone in PLA microcapsules and (B) free pheromone by isothermal TGA at 30 °C for 14 h.

The isothermal TGA curves of the encapsulated pheromone and the free pheromone is shown in **Figure 81.** The release rate for both was found to be non linear. For the encapsulated pheromone, the release rate was calculated to be 0.3 wt% per hour from 100–200 min and 0.13 wt% per hour from 400–600 min. On the other hand, the release rate for the free pheromone was calculated to be 0.6 wt% per hour from 100–200 min and 0.3 wt% per hour from 400–600 min. This clearly indicates that the release rate for the free pheromone was much faster as compared to the release rate of the encapsulated pheromone for both the time intervals.

6.7. Conclusion

The preparation of pheromone-loaded biodegradable microcapsules was carried out using three methods. The first method was coacervation in which PVA was used as the wall material and glutaraldehyde, a water soluble aldehyde, was used to crosslink the polymer wall. The average particle diameter was calculated as 2 to 4 µm. However, only a little amount of the pheromone could be encapsulated inside the microcapsules. The use of a model substance, ethyl caprate in place of the pheromone increased the amount of encapsulation to more than 70% which was confirmed by thermogravimetric analysis. This showed that pheromone having a dodecyl aliphatic chain proved to be more

hydrophobic in terms of affinity to PVA as compared to ethyl caprate with a shorter aliphatic chain.

The second method, which was quite similar to coacervation, distinguished only in the use of tween® 85 as an emulsifier and benzaldehyde, an oil soluble aldehyde, as a crosslinker of the polymer wall. The particle size distribution was found to be 2-10 μm. However, the thermogravimetric analysis again proved the presence of very little amount of pheromone inside the microcapsules. To improve the quantity of encapsulated pheromone, two modifications were tried. In one, PVA with low degree of hydrolysis was used, which could increase the hydrophobicity of PVA and thus the affinity to the pheromone. And in the second, the pheromone was dissolved in 1-decanol, a solvent containing hydroxyl groups. However, none of the methods above succeeded in increasing the amount of encapsulated pheromone. Finally, using cryo SEM it was established that the microparticles prepared via this emulsion/polymer crosslinking method were found to be microspheres and not microcapsules. This meant that the pheromone was not present as a core material but was dispersed inside the polymer matrix or was absorbed at the surface.

Pheromone-loaded PLA microcapsules were successfully prepared using emulsion-evaporation method. The maximum quantity of the pheromone encapsulated was found to be 60 wt% as proved by thermogravimetric analysis. The presence of microcapsules was shown by cryo SEM which confirmed the existence of hollow structures. The average particle size of the microcapsules was calculated to be 2 to 3 μm. Through isothermal TGA it was established that the release rate of the pheromone contained in the PLA microcapsules was much slower compared to the release rate of free pheromone. The electrospinning of these pheromone-loaded biodegradable PLA microcapsules from water, a non-toxic solvent, can be a step further in the field of green electrospinning.

7. Preparation and electrospinning of stable secondary dispersions using miniemulsion

7.1. Aim and motivation

After the successful preparation of dispersions of water-insoluble biodegradable polyesters in water with additives like pheromone for electrospinning, polyesters with sufficient hydrophilicity were prepared to generate good secondary aqueous dispersions.
The need for processing of biodegradable polyesters by "green electrospinning" from water to yield water stable polyester nanofibers requires the development of a high solid content polyester dispersion in water where the glass transition point of the polyester is relatively low. The concept was to prepare polyesters which are well dispersible in water with low glass transition temperature. Nanofibers consisting of spherical polyester particles with low glass transition would result in blending of the particles and thereby mechanical stabilization of the nanofibers.[133] Low molecular weight polyesters i.e. oligolactides (OLA) could serve as a good matrix for the encapsulation of pheromones, with a relative large molar fraction of hydrophilic alkoxy and carboxy end groups to generate good secondary dispersions in water.
High content secondary dispersions of OLA, for their use for an all-water-based preparation of biodegradable polyester coatings and nanofiber nonwovens filled with a functional additive, the pheromone, for biotechnical plant protection against *Lobesia botrana*, the grape vine moth was realized.

7.2. Concept

Miniemulsions are well known to yield stable polymer dispersions.[57] Until now, the concept of miniemulsions has only been applied to prepare stable dispersions in which small, homogeneous and stable droplets of monomers are initially generated and then polymer reactions take place to transform them into polymer latexes. Crucial is the use of a hydrophobe additive in the monomer/tenside mixture to prevent Ostwald ripening of the monomer droplets.

We hypothyzed that in secondary dispersions hydrophobe additives like the pheromone used here, could significantly stabilize the dispersions of a polymer like OLA in water. Hence, the concept of miniemulsions was applied to prepare stable dispersions containing the pheromone as the hydrophobe.

Oligolactide (OLA) with low glass transition was prepared by conventional polycondensation of lactic acid. High solid content secondary dispersions containing OLA/pheromone were prepared and were processed into water stable polyester nanofibers by electrospinning. OLA was dissolved in acetone and mixed with Brij® S20 and (E,Z)-7,9-dodecadien-l-yl acetate, the pheromone of *Lobesia botrana,* the grape vine moth.

7.3. Results and discussion

7.3.1. Synthesis of the oligolactide

Oligolactide (OLA) was prepared by polycondensation of D,L-lactic acid for 16 h. The temperature was increased from 100 °C to 200 °C stepwise and water was removed simultaneously by vacuum distillation **(Figure 82)**.

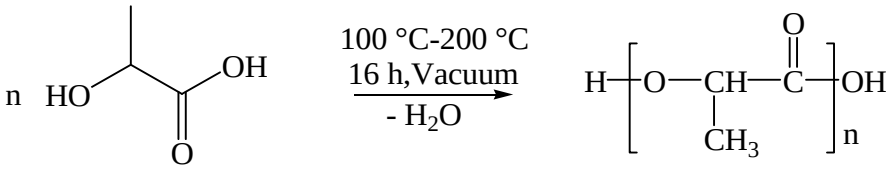

Figure 82. Polycondensation of D,L-lactic acid to form oligolactide.

The expected chemical structure of the OLA was confirmed by ^{1}H-NMR, ^{13}C-NMR, and APCI.

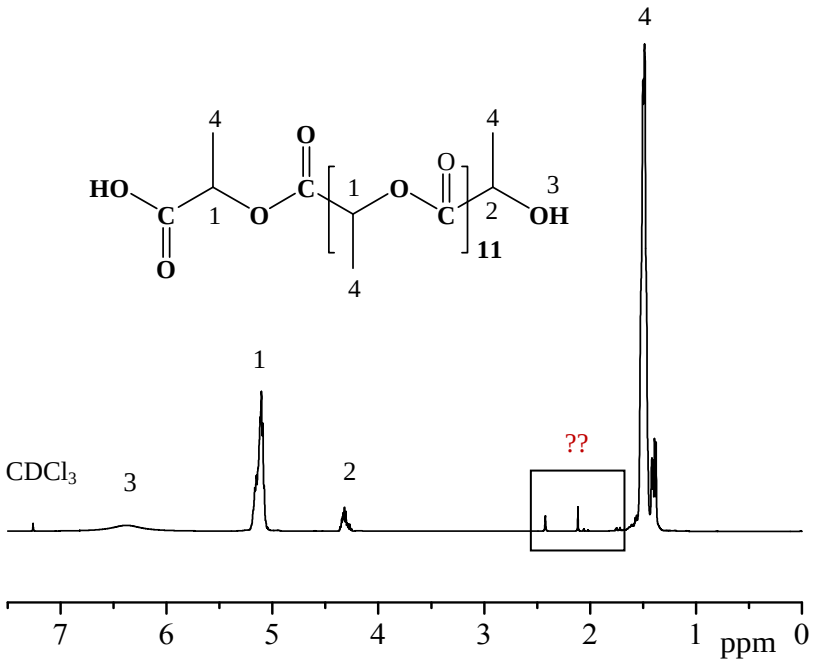

Figure 83. ^{1}H-NMR-Spectrum (400 MHz, $CDCl_3$) of the oligolactide prepared by polycondensation of D,L-lactic acid for 16 h.

The oligolactide formed was characterized by ^{1}H-NMR spectroscopy. The NMR spectrum **(Figure 83)** showed the presence of all the characteristic peaks. The peaks at δ = 2.1 ppm and δ = 2.4 ppm belonged to the side products resulting from overheating of lactic acid. Comparison of integrals of the –CH protons at δ = 5 ppm and the –CH protons at δ = 4.2 ppm gave a ratio of 12:1 which implied that there were 13 repeating units in the oligolactide which amounted to M_n ~ 954 Da.

Since the molecular weight calculated by ^{1}H-NMR spectroscopy was below 1000 Da, it was difficult to analyze the oligolactide by normal GPC. The oligomer THF GPC did not show any peak due to the presence of hydroxyl and carboxyl groups as the end groups which made the oligolactide highly polar, thereby decreasing the solubility in THF.

The molecular weight distribution of the oligolactide was determined by using Atmospheric Pressure Chemical Ionization (APCI) mass spectroscopic technique. It is a form of chemical ionization that takes place at atmospheric pressure. The APCI spectra were taken in both positive and negative ion modes. The negative ion APCI mode is a

good technique to detect the presence of an acidic group capable of losing a proton easily.

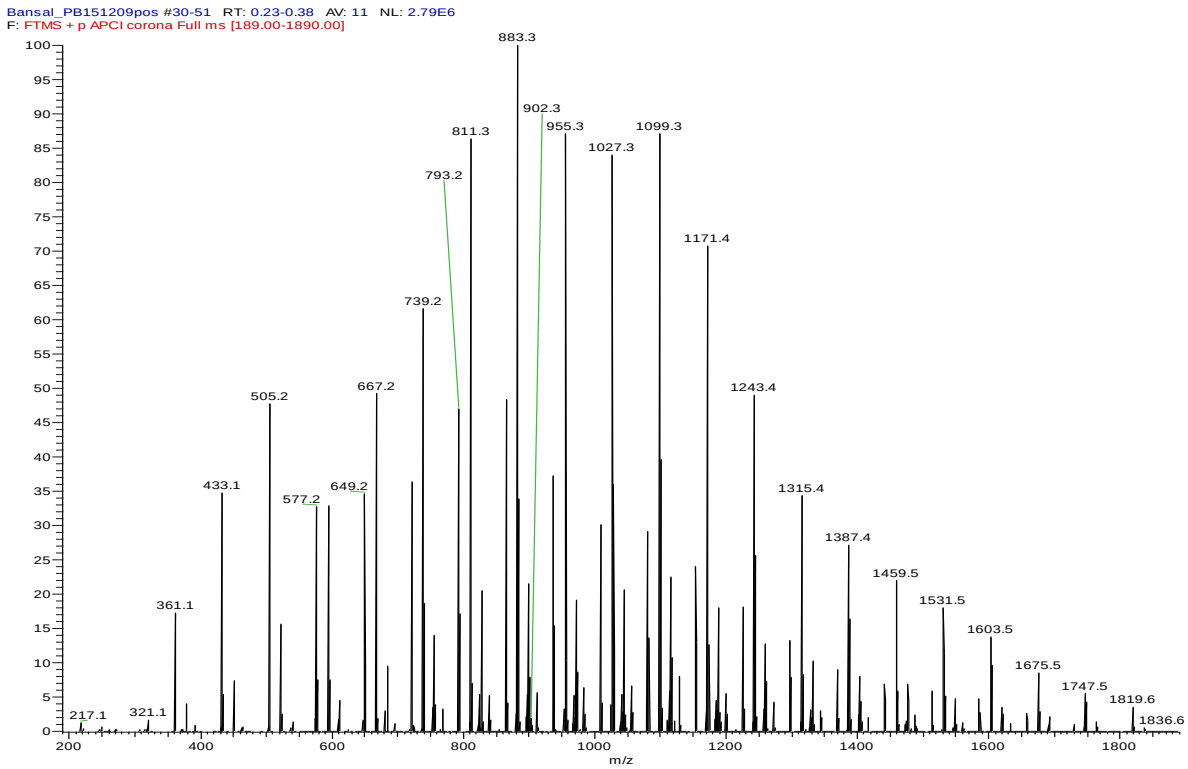

Figure 84. Positive mode APCI Mass Spectrum of the oligolactide.

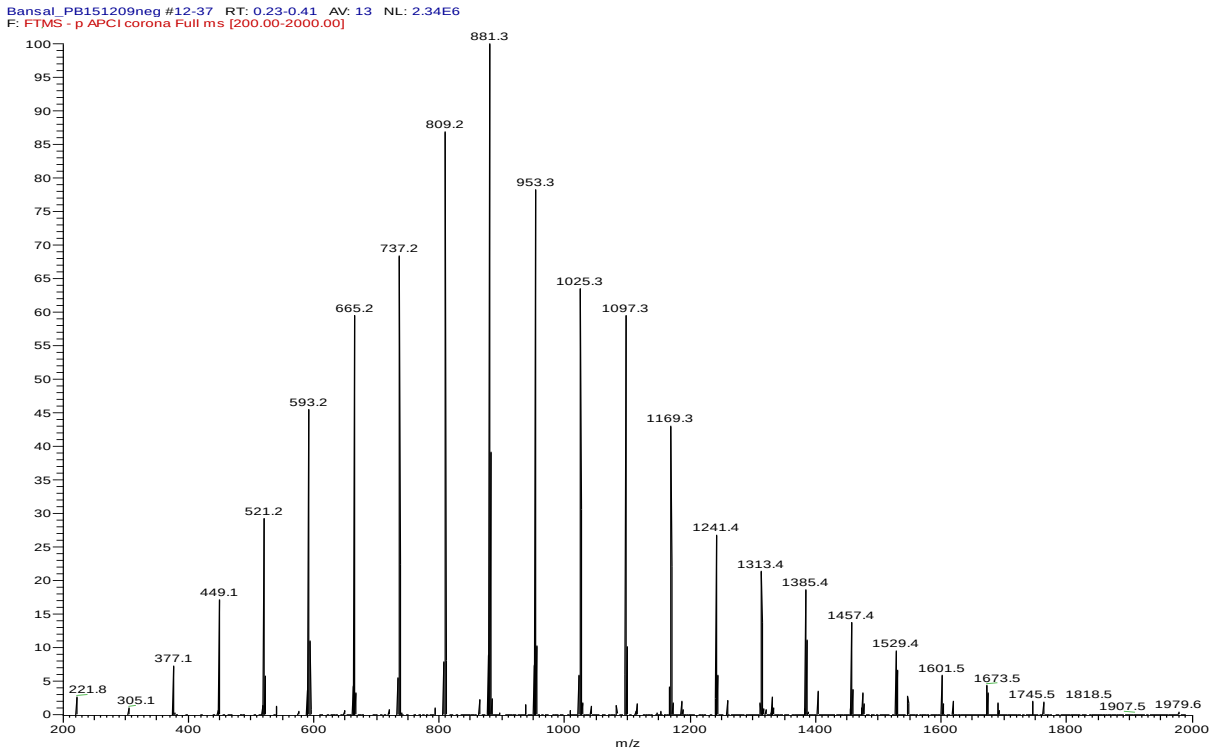

Figure 85. Negative mode APCI Mass Spectrum of the oligolactide.

The APCI mass spectrum in the positive mode **(Figure 84)** showed the presence of two different kinds of peaks, one for the open-chain OLA and the other for cyclic OLA. The difference between any two adjacent peaks is 18 units which corresponded to water. Thus, the peak at m/z = 649 corresponded to the cyclic OLA while the peak at m/z = 667 corresponded to the open-chain OLA. However, the intensity of the peaks of cyclic OLA was found to be higher than the open-chain OLA only in the region of low m/z values. As the m/z value increased, the intensity of the open-chain OLA also increased. Therefore, cyclic lactides were formed during polycondensation as side products, but were found to be more predominant in the low molecular weight region. With increasing molecular weight, open-chain OLA became more predominant.

The APCI mass spectrum in the negative mode **(Figure 85)** confirms the presence of carboxylic group as the end group. On comparing the positive and negative modes, there is a decrease of 2 units in the m/z values, for example the peak at m/z = 883 in the positive ion mode ($[M+H]^+$) and m/z = 881 in the negative ion mode ($[M-H]^-$). This

confirms that a proton can be removed with a lot of ease from the OLA which is likely only due to the presence of an acidic group.

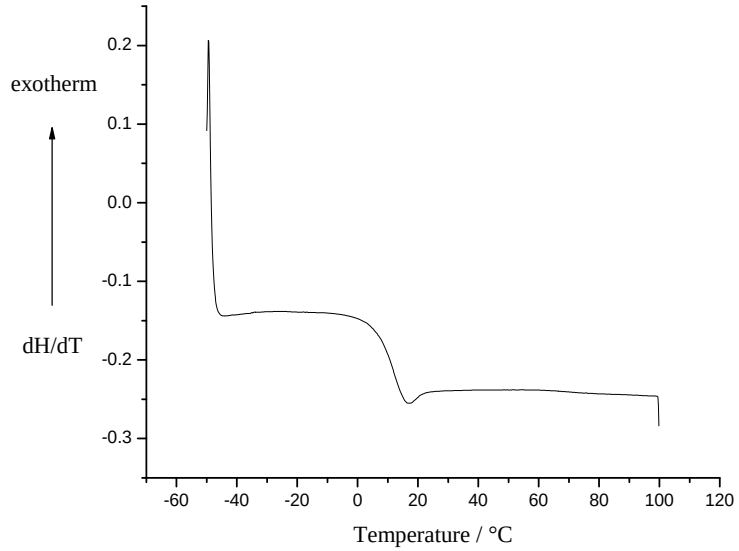

Figure 86. DSC thermogram of the OLA prepared by polycondensation of D,L-lactic acid.

The Differential Calorimetric (DSC) analysis of the OLA was performed from a temperature of -50 to 100 °C at a heating rate of 10 °C / min. The second heating cycle was considered for the determination of the glass transition temperature which was found to be between 12-15 °C as shown in **Figure 86**.

7.3.2. Synthesis of OLA dispersion

OLA dispersion with high solid content (10 wt%) was prepared by the solvent displacement method with pheromone acting as the hydrophobe to stabilize the dispersion.

In another experiment, the OLA was dissolved in acetone. After addition of a solution of water and Brij® S20, ultrasound was applied. Finally, acetone was removed by slow evaporation under mild air stream at 20 °C. Following this procedure, precipitation of OLA occurred with pheromone as an oily residue on the water surface **(Figure 87A).** The dispersion of OLA and Brij® S20 together with pheromone resulted in stable milky dispersions without any visible agglomeration and segregation of pheromone on the water surface **(Figure 87B).** Particle sizes of the dispersion were measured using oil

immersion microscopy and the average diameter was found to be typically in the range of 1-2 μm.

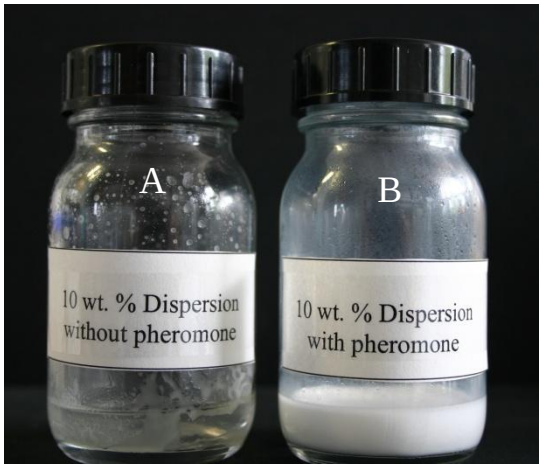

Figure 87. Photos of (A) unstable 10 wt% OLA dispersion without pheromone and (B) a stable aqueous dispersion by solvent displacement method of 10 wt% OLA, 10 wt% pheromone, and 1wt% Brij® S20 after ultrasonification and removal of acetone.

Moreover, the effect of hydrophilicity of OLA in the preparation of stable secondary dispersions was investigated by preparing a 10 wt% aqueous dispersion containing pheromone/Brij® S20 without the addition of OLA**.** The image in **Figure 88,** which was taken two days after the preparation of the dispersion shows that the dispersion was highly unstable.

Figure 88. Unstable 10 wt% dispersion without OLA.

Furthermore, the formation of microparticles was confirmed by analyzing the dispersion under the fluorescence microscope in normal light and UV-light for a 1 wt% OLA dispersion containing the pheromone dissolved in a fluorescent dye, Coumarin 6 **(Figure 89)**.

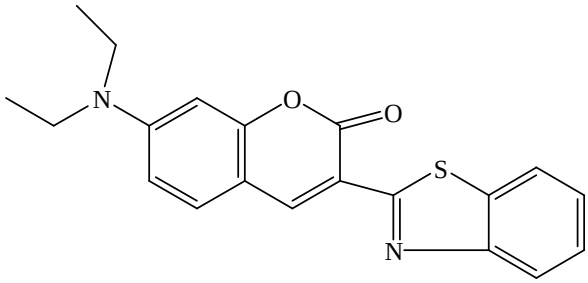

Figure 89. Chemical structure of Coumarin-6.

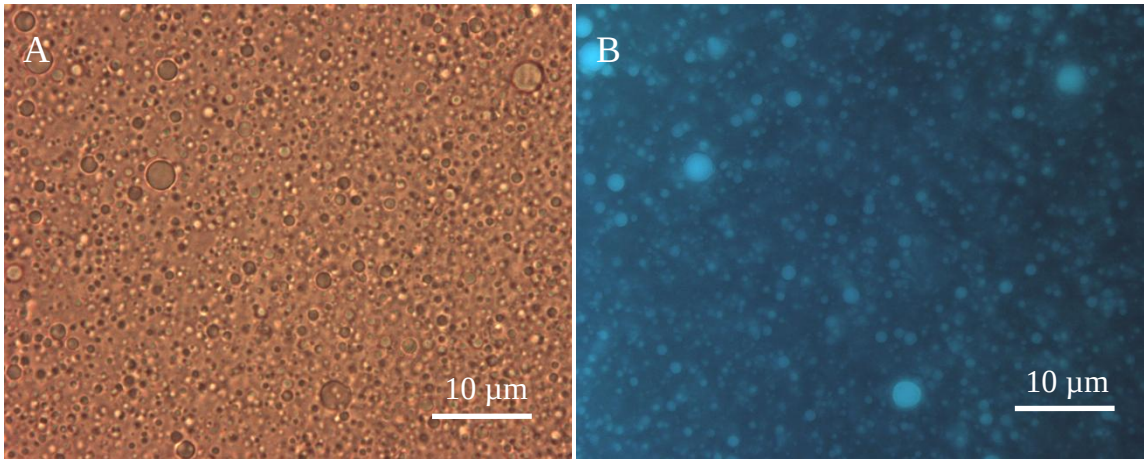

Figure 90. Pheromone containing OLA microparticles under (A) normal light (B) UV-light for a 1wt% aqueous OLA dispersion using oil immersion microscopy

The presence of the pheromone inside the microparticles is also confirmed by the images in UV-light **(Figure 90B).**

The average particle size and the stability of the dispersion were investigated using different concentrations of the pheromone in the dispersion. The concentration of the pheromone was increased with respect to the OLA in a 1 wt% aqueous dispersion.

Table 16. Average particle size and stability of the dispersion with the change in concentration of pheromone in a 1wt% aqueous OLA dispersion.

S.No.	OLA:Pheromone	Stability of the dispersion	Average diameter / μm
1	1:0.1	unstable	1.9
2	1:0.2	unstable	2.1
3	1:0.3	unstable	2.0
4	1:0.5	stable	1.8
5	1:0.7	stable	1.9
6	1:0.9	stable	1.6
7	1:1	stable	1.6

Table 16 shows that the dispersion containing the pheromone in the same weight ratio as the oligolactide showed the lowest average particle size and was also found to be stable at room temperature. However, the dispersions containing the pheromone in 10 wt%, 20 wt% and 30 wt% ratios were found to be unstable with larger particle diameters. Hence, the maximum amount of pheromone required to stabilize the dispersion was found to be around 50 wt%.

The surfactant also plays an important role in stabilizing a dispersion. The function of the surfactant is to suppress coalescence. Hence, the presence of a surfactant is as important as the presence of the hydrophobe. Brij® S20 **(Figure 91)** gave the best results from different tensides tested in varying amounts for the dispersion of OLA in combination with pheromone **(Table 17)**.

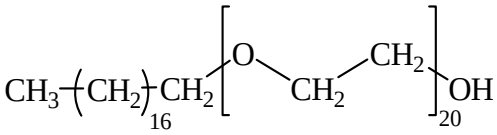

Figure 91. Chemical structure of the surfactant Brij® S20 (Polyoxyethylene (20) stearyl ether).

Table 17. Stability of 10 wt% aqueous dispersions of OLA and pheromone as a function of different tensides.

S.No.	Tenside (10 wt%)	Stability of the dispersion	Average diameter / µm
1	SDS	unstable	1.7
2	Brij® 35P	unstable	1.8
3	Pluronic F-68	unstable	1.8
4	Brij® S20	stable	1.9

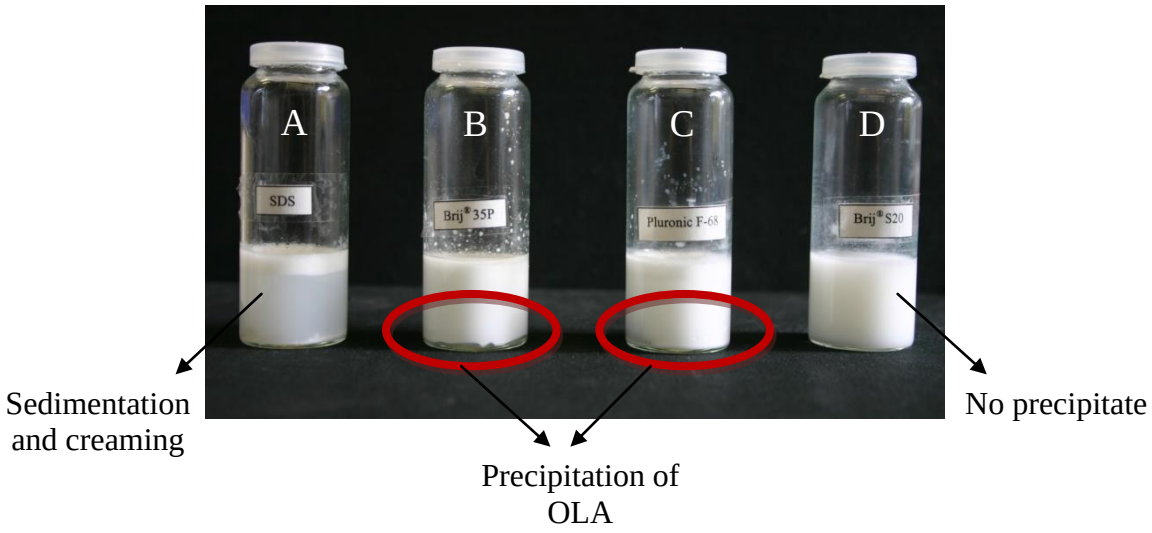

Figure 92. 10 wt% OLA dispersions with different tensides (A) SDS (B) Brij® 35P (C) Pluronic F-68 and (D) Brij® S20.

Precipitation of OLA was observed just two days after the preparation of the dispersions in all cases except the one prepared by using Brij® S20, as evident from **Figure 92**. No visible segregation or agglomeration was observed in 10 wt% OLA aqueous dispersions prepared by using Brij® S20 even after two weeks. It was concluded that the addition of Brij® S20 as the non-ionic surfactant gave the best results in terms of stability and particle size. However, the particle size was almost the same for all the surfactants. For further investigations, Brij® S20 was used as the surfactant.

The role of the surfactant was further investigated by preparing 1 wt% dispersion containing OLA/pheromone (1:1) without the surfactant, which resulted in the formation of a highly unstable dispersion **(Figure 93)**.

Figure 93. 1 wt. % OLA/pheromone (1:1) dispersion prepared without the addition of the surfactant, Brij® S20.

Furthermore, the surfactant concentration was varied with respect to the OLA to see the effect on the particle size for 10 wt% dispersions.

Table 18. The change in the average particle size with change in concentration of the surfactant, Brij® S20, for 10 wt% OLA dispersions.

S.No.	OLA:Brij® S20	Stability of the dispersion	Average diameter / µm
1	1:0.1	stable	1.9
2	1:0.5	stable	0.8
3	1:1	unstable	3.0
4	1:1.5	unstable	1.9
5	1:2	unstable	1.8

As evident from **Table 18,** the dispersion containing the surfactant with weight ratio OLA: Brij® S20 of 1:0.5 gave the smallest particle diameter of 800 nm. Moreover, there was a reduction in the average particle size with an increase in the concentration of the surfactant from OLA:Brij® S20 = 1:1 to 1:2. However, for higher concentrations, the surfactant precipitated out on the walls of the vessel to give an unstable dispersion.

The influence of different hydrophobes on the stability of the dispersion was investigated. As hydrophobes, many different materials have been used to prepare miniemulsions. But as a standard material, hexadecane has been used. Other than this, silanes, siloxanes, isocyanates, fluorinated alkanes, have also been used as hydrophobes to suppress the Ostwald Ripening.[55] To investigate the influence of different hydrophobes, each of these hydrophobes was added to prepare 1 wt% dispersion and the particle size and the stability was compared.

Table 19. Stability and particle size of 1 wt% aqueous dispersions of OLA (1 wt%) and Brij® S20 (1 wt%) as a function of the different additives (1 wt%) replacing the pheromone.

S.No.	Hydrophobe	Structure	Stability of the dispersion	Average diameter / µm
1	Hexadecanol	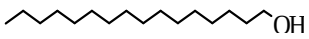	unstable	2.0
2	n-decane		unstable	2.1
3	Dodecane	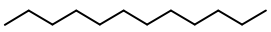	unstable	1.9
4	Tetradecane	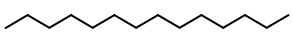	unstable	2.1
5	Hexadecane		unstable	2.3
6	Octadecane	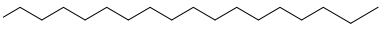	unstable	1.9
7	Stearyl acrylate	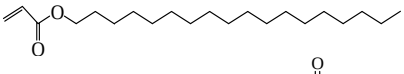	unstable	1.7
8	Octyl acetate	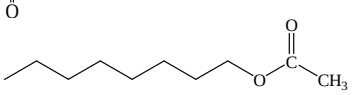	stable	1.6

Hydrophobic compounds like hexadecane, cetyl alcohol (hexadecanol), which are typically used as hydrophobes in miniemulsions yielded dispersions with lower stability **(Table 19).** All the hydrophobes showed almost the same particle size distributions and mean diameters. However, octyl acetate which showed structural analogy to the pheromone yielded dispersions with similar results like the pheromone. Stable dispersions up to 10 wt% were observed by using octyl acetate in place of pheromone as shown in **Figure 94**.

Figure 94. (A) 1 wt% and (B) 10 wt% OLA dispersions (average particle size = 2.1 µm) stabilized by the addition of octyl acetate replacing the pheromone.

7.3.3. Influence of different parameters on particle size and the stability of the dispersion

The effect of change of different parameters on the stability and the average particle size was investigated. The measurements were taken after the complete removal of acetone from the dispersions.

7.3.3.1. Influence of the duration of the ultrasonic treatment

The influence of the duration of the ultrasound treatment on the particle size was investigated. **Table 20** shows the particle size of the 10 wt% aqueous OLA dispersions prepared by ultrasonic treatment for different time intervals.

Table 20. The change in the average particle size and stability with change in duration of the Ultrasonic treatment for 10 wt% OLA dispersions.

S.No.	Duration of the Ultrasonic treatment	Stability of the dispersion	Average diameter / μm
1	30 s	stable	1.7
2	1 min	stable	2.0
3	2 min	stable	2.3
4	4 min	stable	1.9
5	6 min	stable	1.9
6	8 min	unstable	2.5
7	10 min	unstable	2.6

There was a strong dependence of the particle size on the duration of the ultrasound treatment. The average particle size was found to be the smallest for the dispersions treated with ultrasound for 30 s. The dispersion treated with ultrasound was found to be more stable than the dispersion without any ultrasound treatment. With increase in the time for ultrasonification, the average diameter increased and the stability decreased. For further investigations, the dispersions were treated with ultrasound for 4 min to see the influence on particle size by other factors. Plot in **Figure 95** shows the dependence of average particle size on the duration of the ultrasonic treatment.

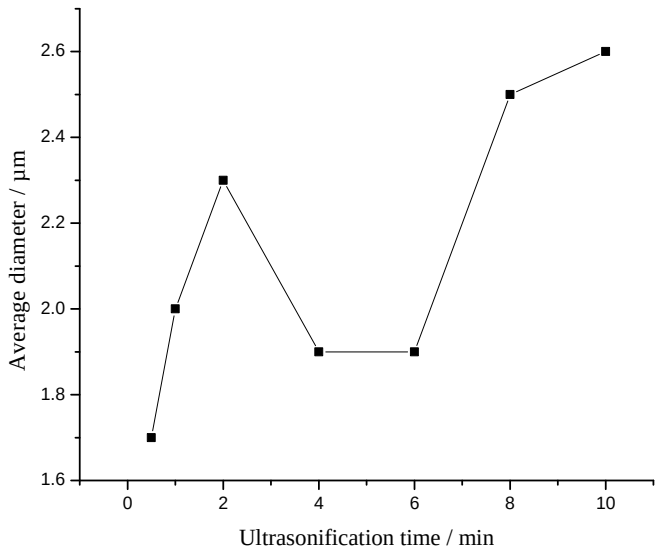

Figure 95. Plot showing dependence of average particle size on duration of the ultrasonic treatment for 10 wt% OLA dispersions.

7.3.3.2. Influence of the output power of the ultrasonic sonotrodes

Increasing the energy density in the continuous emulsification process has a significant effect on the droplet size of an emulsion. The influence of the output power of the ultrasound sonotrodes on the particle size was investigated. The table below shows the average particle sizes of the 10 wt% OLA dispersions prepared by using different output power of the ultrasound.

Table 21. The change in the average particle size and stability with change in the output power of the Ultrasonic for 10 wt% OLA dispersions.

S.No.	Output Power / W	Stability of the dispersion	Average diameter / µm
1	20	unstable	1.8
2	40	unstable	2.2
3	60	stable	1.9
4	70	stable	1.9
5	80	stable	2.1

The output power has no major influence on the average particle size as evident from **Table 21.** With increase in the output power, there was not much change in the particle diameters. However**,** for lower output power of the ultrasonic sonotrodes, the stability of the dispersions was found to be much less.

7.3.3.3. Influence of the volume ratio of organic phase to aqueous phase

The volume of the organic phase is essential for proper dispersion of the OLA. The volume of the organic phase should be small to minimise the use of organic solvents However, if it is too small, the OLA may not be properly dispersed in the continuous aqueous phase. The volume ratio of the organic phase and the aqueous phase was studied by changing the concentration of acetone with respect to water. For this, 1 g of the OLA was dissolved in various volumes of acetone and added to 10 mL of the surfactant solution. **Table 22** shows the summarized data and **Figure 96** shows the plot between the average particle diameter with the change in the volume ratio between the organic phase and the aqueous phase.

Table 22. The change in the average particle size with change in volume ratio of organic phase to the aqueous phase for 10 wt% OLA dispersions.

S.No.	Acetone	Water	Stability of the dispersion	Average diameter / μm
1	1 mL	10 mL	stable	1.9
2	3 mL	10 mL	stable	2.0
3	5 mL	10 mL	stable	2.2
4	7 mL	10 mL	unstable	2.1
5	9 mL	10 mL	unstable	2.2
6	10 mL	10 mL	unstable	3.0

The particle size of the dispersion did not change much with increase in the volume of the organic phase. The dispersion with 1:1 ratio of organic phase to aqueous phase showed the largest mean diameter. In addition, with increase in the amount of the organic phase, the dispersability of the oligolactide in water decreased and the dispersion became highly unstable.

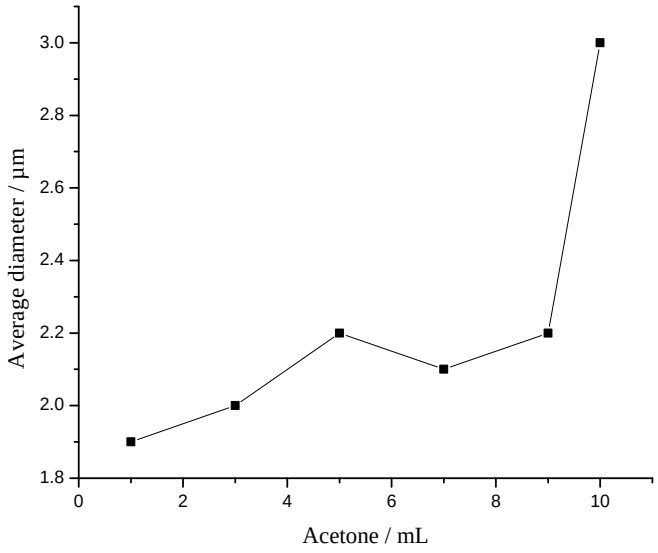

Figure 96. Plot showing dependence of average particle size on volume ratio between organic phase and aqueous phase for 10 wt% OLA dispersions.

The role of the pheromone in stabilizing the dispersion as a hydrophobe and not as a surfactant was further investigated by an attempt to determine its Critical Micelle concentration (CMC) using the surface tension measurements. A graph of surface

tension vs. concentration was plotted. Since the pheromone is water insoluble, the surface tension was measured using acetone as solvent.

Surface tension of acetone at 20 °C = 23.7 mN/m

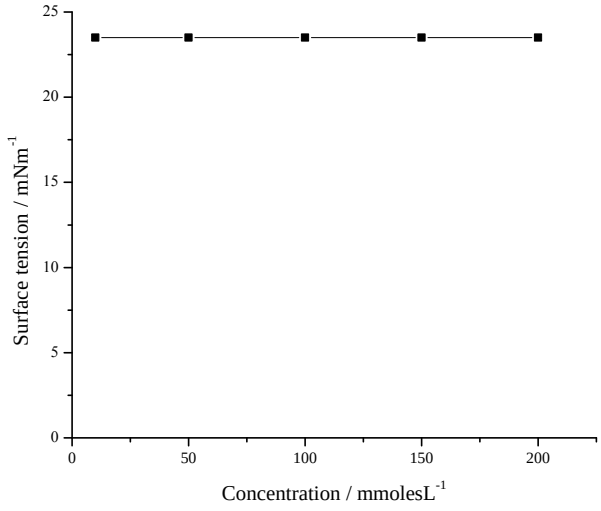

Figure 97. Plot of surface tension with change in concentration of pheromone.

There was no change in the surface tension with the increase in concentration of the pheromone **(Figure 97).** This defies the role of the pheromone as a "surfactant" in stabilizing the dispersion.

7.3.4. Preparation of OLA dispersions by up-concentration via dialysis

The solid content of the dispersions prepared so far was increased drastically without aggregation by osmosis similar to the procedure described by C Vauthier.[134] Here, a dialysis tube containing a 10 wt% aqueous dispersion of OLA, pheromone, and Brij® S20 was placed in a PVA solution (15 wt% in water). After 72 hour of dialysis, stable aqueous dispersions of OLA up to 32 wt% with an average particle size of 1.8 µm remained in the dialysis tube **(Figure 98)**.

Figure 98. Stable 32 wt% OLA/Brij® S20/pheromone dispersion prepared via dialysis.

7.3.5. Electrospinning of OLA/Brij® S20/pheromone in PHA-*b*-MPEG with PEO

Suspension electrospinning with water soluble polymers like poly(vinylpyrrolidone), PVA and PEO have shown best results in terms of spinnability and fiber shape. Electrospinning of 1 wt% OLA dispersion containing pheromone and fluorescent dye, Coumarin 6 was carried out with a 16 wt% water-based dispersion of PHA and α-hydroxy-ω-methoxy-PEG (M_n = 5000 Da) diblock copolyester **(Figure 99)**. The PHA-*b*-MPEG dispersion was used owing to its high solid content and good electrospinnability. High molecular weight PEO (M_w = 900000 Da) was used as the template polymer.[135] The synthesis of the diblock copolyester, preparation of the dispersion and the electrospinning experiments were carried out by Kathrin Bubel.[135]

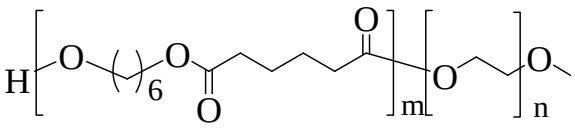

Figure 99. Structure of Polyhexyleneadipate-*block*-methoxypolyethyleneglycol (PHA-*b*-MPEG).

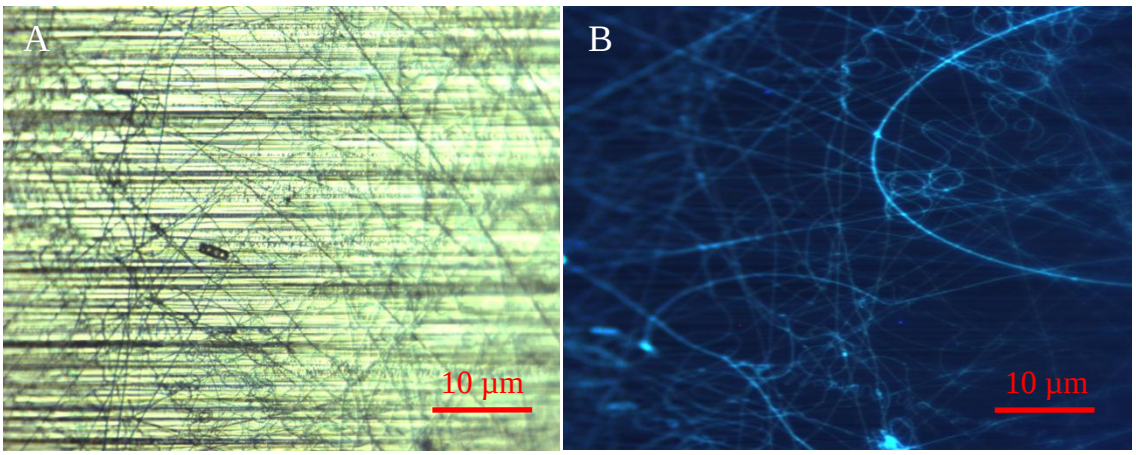

Figure 100. Electrospun fibers of 1 wt% OLA dispersion containing a water-based dispersion of diblock copolyester PHA-*b*-MPEG and PEO as the matrix polymer under the fluorescence microscope in (A) normal light and (B) UV-light.

The image of the electrospun fibers under UV-light **(Figure 100B)** confirmed the presence of microparticles. Since 1 wt% of the OLA dispersion was used for electrospinning, the concentration of the microparticles in the fibers was very high. Furthermore, electrospinning of the 1 wt% OLA/Brij® S20/pheromone dispersion was carried out using PHA-*b*-MPEG dispersion (16 wt%) with PEO as the template polymer. After electrospinning, the fibers were treated with water in order to test the water stability of the fibers. The SEM images of the as spun fiber mats and the water treated fiber mats are shown in **Figure 101**.

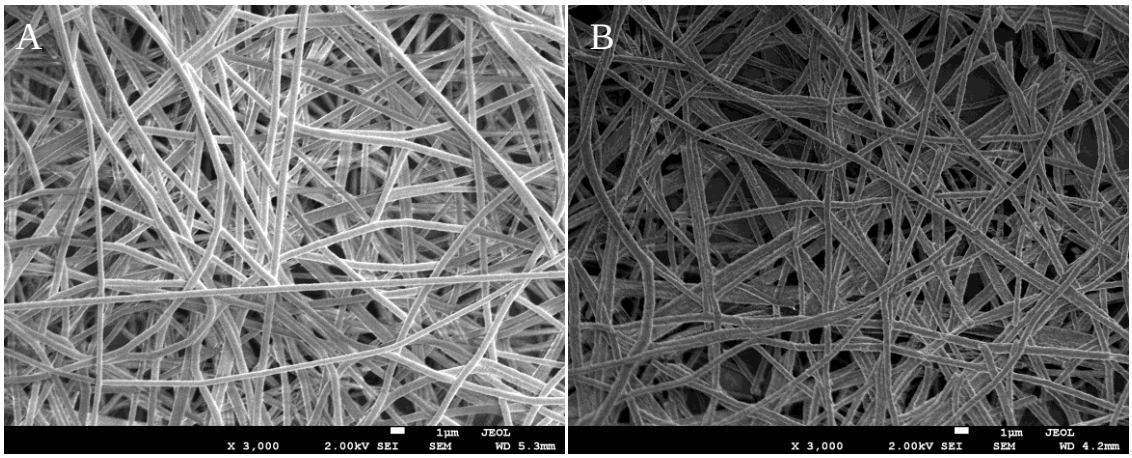

Figure 101. SEM images of electrospun fibers of 1 wt% OLA/Brij® S20/pheromone aqueous dispersion with PHA-*b*-MPEG dispersion and PEO (A) before water treatment and (B) after water treatment for 24 h at 20 °C.

The average diameter of the non water treated fibers was found to be 500 nm. The water treated fibers showed no sign of swelling as the average fiber diameter was 510 nm. Hence, there was no change in the average diameter and fiber morphology after water treatment for 24 h at 20 °C. However, the particles from the dispersion could not be identified after electrospinning or after water treatment. This was because the particles were smoothened during fiber formation, which was also reported by Stoiljkovic et al. for polyacrylate fibers upon suspension electrospinning.[133]

7.3.6. Release experiments

The release experiments of the pheromone containing OLA dispersion were also carried out. The dispersion with high solid content of 32 wt%, obtained by a combination of solvent displacement method and osmosis, was used for this purpose. The presence of pheromone in the microparticles was confirmed by the retarded release of the pheromone from the dispersion as compared to the free pheromone.

The 32 wt% OLA dispersion containing pheromone and Brij® S20 was mixed with the PHA-*b*-MPEG dispersion and PEO, acting as the template polymer. The high solid content of the OLA dispersion and the presence of PHA-*b*-MPEG dispersion mixed with PEO gave the resulting solution a good film-forming property.

Films prepared by solvent casting were analyzed by isothermal TGA at a temperature of 30 °C for 4 h under inert atmosphere. The rate of evaporation of the pheromone was studied with time. Similarly, another solution containing free pheromone with PHA-*b*-MPEG dispersion and PEO was prepared and the isothermal TGA was carried out at the same temperature under the same conditions.

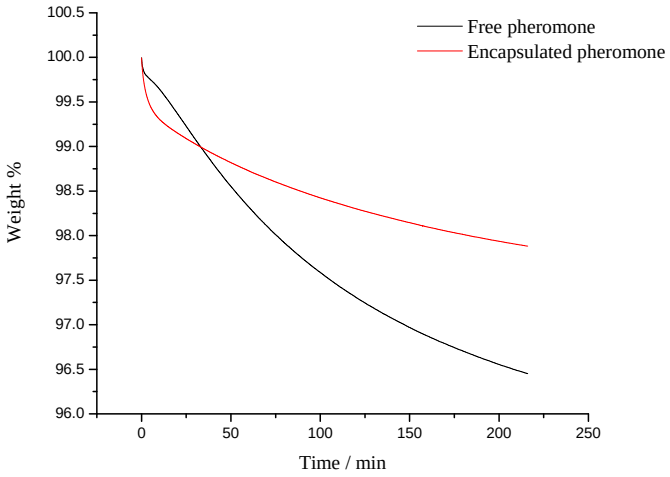

Figure 102. Comparison of the release rates of (A) free pheromone and (B) pheromone in OLA dispersion by isothermal TGA at 30 °C for 4 h.

Figure 102 shows the isothermal TGA curves for the pheromone in the 32 wt% OLA dispersion and for the free pheromone**.** The release rate for both was found to be non linear. The release rate for the pheromone in the OLA dispersion for the first 25 min was found to be 2.1 wt% per hour while for the free pheromone it was found to be 1.9 wt% per hour. For the pheromone in the dispersion, the release rate from 100-200 min was calculated to be 0.29 wt% per hour while for the free pheromone, the release rate was calculated to be 0.62 wt% per hour. This shows that the release rate was quite comparable for the first 25 min, but with time the release rate for the pheromone in the OLA microparticles decreased as compared to the free pheromone. The comparable rates in the beginning are attributed to the release of small amount of free pheromone present in the OLA microparticles. When all the free pheromone got released from the OLA microparticles, then the rate decreased. This shows that the OLA dispersion contains

only a small amount of pheromone in the free state while a major part is either dispersed in the OLA matrix or encapsulated inside the OLA microparticles.

Furthermore, for the pheromone to be present in the OLA microparticles, it is important that it is miscible with the OLA. The miscibility of pheromone in OLA was proved by DSC analysis of a mixture containing 34 wt% pheromone with respect to OLA. The DSC analysis was performed from a temperature of -50 to 50 °C at a heating rate of 10 °C / min **(Figure 103)**.

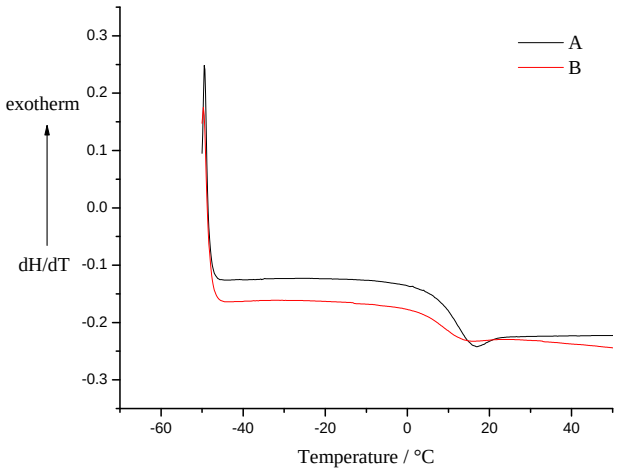

Figure 103. DSC thermogram of (A) OLA (B) 34 wt% pheromone mixed with OLA.

From the DSC curves, the glass transition temperature of the OLA was found to be 12 °C. On mixing 34 wt% pheromone with OLA, the glass transition temperature of the OLA decreased to 9 °C. This shows that the pheromone acts as a plasticizer. It embeds itself between the chains of the OLA, thereby increasing the distance between them, and lowering the glass transition temperature of the OLA. This proves the miscibility of the pheromone in OLA and hence the presence of pheromone in the OLA microparticles.

7.4. Conclusion

Biodegradable oligolactides (OLA) were dispersed in water to concentrations of about 10 wt%. The addition of the pheromone (E,Z)-7,9-dodecadien-l-yl acetate in combination with Brij® S20 to oligolactide (OLA) resulted in aqueous dispersion of a total hydrophobic content (OLA, pheromone, Brij® S20) of up to 32 wt% applying the

combination of solvent displacement method and osmosis. The OLA/pheromone dispersions were stable for several weeks without any sedimentation. These dispersions, in combination with secondary aqueous dispersion of a blockcopolyester and a small amount of PEO, were processed into corresponding nanofibers after electrospinning. The resulting fibers did not show any change in diameter or morphology after water treatment for 24 h at 20 °C.

The role of the pheromone as a secondary dispersion hydrophobe was successfully proved by preparation of stable aqueous OLA dispersions up to 10 wt% using the solvent displacement method. No stable dispersion of OLA in water was possible without pheromone as well as no stable dispersions of pheromone were possible without OLA. The minimum pheromone concentration required to give stable dispersions was found to be 50 wt%. No stable dispersions were possible below this concentration. The average particle size of the dispersion was found to be 1-2 μm by using oil immersion microscopy. Brij® S20 as the surfactant was the most effective in giving stable dispersions with OLA/pheromone. No stable dispersion in water was possible without the surfactant. Replacement of pheromone by classical hydrophobes used for miniemulsions did not yield stable dispersions but the addition of octyl acetate, which shows structural similarity to the pheromone, yielded stable dispersions in water up to 10 wt%.

Release study of the pheromone was carried out by isothermal thermogravimetric analysis of free pheromone and the pheromone in the OLA dispersion at 30 °C for 4 h. The much slower release rate of the pheromone in the OLA dispersion proved its presence as an encapsulated material or in the OLA matrix rather than in a free state in the dispersion. In addition, the presence of pheromone in the OLA microparticles was further proved by the decrease in the glass transition temperature of the OLA on mixing it with 34 wt% pheromone.

8. Experimental part

8.1. Materials

Acetic acid, 99.8%	KMF Laborchemie, used as received
Acetone	BASF, distilled before use
Bayresit VPLS 2331	Bayer MaterialScience, used as received
Bayhydrol A242	Bayer MaterialScience, used as received
Bayhydur XP 2655	Bayer MaterialScience, used as received
Benzaldehyde	Aldrich, used as received
Brij® 78 / Brij® S20	Aldrich, used as received
Brij® 35P	Fluka, used as received
Concentrated HCl, 37%	Aldrich, used as received
Chloroform-d[1]	Roth, used as received
D,L-lactic acid (90% in water)	Aldrich, purified by distillation
1-Decanol, 99%	Acros Organics, used as received
Decyltrimethoxysilane (DTMS)	Aldrich, used as received
Dodecane, 99%	Aldrich, used as received
n-Dodecyltriethoxysilane, 95%	Alfa Aesar, used as received
Ethanol	BASF, distilled before use
Ethyltrimethoxysilane, 97%	Alfa Aesar, used as received
E7, Z9-Dodecadienyl-1-acetate	Trifolio-M GmbH, used as received
Glutaraldehyde solution (25 wt% in water)	Aldrich, used as received
Glyoxal solution (40 wt% in water)	Aldrich, used as received
Hexadecane, 98%	Fluka, used as received

1-Hexadecanol, 99%	Aldrich, used as received
n-Hexyltrimethoxysilane, 97%	Alfa Aesar, used as received
Methanol CHOMASOLV®	Aldrich, used as received
Monochlortriazinyl-beta-cyclodextrin Na-salt (Cavasol ® W7 MCT)	Wacker Fine Chemicals, used as received
Octyl acetate, 99+ %	Acros Organics, used as received
n-Octyltriethoxysilane, 95%	Alfa Aesar, used as received
1H,1H,2H,2H-Perfluorooctyltriethoxysilane	Alfa Aesar, used as received
Pluronic F-68	BioChemica ®, used as received
Poly(vinyl alcohol) (56-98)	KSE GmbH, used as received
Poly(vinyl alcohol) (3-96)	KSE GmbH, used as received
Poly(vinyl alcohol) (28-99)	KSE GmbH, used as received
Poly(vinyl alcohol) (10-98)	KSE GmbH, used as received
Poly(L-lactide) (L210, M_w = 380000)	Boehinger, used as received
Sodium dodecyl sulfate	Chemical store University of Marburg, used as received
Sodium sulfate	Chemical store University of Marburg, used as received
Tetraethyl orthosilicate (TEOS) (99.999% metals basis)	Aldrich, used as received
Tetradecane, 99%	Acros Organics, used as received
Tween® 85	Acros Organics, used as received

8.2. Characterization

8.2.1. Contact angle measurement

The water contact angle of the samples was measured in the group of Prof. Dr. Norbert Hampp in the Physical Chemistry Department at Philipps-University Marburg with a Contact Angle Measuring System G10 from the Kruess Company. Drop Shape Analysis Software was used for the measurement. An average of at least five droplets of 3 mg of distilled water was taken.

8.2.2. Electron microscopy

The SEM images were obtained with the help of the JSM-7500F (JEOL) scanning electron microscope, with a voltage of 2-4 kV. The samples were directly put on the sample holder using a conductive tape. They were then coated with a layer of gold to increase the conductivity of the sample and to get a better image on the detector.
The morphology and the diameter of the PVA / cavasol fiber mat was determined using Scanning electron microscopy (SEM) (CamScan Series 4, Cambridge Scanning Company Limited). The fibres were coated with gold in an Edwards Auto 306 sputter-coater at $< 5 * 10^{-5}$ mbars.

8.2.3. Thermal analysis

The thermal analysis of the samples was done by using the Mettler thermal analyzers having 851 Thermogravimetric (TG) and 821 Differential Scanning Calorimetry (DSC) modules from the company Mettler Toledo. The thermal stability was determined under nitrogen atmosphere (flow rate = 50 mL/min). The thermal degradation was studied by heating 8-12 mg of the sample from room temperature to 800 °C at a heating rate of 10 °C/min. DSC scans were recorded under nitrogen atmosphere at a heating rate of 10 °C/min. A sample size between 5-10 mg was used in each experiment. The glass transition temperature was obtained from the second heating cycle using STARe software.

8.2.4. Mechanical property

The tensile strength of the samples was measured using Zwick/Roell Materials Testing machine (Type: KAF-TC). The samples were cut in the shape of a bone with a total length of 80.6 mm. It was then mounted directly onto the clamps having a grip to grip separation of 35 mm at the start position. The software used was testXpert II. The values for the density of the material to be measured and the weight of each sample were fed before the measurement began. The curves for stress versus strain were recorded. Each measurement was repeated 5 times and an average value was taken.

8.2.5. Infrared spectroscopy (FTIR)

The IR spectra were measured on a FT-IR spectrometer of type Excalibur Series with an attached IR microscope of the type UMA 600 from Digilab. Infrared spectroscopy (IR) was performed by means of Digilab (Excalibur series) instrument with ATR crystal ZnSe and WinIRPro software version 3.3.

8.2.6. Wide angle X-ray diffraction (WAXD)

X-ray diffraction patterns were recorded on a Siemens D-5000 wide-angle diffractometer (Siemens, Germany) equipped with DiffracPlus 3.0 software at room temperature. The samples were mounted on an aluminum cantilever and Nickel filtered Cu-Kα radiation was used as an X-ray source. The scattering angle (2θ) varied from 3° to 33° and the measuring time was 25 h.

8.2.7. NMR spectroscopy

^{1}D NMR was measured in the NMR Department at Philipps-University Marburg. ^{1}H and ^{13}C NMR spectra were measured using the Bruker DRX-400 spectrometer. MestRec version 4.9.9.6 software was used for the analysis of the spectra. The signal for the normal deuterated solvent used to measure the NMR is as follows: $CDCl_3$ (^{1}H-NMR = 7.26 ppm, ^{13}C-NMR = 77.0 ppm).

8.2.8. Pore size measurement

The pore size of electrospun fiber mats was determined using the Capillary Flow Porometer (Porous Materials Inc., CFP-1200-AEXL). The sample was saturated with a wetting liquid, Galwick (Surface tension = 15.9 dynes/cm). The wetting liquid spontaneously fills up the pores of the sample. A pressurized non-reacting gas is allowed to displace the liquid from the pores and permit gas flow. The gas pressure and the flow rates are simultaneously measured using the Wet Up / Dry Up method. The measurement and analysis of the results was done using the Capwin software.

8.2.9. Mass spectroscopy

Mass spectroscopy of the samples was performed in the routine analysis centre of the Chemistry Department at Philipps-University Marburg. Atmospheric Pressure Chemical Ionization (APCI) was used to determine the end groups of the low molecular weight Poly (lactides).

8.2.10. Fiber diameter measurement

Images obtained by SEM were used to determine the fiber diameter of the electrospun fiber mats. The software Image J was used to calculate the fiber diameter. An average of at least 50 values was taken for each sample to get the average fiber diameter of that sample.

8.2.11. Surface tension measurement

The surface tension was measured to determine the Critical Micelle Concentration (CMC) of pheromone at 20 °C using Dataphysics DCAT 11 Surface tension measuring device equipped with Wilhelmy-Plate. About 40 mL of the solution was filled into a clean, dry quartz glass container and the surface tension was measured. The surface tension was calculated from the measured values using the software SCAT 12.

8.2.12. Optical microscopy

The optical microscope of the type Leica DMRX was used to measure particle sizes using the oil immersion technique. This was achieved by immersing both the objective lens and the specimen in a transparent oil of high refractive index. Leica 100× oil immersion objective and Leica standard immersion oil was used for this purpose. The images were obtained using the software Leica DC Viewer. An average of the diameter of at least 100 particles was taken to determine the mean particle diameter for each sample, which was calculated using Image J. Leica DMRX fluorescence microscope was used to obtain the fluorescent microscopy images.

8.3. Preparation of solutions

8.3.1. PVA / cavasol solution for electrospinning

A 10 wt% solution of PVA (M_w = 195000 Da) in water was prepared by adding 100 g of PVA in 900 g of distilled water, followed by vigorous mixing and constant heating at 90° C for 12 h to get a homogeneous solution. 5 wt% aqueous solution of cavasol was added to the PVA solution with a weight ratio PVA to cavasol of 1:0.1. 10 wt% of sodium dodecyl sulfate (SDS) was added to it as a surfactant.

Table 23. The amount of various chemicals added to prepare PVA / cavasol solution in different concentrations.

PVA:cavasol	Amount of 10 wt% PVA solution added / g	Amount of cavasol added / g	Amount of water added / g	Amount of SDS added / g
1:0.1	10	0.1	2	0.01
1:0.2	10	0.2	4	0.01
1:0.3	10	0.3	6	0.01
1:0.4	10	0.4	8	0.01
1:0.5	10	0.5	10	0.01
1:0.6	10	0.6	12	0.01
1:0.7	10	0.7	14	0.01
1:0.8	10	0.8	16	0.01
1:0.9	10	0.9	18	0.01
1:1	10	1	20	0.01

Electrospinning parameters

Voltage = 30 kV

Distance between the electrodes = 20 cm

Needle diameter = 0.55 mm

Flow rate = 0.51 mL/h

Aluminium foil was used as a substrate for collecting the electrospun fibers.

8.3.2. PVA / borax crosslinked fiber mats

A 10 wt% solution of PVA (M_w = 195000 Da) in water was prepared by dissolving 100 g of PVA in 900 g of deionized water. The solution was homogenized by constant stirring and heating at 90° C for 12 h. 0.5 g (50 wt%) of sodium dodecyl sulfate (SDS) was added to 10 g of this 10 wt% PVA solution as a surfactant.

Electrospinning parameters

Voltage = 20 kV

Distance between the electrodes = 21 cm

Needle diameter = 0.55 mm

Flow rate = 0.51 mL/h

Aluminium foil was used as a substrate for collecting the electrospun fibers.

Borax solution was prepared by dissolving 0.1 g borax in 4.04 g of water with a weight ratio PVA to borax of 1:0.1. A defined piece of the electrospun fiber mat was dipped into the borax solution for 1 min. It was then left to dry for about 24 h at room temperature.

Table 24. The amount of various chemicals added to prepare PVA / borax crosslinked fiber mats.

Amount of 10 wt% PVA solution added / g	Amount of borax added / g	Amount of water added / g	Amount of SDS added / g
10	0.1	4.04	0.5

8.3.3. PVA / benzaldehyde solution

A 10 wt% solution of PVA (M_w = 195000 Da) in water was prepared. Benzaldehyde was added to the PVA solution with a weight ratio PVA to benzaldehyde of 1:0.2. Sample films of PVA / benzaldehyde solution were prepared by solvent casting method.

Table 25. The amount of various chemicals added to prepare PVA / benzaldehyde solution.

Amount of 10 wt% PVA solution added / g	Amount of benzaldehyde added / g
10	0.2

8.3.4. PVA / glutaraldehyde solution

A 10 wt% solution of PVA (M_w = 195000 Da) in water was prepared. A glutaraldehyde solution (25 wt% in water) was added to the PVA solution with a weight ratio PVA to glutaraldehyde of 1:0.4. Films of PVA / glutaraldehyde solution were prepared by solvent casting.

Table 26. The amount of various chemicals added to prepare PVA / glutaraldehyde solution.

Amount of 10 wt% PVA solution added / g	Amount of glutaraldehyde solution added / g
10	0.4

8.3.5. PVA / glutaraldehyde solution under acidic conditions

Glutaraldehyde solution in water was prepared with a weight ratio PVA to glutaraldehyde of 1:0.6. 2-3 drops of conc. H_2SO_4 was added to it.
PVA fiber mat was electrospun from a 10 wt% solution of PVA (M_w = 195000 Da) in water. 10 wt% sodium dodecyl sulfate was added as a surfactant in the electrospinning solution. A defined piece of the electrospun fiber mat was dipped into the acidified glutaraldehyde solution for 1 min and the solubility in water was tested.

Table 27. The amount of various chemicals added to prepare PVA / glutaraldehyde solution.

Amount of 10 wt% PVA solution added / g	Amount of glutaraldehyde solution added / g	Amount of SDS added / g
10	0.6	0.1

8.3.6. PVA / glyoxal solution under acidic conditions

A 10 wt% solution of PVA (M_w = 195000 Da) in water was prepared. The glyoxal solution (40 wt% in water) was added to this PVA solution with a weight ratio PVA:glyoxal of 1:0.2. To this 1 drop of concentrated hydrochloric acid (37%) was added as a catalyst.

Table 28. The amount of various chemicals added to prepare PVA / glyoxal solution.

Amount of 10 wt% PVA solution added / g	Amount of glyoxal solution added / g
10	0.2

Electrospinning parameters

Voltage = 20 kV

Distance between the electrodes = 20 cm

Needle diameter = 0.55 mm

Flow rate = 0.51 mL/h

Aluminium foil was used as a substrate for collecting the electrospun fibers.

8.3.7. Preparation of the sol-gel solutions for coating

The coating solution containing TEOS (Tetraethyl orthosilicate) and DTMS (n-decyltrimethoxysilane) was prepared with the molar compositions of:

$$TEOS:DTMS:ethanol:H_2O:HCl = 0.5:0.1:20:11:0.008$$

followed by continuous stirring at room temperature for 24 h. The PVA samples heated at 180 °C for 3 min were coated with this sol-gel solution by immersing the samples into the solution for 10 s – 2 min. The dipping experiments were carried out with the help of a dip-coater. The samples were then dried in air for 24 h. DTMS was used under inert atmosphere since if exposed to air, it undergoes self polymerization.

Table 29. Mole ratio, molecular weights and densities of the chemicals used in the preparation of the sol-gel solution.

Mole ratio	Chemical	Molecular weight / $gmol^{-1}$	Density / gcm^{-3}
0.5	TEOS	208.32	0.94
0.1	DTMS	262.46	0.9
20	Ethanol	46	0.789
11	Water	18	1
0.008	Conc. HCl	36.46	1.19

Table 30. Volume of the chemicals required to prepare 50 mL of the sol-gel solution.

Chemical	Volume / mL
TEOS	3.67
DTMS	0.96
Ethanol	38.76
Water	6.57
Conc. HCl	0.008

Different silanes used in the sol-gel solution to investigate the change in the hydrophobic character of the cured PVA fiber mats were added in the same molar composition:

TEOS:Silane:ethanol:H_2O:HCl = 0.5:0.1:20:11:0.008

Table 31. Molecular weights, densities and volumes of the different silanes added to prepare 50 mL of the sol-gel solution.

Silane	Molecular weight / $gmol^{-1}$	Density / gcm^{-3}	Volume / mL
Ethyltrimethoxysilane	150.25	0.94	0.53
Hexyltrimethoxysilane	206.35	0.92	0.74
Octyltriethoxysilane	276.49	0.94	0.97
Dodecyltriethoxysilane	332.59	0.88	1.22
1H,1H,2H,2H-Perfluorooctyltriethoxysilane	468.29	1.44	1.07

The sol-gel solution containing Bayresit VPLS 2331 was prepared by mixing 0.75 mL of Bayresit VPLS 2331 and 0.51 mL of DTMS (under argon). 42 mL of ethanol and 7 mL of water were added to it. Finally, 0.01 mL of conc. HCl (37%) was added. The solution was stirred continuously for 24 h at room temperature.

8.3.8. PVA / polyurethane dispersion for electrospinning

Polyurethane was prepared from a polyisocyanate and a polyol from the Bayer MaterialScience. The isocyanate used was Bayhydur XP 2655, a hydrophilic aliphatic polyisocyanate based on hexamethylene diisocyanate (HDI). The polyol was Bayhydrol A242, a polyacrylic resin containing hydroxyl groups. The polyol and the polyisocyanate were added such that the ratio between the two monomers was 1:1.

10 wt% PVA (M_w = 195000 Da) solution in water was prepared. The polyurethane mixture was added to it in weight ratio 1:1. Sodium dodecyl sulfate was added as a surfactant in the weight ratio PVA:SDS of 1:0.01. The resulting solution was electrospun after stirring for half an hour. Prolonged stirring was avoided because it resulted in crosslinking, making electrospinning difficult.

Electrospinning parameters

Voltage = 20 kV

Distance between the electrodes = 12 cm

Needle diameter = 0.55 mm

Flow rate = 0.51 mL/h

Aluminium foil was used as a substrate for collecting the electrospun fibers.

8.3.9. Microencapsulation by Coacervation

8.3.9.1. Determination of the cloud point temperature

To determine the cloud point temperature, a test tube containing 10 mL of 2 wt% PVA (M_w = 16000 Da, degree of hydrolysis = 96%) solution was dipped in a thermostated water bath maintained at 10 °C. Then, a predetermined amount of 20 wt% aqueous sodium sulfate solution was added to it dropwise. After the addition, the temperature of the bath was slowly increased at the rate of 1 °C/min. The onset of phase separation was observed and the cloud point temperature was noted down.

8.3.9.2. Preparation of pheromone loaded microcapsules

50 mL of 2 wt% PVA (M_w = 16000 Da, degree of hydrolysis = 96%) solution was taken in a three-necked round bottom flask. To this 15 mL of 20 wt% aqueous sodium sulfate solution was added dropwise at a temperature of 10 °C. 2 mL of the pheromone was then slowly added to this PVA / sodium sulfate solution. The temperature of the bath was slowly increased at the rate of 1 °C/min from 10 °C to the cloud point temperature. This increase in temperature was accompanied by vigorous agitation with the help of the Ultra Turrax homogenizer. The crosslinking was brought about by the addition of 6 mL of the crosslinking solution consisting of methanol (16.67 % vol.), acetic acid (5% vol.), sulfuric acid (0.167% vol.) and glutaraldehyde (25% vol.). The crosslinking reaction was carried out at the cloud-point temperature for 24 h. The obtained microcapsules were sieve filtered, washed with distilled water several times and stored in 1 wt% aqueous sodium sulfate solution.

8.3.9.3. Preparation of ethyl caprate loaded microcapsules

50 mL of 2 wt% PVA (M_w = 16000 Da, degree of hydrolysis = 96%) solution was taken in a three-necked round bottom flask. 15 mL of 20 wt% aqueous sodium sulfate solution was added dropwise to it at a temperature of 10 °C. Subsequently, 2 mL of ethyl caprate

was slowly added to this PVA / sodium sulfate solution. The temperature of the bath was slowly increased at 1 °C/min from 10 °C to the cloud point temperature. This increase in temperature was accompanied by vigorous agitation with the help of the Ultra Turrax homogenizer. 6 mL of the crosslinking solution consisting of methanol (16.67% vol.), acetic acid (5% vol.), sulfuric acid (0.167% vol.) and glutaraldehyde (25% vol.) was then added to bring about crosslinking of poly(vinyl alcohol). The crosslinking reaction was carried out at the cloud-point temperature for 24 h. The obtained microcapsules were sieve filtered, washed with distilled water several times and stored in 1 wt% aqueous sodium sulfate solution.

8.3.10. Microencapsulation by emulsion / crosslinking method

8.3.10.1. Preparation of microcapsules

50 mL of 3 wt% PVA (M_w = 61000 Da and degree of hydrolysis of 98%) solution was taken in a 100 mL round bottom flask. Tween® 85 (polyethylene glycol sorbitan trioleate) (66.6 wt%) was added as a surfactant. 2 mL of the pheromone was added to it subsequently. The mixture was dispersed by agitating it for 15 min using the Ultra Turrax homogenizer at a temperature of 323 K. Benzaldehyde (20 wt%) and conc. HCl (1 wt%) were added to it for crosslinking of the polymer wall at the same temperature. A white milky dispersion was obtained. The microcapsules were separated by drying the obtained dispersion at room temperature for 24 h.

8.3.10.2. Preparation of microcapsules with 1-decanol

In the microencapsulation process, 50 mL of 3 wt% PVA (M_w = 61000 Da and degree of hydrolysis of 98%) solution was taken in a 100 mL round bottom flask. Tween 85 (polyethylene glycol sorbitan trioleate) (66.6 wt%) was added as a surfactant. A 10 wt% pheromone solution in 1-decanol was prepared and 2 mL of this solution was added to it subsequently. The mixture was dispersed by agitating it for 15 min using the Ultra Turrax homogenizer at a temperature of 323 K. Benzaldehyde (20 wt%) and conc. HCl (1 wt%) were added to it for crosslinking of the polymer wall at the same temperature. The microcapsules were separated by drying the obtained dispersion at room temperature for 24 h.

8.3.11. Microencapsulation by solvent evaporation method

8.3.11.1. Preparation of microcapsules

200 mg of PLA (L210, M_w = 380000) was dissolved in 10 mL of dichloromethane (DCM). Pheromone was added to it in varying amounts. The resultant organic solution was added to 70 mL of PVA (M_w = 14,000 Da and degree of hydrolysis = 85%) used as a surfactant (1 wt%) and emulsified using the Ultra Turrax for 5 min. The system was then stirred continuously for 24 h at room temperature and atmospheric pressure to evaporate DCM completely. The particles obtained were then centrifuged, washed several times with distilled water

8.3.12. Synthesis of oligolactide (OLA) by polycondensation

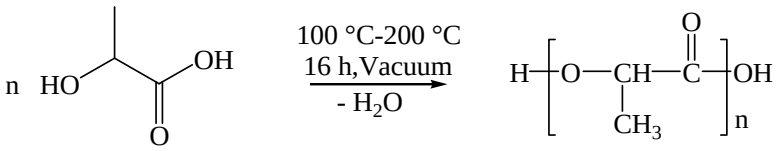

200 g of D,L-lactic acid (90% in water) was weighed in a clean and dried 500 mL round bottom flask. The temperature was increased to 100 °C to distill off the 10% water present in the monomer without applying vacuum to prevent distillation of D,L-lactic acid (Boiling point = 122 °C @ 12 mmHg). The heating was then increased stepwise to 200 °C simultaneouly removing water by vacuum distillation. The polycondensation reaction was carried out for 16 h.

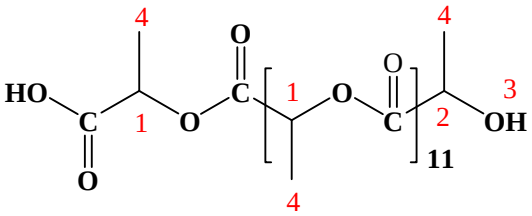

^{1}H-NMR (400 MHz, $CDCl_3$): δ/ppm = 1.37 -1.60 (m, $C4H_3$)
4.25 - 4.35 (m, C2H)
5.07 - 5.16 (m, C1H)
6.3 (broad, s, OH)

^{13}C-NMR (400 MHz, $CDCl_3$): δ/ppm = 15, 16, 19, 20 (CH_3)
66, 68, 69, 70, 72 (CH)
169, 174, 175 (C=O)

DSC: T_g = 12-15 °C

8.3.13. Synthesis of OLA dispersions

All OLA dispersions were prepared under similar conditions. The OLA was dissolved in acetone and pheromone and added to the aqueous phase containing a surfactant. The mixture was sonicated for a few minutes. Ultrasound treatment was performed with an ultrasonic device (Bandelin electronic UW 60, Bandelin Sonoplus HD 60 adapter, power 70 W). The dispersions were stirred at room temperature for 24 h until acetone had evaporated completely. Both creaming and sedimentation were observed in some of the dispersions after allowing them to stand for a few days. All the dispersions were decanted and centrifuged at 14000 rpm for 10 min to determine the particle size by oil immersion microscopy.

8.3.13.1. Synthesis of 1 wt% OLA/pheromone/Brij® S20 dispersion

0.1 g of the OLA was dissolved in 2.5 mL acetone. To this, 0.1 g of the pheromone was added. The components were mixed together and added to 10 mL aqueous solution containing 0.1 g of Brij® S20. The resulting dispersion was subjected to ultrasound for 4 min and then purged under mild air stream at 20 °C to remove acetone.

8.3.13.2. Synthesis of 10 wt% OLA/pheromone/Brij® S20 dispersion

1 g of the OLA was dissolved in 5 mL acetone. After addition of a solution of 10 mL of water and 0.1 g Brij® S20, the mixture was subjected to ultrasound for 4 min. The resulting dispersion was purged under a mild air stream at 20 °C to remove acetone.

8.3.13.3. Synthesis of 1 wt% OLA/pheromone/Coumarin 6/Brij® S20 dispersion

0.6 g of the OLA was dissolved in 20 mL acetone. A mixture of 1.78 g of the pheromone and 2.9 mg of Coumarin 6 was added to it. The components were mixed together and added to 60 mL aqueous solution containing 0.6 g of Brij® S20. The resulting dispersion was subjected to ultrasound for 4 min and then purged under mild air stream at 20 °C to remove acetone.

8.3.14. Synthesis of Polyhexyleneadipate-*block*-methoxypolyethyleneglycol (PHA-*b*-MPEG)

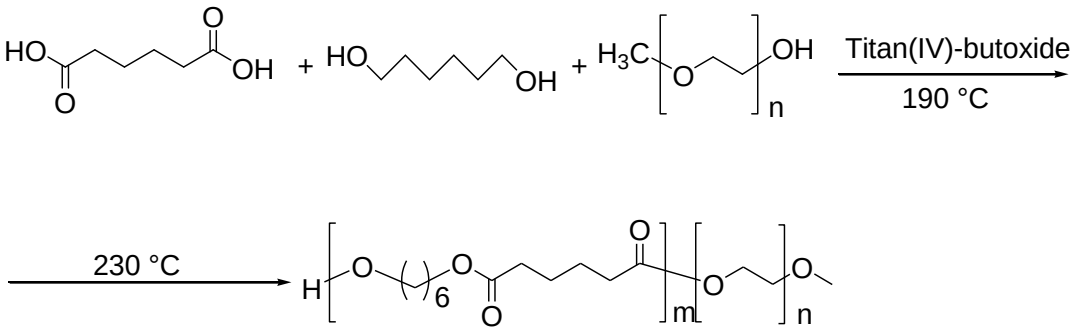

The synthesis of the diblock copolyester was performed by melt polycondensation using adipic acid, 1,6-hexanediol and α-hydroxy-ω-methoxy-PEO (M_w = 5000 Da). Titanium butoxide was used as the catalyst followed by a subsequent addition of polyphosphoric acid to prevent side reactions and thermal decomposition.[135]

8.3.15. Synthesis of PHA-*b*-MPEG dispersion (2.5 wt%) in water

0.5 g of PHA-*b*-MPEG (M_n = 6400 Da, PDI = 2.1) was dissolved in 12.5 mL of acetone. After addition of a solution of 20 mL of water and 0.05 g Brij® 78, the mixture was subjected to ultrasound for 4 minutes. The resulting suspension was purged under mild air stream at 20 °C to remove acetone.

Upconcentration of 2.5 wt% dispersion of PHA-*b*-MPEG (M_n = 6400 Da, PDI = 2.1, particle size = 108 nm) to 16 wt% was carried out by dialysis. 500 mL of the dispersion were filled in a dialysis tube with a length of 15 cm and placed in 6 L of an aqueous solution of PVA (15 wt%). After 100 h, the tube was removed from the PVA solution and rinsed with water and dried. The solid content of PHA-*b*-MPEG was obtained by freeze drying and weighing.[135]

8.3.16. Preparation of solution for electrospinning of 1 wt% OLA/pheromone/Coumarin 6/Brij® S20 dispersion/16 wt% PHA-*b*-MPEG dispersion/PEO

2 g of 1 wt% OLA/pheromone/Coumarin 6/Brij® S20 dispersion was mixed with 8 g of 16 wt% PHA-*b*-MPEG dispersion. 0.4 g of PEO (M_w = 900000) was added to it.

Electrospinning parameters
Voltage = 15 kV
Distance between the electrodes = 22 cm
Needle diameter = 0.55 mm
Flow rate = 0.05 mL/min
Aluminium foil was used as a substrate for collecting the electrospun fibers.

8.3.17. Preparation of solution for electrospinning of 1 wt% OLA/pheromone/Brij® S20 dispersion/16 wt% PHA-*b*-MPEG dispersion/PEO

1 g of 1 wt% OLA/pheromone/1 Brij® S20 dispersion was mixed with 4 g of 16 wt% PHA-*b*-MPEG dispersion. 0.2 g of PEO (M_w = 900000) was added to it.

Electrospinning parameters
Voltage = 15 kV
Distance between the electrodes = 22 cm
Needle diameter = 0.55 mm

Flow rate = 0.05 mL/min

Aluminium foil was used as a substrate for collecting the electrospun fibers.

8.3.18. Dialysis

Dialysis of the 10 wt% oligolactide dispersion containing the pheromone was carried out to prepare dispersions of higher concentration. A larger batch of a new aqueous dispersion of OLA (10 wt% of OLA, M_n ~ 954 Da, particle size = 1.9 µm) was used for the up-concentration by dialysis. A dialysis membrane Spectra Por® (MWCO = 1000; Normal width = 38 mm, Diameter = 24 mm) was used. The dialysis tubes were precleaned by treatment with deionized water for 20 min.

50 mL of the 10 wt% dispersion was filled in the dialysis tube with a length of 10 cm and placed in 800 mL of an aqueous solution of 15 wt% PVA solution (M_w = 14000 Da) for 72 h at room temperature. After 72 h, the tube was removed from the PVA solution and rinsed with water and dried. Solid content of OLA was obtained by freeze drying and weighing.

The dialysis was stopped after 72 h to avoid agglomeration. The particle size and particle size distribution remained unchanged after concentration. In theory, the dispersion could be further concentrated until equilibrium is reached on both sides of the dialysis membrane.[134] No visible agglomeration was formed even after storing the concentrated dispersion for two weeks.

8.3.19. Preparation of solution for release study of the pheromone

Two solutions were prepared to study the release rate of the pheromone. The first solution was prepared by mixing 5 g of 32 wt% OLA/pheromone/Brij® S20 dispersion (prepared by a combination of solvent displacement method and dialysis), 5 g of 2.5 wt% PHA-*b*-MPEG dispersion and 0.4 g of PEO (M_w = 900000) as the template polymer.

The other solution was prepared by the addition of 5 g of 2.5 wt% PHA-*b*-MPEG dispersion, 0.4 g of PEO (M_w = 900000) and 1 g of free pheromone. Sample films for analysis were prepared from both the solutions by solvent casting method.

9. Zusammenfassung

Wasserstabile und bioabbaubare Nanofasern konnten erfolgreich durch Electrospinning einer Kombination bestehend aus einer sekundären wässrigen Dispersion von Oligolactid (OLA) und einem Blockcopolyester hergestellt werden. Die stabile wässrige Dispersion von OLA mit einem Feststoffanteil von bis zu 10 wt% und dem Pheromon von *Lobesia Botrana,* dem bekreuzten Traubenwickler, beladen, wurde hierzu über *Solvent Displacement Method* dargestellt. OLA wurde mittels konventioneller Polykondensation von Milchsäure hergestellt. In Gegenwart des Pheromons, das als hydrophobes Additiv der sekundäreren Dispersion wirkt, und OLAs mit seinen hydrophilen Alkoxy und Carboxy Endgruppen konnte erfolgreich eine stabile Dispersion hergestellt werden. Wässrige Dispersionen mit einem hydrophoben Anteil von bis zu 32 wt% konnte indes erzielt werden, in dem eine Kombination aus *Solvent Displacement Method* und Osmose verwendet wurde. Die durchschnittliche Partikelgröße lag zwischen 1-2 µm. Ohne wenigstens eine der beiden Komponenten Pheromon oder OLA konnte allerdings keine stabile Dispersion erhalten werden. Der Austausch des Pheromons durch ein in der Miniemulsion verwendetes, klassisches Hydrophob, wie zum Beispiel Hexadecan oder 1-Hexadecanol, führte zu keiner stabilen Dispersion. Jedoch konnte mit Octylacetat, welches eine Struktur ähnlich des Pheromons besitzt, eine stabile Dispersion mit einem Feststoffgehalt von bis zu 10 wt% dargestellt werden. Diese Art von wässriger Polyester Formulierung ist vielversprechend und eröffnet neue Perspektiven für Anwendungen wie der kontrollierten Freisetzung von Biomaterialien wie Pheromonen und Pharmazeutika. Diese wiederum können für weitere Arbeitstechniken, wie zum Beispiel, Filmherstellung und Beschichtung, verwendet werden. Da bei solchen Formulierungen der Einsatz von gefährlichen, organischen Lösungsmittel komplett vermieden wird, könnten sie zudem auch für Anwendungen im medizinischen Bereichen, der Pharmazie und der Agrarwirtschaft eingesetzt werden.

Auf einem ähnlichem Konzept basierend wurden mit Pheromon beladende Mikrokapseln aus bioabbaubaren Polymeren erfolgreich hergestellt. Dieses sollten eingesetzt werden, um die Fortpflanzung von *Lobesia Botrana* zu unterbinden. Bei der Herstellung der Mikrokapseln wurden dabei verschieden Methoden wie Koazervation, Emulsion/Vernetzung und *Solvent Evaporation* verwendet. Die beiden ersten Methoden

ergaben Dispersionen mit einem sehr geringen Anteil Pheromon, welches eine Limitierung der kontrollierten Freisetzung des Pheromons aus den Mikrokapseln auf dem Feld nach dem Elektrospinnen bedeuten könnte. Über *Solvent Evaporation Method* konnte der Anteil an Pheromon in den Polylactid Mikrokapseln indes bis auf 60 wt% gesteigert werden. Die Mikrokapseln selbst konnte mittels Cryo-SEM nachgewiesen werden. Die durchschnittliche Partikelgröße der Mikrokapseln lag hierbei zwischen 2 bis 3 µm. Die durchgeführten Freisetzungsstudien belegten, dass die Freisetzungrate des Pheromons in den PL-Kapseln wesentlich langsamer erfolgte, als beim freien Pheromon.

Des Weiteren wurde der bioabbaubare, wasserlösliche Polyvinylalkohol (PVA) vernetzt, um diesen für verschiedene Anwendungsbereichen wie zum Beispiel Microverkapselungen einzusetzen. Hierzu wurden verschiedene chemische und physikalische Vernetzungsmethoden durchgeführt. Beim Electrospinning wurde PVA mit chemikalischen Crosslinkern wie Glyoxal und Cavasol versponnen und anschließend die erhaltenden PVA-Fasern mit Agentien wie Borax und Glutaraldehyde nachbehandelt. Allerdings konnte bei keiner der oben genannten Prozeduren wasserstabile Fasern erhalten werden. Erst durch das Tempern der Fasern bei 180 °C für 3 min konnten wasserunlösliche PVA-Fasern erhalten werden. Der prozentuale Gewichtsverlust wurde berechnet und betrug nach einer 24-stündigen Wasserbehandlung bei RT 1,5%. Die Fasermatten behielten bis 70 °C ihre Wasserstabilität bei. Die Röntgenbeugungsmessung zeigte, dass der Grund für die Wasserunlöslichkeit auf eine Veränderung des Kristallinitätsgrads zurückzuführen ist. Bei der isothermen Thermogravimetrischen Analyse der Fasermatte konnte keine Abspaltung von Wasser festgestellt werden. Dieses schließt aus, dass eine Vernetzungsreaktion der einzelnen Hydroxylgruppen untereinander stattfand. Eine Vernetzung von PVA konnte zudem auch mit Polyurethanen erzielt werden. Hierfür wurde eine Polyurethan Dispersion zusammen mit PVA aus Wasser versponnen und anschließend für 2 h bei 60 °C gehalten, um die wasserstabilen Fasern zu erhalten. Der prozentuale Gewichtsverlust betrug nach 24-stündiger Wasserbehandlung bei RT 11% und nach 9-stündiger Wasserbehandlung bei 90 °C 14%. Die Fasermorphologie und der Faserdurchmesser, blieben indes unverändert und wurden mittels SEM Bilder bewiesen.

Zudem wurde eine Sol-Gel-Behandlung durchgeführt, um die Hydrophobizität der PVA - Fasermatten zu erhöhen, indem Tetraethylorthosilicat (TEOS) und *n*-Decyltrimethoxysilan (DTMS) eingesetzt wurden. Der Kontaktwinkel betrug 144°, dieses bedeutet eine geringe

Oberflächenbenetzung. Die Fasermorphologie der PVA-Fasern blieb nach dem Beschichten weiterhin erhalten und wurde mittels SEM Bildern belegt. Des Weiteren wurden die Fasern mit Superhydrophobizität ausgestattet, indem sie mit einer Sol-Gel-Lösung beschichtet wurde, die eine Perfluorooctyltriethoxysilangruppe als organische Funktionalität zusammen mit TEOS enthielt. Der Kontaktwinkel lag bei über 150°. Auf ähnliche Art und Weise wurde eine Sol-Gel-Beschichtung von Keramikoberflächen durchgeführt, welches zu einer stark reduzierten Benetzbarkeit der Oberfläche führte. Dieses beweist, dass die Sol-Gel-Benetzung eine effektive Methode ist, welche neue Eigenschaften wie Hydrophobizität sowohl in elektroversponnene Materialien, als auch auf Keramikoberflächen induzieren kann.

10. Summary

Water stable and biodegradable nanofibers were successfully prepared by electrospinning of a combination of secondary aqueous dispersions of oligolactide (OLA) and a blockcopolyester. Stable aqueous dispersions of OLA up to 10 wt% loaded with the pheromone of *Lobesia Botrana*, the grapevine moth, were prepared using solvent displacement method. OLA was prepared by conventional polycondensation of lactic acid. The presence of OLA with hydrophilic alkoxy and carboxy end groups and pheromone as a secondary dispersion hydrophobe additive, succeeded in giving stable dispersions in water. Aqueous dispersion of a total hydrophobic content of up to 32 wt% was prepared applying the combination of solvent displacement method and osmosis. The average particle size of the dispersions was about 1-2 µm. No stable dispersions were possible without the pheromone or without the OLA. Replacement of the pheromone with classical hydrophobes used in miniemulsions for example hexadecane, hexadecanol (cetyl alcohol) did not yield stable dispersions. However, octyl acetate having structural analogy to the pheromone gave stable dispersions in water up to 10 wt%. This type of aqueous polyester formulation is highly effective in providing novel perspectives in applications such as controlled release of biomaterials like pheromone, in this case, and drugs. These could also be used for other processing techniques, for example, film preparation and coatings. Since such formulations completely eliminate the use of harmful organic solvents for processing, they can be highly effective for applications in the fields of medicine, pharmacy and agriculture.

Based on a similar concept, dispersions with pheromone loaded microcapsules were successfully prepared for mating disruption in *Lobesia Botrana* using biodegradable polymers. Different methods of microencapsulation were carried out like coacervation, emulsion/crosslinking and solvent evaporation. The first two methods yielded in dispersions with very low amount of pheromone which could be a limitation for controlled release of the pheromone from the microcapsules on the fields after electrospinning. However, polylactide microcapsules containing about 60 wt% pheromone were prepared using solvent evaporation method. The presence of microcapsules was confirmed by cryo SEM. The average particle size of the

microcapsules was found to be 2 to 3 µm. The release studies carried out established that the release rate of the pheromone in the polylactide microcapsules was much slower as compared to that of free pheromone.

Furthermore, crosslinking of water soluble biodegradable polymer, poly(vinyl alcohol) (PVA) was brought about for use in various applications including microencapsulation. Various chemical crosslinking methods and physical methods were carried out. Electrospinning of PVA with chemical crosslinking agents like glyoxal and cavasol was brought about, including post treatment of the electrospun PVA fibers with agents like borax and glutaraldehyde. None of the above procedures resulted in fibers stable in water at low and high temperatures. However, a heat treatment carried out at 180 °C for 3 min brought about water insolubility of PVA fiber mats. The percentage weight loss was calculated to be around 1.5% after water treatment at room temperature for 24 h. The mats were also found to be stable in water up to 70 °C. The reason for insolubility was found to be a change in the degree of crystallinity of PVA fibers, which was proved by X-ray diffraction. The isothermal TGA of the PVA fiber mat at 180 °C for 3 min showed a weight loss of around 0.05 wt% which was quite negligible. This eliminated the possibility of any crosslinking reaction which could occur between the hydroxyl groups of PVA at 180 °C. Crosslinking of PVA was also brought about by polyurethane. Polyurethane dispersions in water containing PVA were electrospun and were found to be water stable after heating at 60 °C for 2 h. The percentage weight loss after water treatment for 24 h at room temperature was around 11% and in water at 90 °C for 9 h was around 14%. The fiber morphology and diameter remained unchanged after water treatment which was evident from the SEM images.

In addition, a sol-gel treatment was brought about to induce hydrophobicity onto the cured PVA fiber mats using tetraethyl orthosilicate (TEOS) and n-decyltrimethoxysilane (DTMS) as the active chemicals. The contact angle was found to be 144° showing low surface wetting. The fiber morphology of the cured PVA fibers was retained after coating which was evident from the SEM images. Furthermore, super-hydrophobicity was induced on coating with a sol-gel solution containing perfluorooctyltriethoxysilane as the organic functional group along with TEOS. The contact angle was measured to be more than 150°. In a similar way, sol-gel coating was carried out on ceramic surfaces

which decreased the wettability of the surface to a large extent. This proves that sol-gel coating can be used as an effective method to introduce novel properties like hydrophobicity into electrospinnable materials as well as ceramic surfaces.

11. Literature

[1] D. H. Reneker, W. Kataphinan, A. Theron, E. Zussman, A. L.Yarin, *Polymer* **2001**, *43*, 6785.

[2] K. H. Lee, H. Y. Kim, M. S. Khil, Y. M. Raand, D. R. Lee, *Polymer* **2003**, *44*, 1287.

[3] J. P. Jeum, Y. H. Kim, Y. M. Lim, J. H. Choi, C. H. Jung, P. H. Kang, Y. C. Nho, *J. Ind. Eng. Chem.* **2007**, *13*, 592.

[4] Fabienne Barroso-Bujans, Ricardo Martínez, Mehrdad Yazdani-Pedram, Pedro Ortiz and Holger Frey, *European Polymer Journal* **2007,** *43(4)*, 1288.

[5] SL Timofeevski, EF Panarin, OL Vinogradov, MV Nezhentsev, *Pharm Res.* **1996,** *13(3)*, 476.

[6] The term ‘‘Green Electrospinning’’ was first used, to the best of our knowledge, in: R. Krishnan, J. Venugopal, S. Sundarrajan, S. Ramakrishna, 14th European Conference on Composite Materials, ECCM14, 7-10 June, 2010, Budapest, Hungary.

[7] Andreas Greiner, J. H. Wendorff, *Angew Chem Int Edit* **2007**, *46*, 5670.

[8] J. Doshi and D. H. Reneker, Electrospinning process and applications of electrospun fibers, *J. Electrostat.* **1995**, *35*, 151.

[9] Zhenyu Li, Huimin Huang, Ce.Wang, *Macromolecular Rapid Communications* **2006**, *27(2)*, 152.

[10] Ulrich Boudriot, Roland Dersch, Andreas Greiner, and Joachim H. Wendorff, *Artificial Organs* **2006**, *30*, 785.

[11] Pattama Taepaiboon, Uracha Rungsardthong, Pitt Supaphol, *Nanotechnology* **2006**, *17(9)*, 2317.

[12] Changlu Shao, Hak-Yong Kim, Jian Gong, Bin Ding, Douk-Rae Lee and Soo-Jin Park, *Materials Letters* **2003**, *57* (*9-10)*, 1579.

[13] Michael Bognitzki, Mathias Becker, Martin Graeser, Werner Massa, Joachim H. Wendorff, Andreas Schaper, Dirk Weber, Andre Beyer, Armin Gölzhäuser, and Andreas Greiner, *Advanced Materials* **2006**, *18*, 2384.

[14] Jing Zeng, Xiaoyi Xu, Xuesi Chen, Qizhi Liang, Xinchao Bian, Lixin Yang and Xiabin Jing, *Journal of Controlled Release* **2003**, *92*, 227.

[15] Geert Verreck, Iksoo Chun, Joel Rosenblatt, Jef Peeters, Alex Van Dijck, Jurgen Mensch, Marc Noppe, Marcus E. Brewster, *Journal of Controlled Release* **2003**, *92*, 349.

[16] Y. K. Wang, T. Yong and S. Ramakrishna, *Aust. J. Chem.* **2005b**, *58*, 704.

[17] W. J. Li, C. T. Laurencin, E. J. Caterson, R. S. Tuan and F. K. Ko, *J. Biomed. Mater. Res* **2002**, *60*, 613.

[18] Wenguo Cui, Yue Zhou and Jiang Chang, Sci. Technol. *Adv. Mater*. **2010**, *11*, 014108.

[19] Jason J. Ge, Haoqing Hou, Qing Li, Matthew J. Graham, Andreas Greiner, Darrell H. Reneker, Frank W. Harris, and Stephen Z. D. Cheng, *J Am Chem Soc* **2004**, *126*, 15754.

[20] Zhenyu Li, Huimin Huang, Ce Wang, *Macromolecular Rapid Communications* **2006**, *27*, 152.

[21] M. Gensheimer, M. Becker, A. Brandis-Heep, J. H. Wendorff, R. K. Thauer and A. Greiner, *Advanced Materials* **2007**, *19*, 2480.

[22] Seung-Wuk Lee and Angela M. Belcher, *Nano Letters* **2004**, *4*, 387.

[23] Z. M. Huang, Y. Z. Zhang, M. Kotaki and S. Ramakrishna, *Compos. Sci. Technol.* **2003,** *63*, 2223.

[24] I. S. Chonakis, *J. Mater. Process. Technol.* **2005**, *167***,** 283.

[25] M. Bognitzki, M. Becker, M. Graeser, W. Massa, J. H. Wendorff, A. Schaper, D. Weber, A. Beyer, A. Gölzhäuser and A. Greiner, *Advanced Materials* **2006**, *18*, 2384.

[26] Eugene Smit, Ulrich Bűttner, Ronald D. Sanderson, *Polymer* **2005**, *46*, 2419.

[27] P. Katta, M. Alessandro, R. D. Ramsier, and G. G. Chase, *Nano Letters* **2004**, *4*, 2215.

[28] D. Li, Y. Wang and Y. Xia, *Advanced Materials* **2004**, *16*, 361.

[29] D. Yang, B. Lu, Y. Zhao and X. Jiang, *Advanced Materials* **2007**, *19*, 3702.

[30] Zheng-Ming Huang, Y.-Z. Zhang, M. Kotaki, S. Ramakrishna, *Composites Science and Technology* **2003**, *63*, 2223.

[31] W. E. Teo and S. Ramakrishna, *Nanotechnology* **2006,** *17*, R89.

[32] Shuiliang Chen, Dissertation thesis, Philipps-Universität (Marburg/Lahn), **2010**.

[33] Yoshito Ikada, Hideto Tsuji, *Macromol. Rapid Commun.* **2000**, *21***,** 117.

[34] *Biodegradability of Polymers: Regulations and Methods for Testing*, Dr. Rolff Joachim Müller.

[35] Friederike von Burkersroda, Luise Schedl, Achim Göpferich, *Biomaterials* **2002,** *23*, 4221.

[36] http://en.wikipedia.org/wiki/Polyanhydrides

[37] U. Witt, T. Einig, M. Yamamoto, I. Kleeberg, W.-D. Deckwer, R.-J. Müller, *Chemosphere* **2001,** *44*, 289.

[38] Charlotte K. Williams, *Chem. Soc. Rev.* **2007**, *36*, 1573.

[39] Liqun Ren, Philipps-Universität (Marburg/Lahn), **2008**.

[40] Jae Hyung Park, Mingli Ye and Kinam Park, *Molecules* **2005**, *10*, 146.

[41] *Technical Overview: Microencapsulation*, microtek Laboratories, Inc.

[42] P.Venkatesan, R.Manavalan and K.Valliappan, *J. Pharm. Sci. & Res.* **2009,** *1 (4)*, 26.

[43] Vanessa Carla Furtado Mosqueira, Philippe Legrand, Huguette Pinto-Alphandary, Francis Puisieux, Gillian Barratt, *Journal of Pharmaceutical Sciences*, **2000,** *89(5)*, 614.

[44] O. Behend, H. Schubert, *Ultrasonics Sonochemistry* **2001,** *8*, 271.

[45] O. Behend, K. Ax, H. Schubert, *Ultrasonics Sonochemistry* **2000,** *7*, 77.

[46] http://fedainc.com/7.html

[47] Jinyuan Sun, Philipps-Universität (Marburg/Lahn), **2010**.

[48] Paul Paquin, *International Dairy Journal* **1999**, *9*, 329.

[49] http://www.hielscher.com/ultrasonics/homogenize_01.htm

[50] *Ultrasonic Production of Nano-Size Dispersions and Emulsions:* Thomas Hielscher, ENS'05, Paris, France, 14-16 December **2005**.

[51] http://www.hielscher.com/ultrasonics/disperse.htm

[52] Simon M. Joscelyne and Gun Trägårdh, *Journal of Membrane Science* **2000**, *169*, 107.

[53] http://www.malvern.com/LabEng/industry/colloids/colloids_stability.htm

[54] *Steric Stabilization,* Center for Industrial Sensors and Measurements, Literature Review, **2002,** 1.

[55] http://www.malvern.com/LabEng/industry/colloids/dlvo_theory.htm

[56] Surfactants and Interfacial Phenomena, Third Edition, Milton J. Rosen, *Wiley-*

Interscience.

[57] K. Landfester, *Macromol. Rapid Comm.* **2001**, *22*, 896.

[58] K. Landfester, Adv. Mater. 2001, 13, No. 10, 765.

[59] J. Ugelstad, F. K. Hansen, S. Lange, Makromol. Chem. 1974, 175, 507.

[60] Chi Hun Kim, Myung Seob Khil, Hak Yong Kim, Hyun Uk Lee, Kwang Yeop Jahng, *Journal of Biomedical Materials Research Part B: Applied Biomaterials*, *78B(2)*, 283.

[61] Harindra Vedala, Jun Huang, Xiang Yang Zhou, Gene Kim, Somenath Roy, Won Bong Choi, *Applied Surface Science* **2006,** *252*, 7987.

[62] Se Heang Oh, Soung Gon Kang, Eun Seok Kim, Sang Ho Cho and Jin Ho Lee, *Biomaterials* **2003**, *24(22)*, 4011.

[63] C.A. Finch, *Chemical reactions and stereochemistry of poly(vinyl alcohol), in: Poly(vinyl alcohol) Developments*, John Wiley and Sons, New York **1992**, 281.

[64] S. Inasawa and M. Suzuki (to Showa Denko K.K.), Jap. Pat. Appl. 87/232,444 **1987**.

[65] C. Bergstrom (to Neste Oy), Eur. Pat. Appl. EP 187,040 **1986**.

[66] D. S. Varma, C. Nedungadi, *Journal of Applied Polymer Science* **1976**, *20*, 681.

[67] M. Bravar, V. Rek, and R. Kostelac-.Biffl, *J. Polym. Sci., Polym. Symp.* **1973,** *40*, 19.

[68] Y. Nishijima (to Kanebo Ltd), Jap. Pat. 74/18,915.

[69] Y. Shimosaka and H. Suzuki (to Japan Exlan Co. Ltd), Ger. Offen. DE 2,149,736 **1972**.

[70] Y. Shimosaka and H. Suzuki (to Japan Exlan Co. Ltd), Jap. Pat. 74/48073 **1974**.

[71] J. Bozzay, D. Agoston, I. Rusznak, and L. Torok, *Period. Polytech. Chem. Eng.* **1981**, *25*, 111.

[72] L. M. Shtyagina, V. M. Vainburg, L. E. Vinogradova, *Russ. J. Appl. Chem.* **2001**, *74(8)*, 1408.

[73] G. G. Xu, C. Q. Yang, Y. Deng, *J. Appl. Polym. Sci.* **2004**, *93*, 1673.

[74] Bin Ding, Hak-Yong Kim, Se-Chul Lee,Chang-Lu Shao, Douk-Rae Lee, Soo-Jin Park, Gyu-Beom Kwag, Kyung-Ju Choi ; *Journal of Polymer Science: Part B: Polymer Physics* **2002**, *40*, 1261.

[75] Pattama Taepaiboon, Uracha Rungsardthong and Pitt Supaphol; *Nanotechnology* **2007**, *18*, 175102.

[76] I. Uslu, H. Daştan, A. Altaş, A. Yayli, O. Atakol, M. L. Aksu; *e-Polymers* **2007**, *133*.

[77] J. M. Gohil, A. Bhattacharya and P. Ray; *Journal of Polymer Research* **2006**, *13*, 161.

[78] Xiao-Hong Qin, Shan-Yuan Wang; *Journal of Applied Polymer Science* **2008,** *109*, 951.

[79] M. Krumova, D. López, R. Benavente, C. Mijangos, J. M. Pereña, *Polymer* **2000**, *41*, 9265.

[80] Enlong Yang, Xiaohong Qin, Shanyuan Wang, *Materials Letters* **2008,** *62*, 3555.

[81] J. Ruiz, A. Mantecón, V. Càdiz, *Polymer* **2001**, *42*, 6347.

[82] Li Yao, Thomas W. Haas, Anthony Guiseppi-Elie, Gary L. Bowlin, David. G. Simpson, and Gary E. Wnek; *Chem. Mater.* **2003**, *15*, 1860.

[83] Teresa M R Miranda, Adilson R Goncalves and MT Pessoa Amorim **2001** *Society of chemical Industry, Polymer International.*

[84] Jun Zeng, Haoqing Hou, Joachim H. Wendorff, Andreas Greiner, *Macromolecular Rapid Communications* **2005**, *26*, 1557.

[85] Yurong Liu, Brian Bolger, Paul A. Cahill, Garrett B. McGuinness, *Materials Letters* **2009**, *63*, 419.

[86] Chistina Tang, Carl D. Saquing, Jonathon R. Harding, and Saad A. Khan, *Macromolecules* **2010**, *43*, 630.

[87] Claudia Preininger and Piero Chiarelli, *Talanta* **2001**, *55(5)*, 973.

[88] E. *Z.* Casassa, A. M. Sarquis, C. H. Van Dyke, *Journal of Chemical Education* **1986**, *63, No. 1*, 57.

[89] Hiroshi Ochiai, Yuji Kurita, Ichiro Murakami, *Makromol. Chem.* **1988**, *189*, 351.

[90] Saulute Budriene, Asta Zubriene, Daina Nekrasiene and Gervydas Dienys, *Chemija (Vilnius)* **2002**, 103.

[91] Y. Z. Zhang, J. Venugopal, Z.-M. Huang, C. T. Lim, S. Ramakrishna, *Polymer* **2006** , *47*, 2911.

[92] Krystyna Burczak, Toshiya Fujisato, Motoyoshi Hatada and Yoshito Ikada, *Biomaterials* **1994**, *15(3)*, 231.

[93] Bin Ding, Hak-Yong Kim, Se-Chul Lee, Douk-Rae Lee, and Kyung-Ju Choi, *Fibers and Polymers* **2002**, *3(2)*, 73.

[94] Sung Jun Lee, Se Geun Lee, Hoyoung Kim, Won Seok Lyoo, *Journal of Applied Polymer Science* **2007**, *106*, 3430.

[95] Steffen Hofacker, Markus Mechtel, Michael Mager, Harald Kraus, *Progress in Organic Coatings* **2002**, *45*, 159.

[96] David Avnir, Thibaud Coradin, Ovadia Lev and Jacques Livage, *Journal of Materials Chemistry* **2006**, *16*, 1013.

[97] Abhijit Bandyopadhyay, Mousumi De Sarkar, Anil K. Bhowmick, *J Mater Sci* **2006**, *41*, 5981.

[98] A. Bandyopadhyay, M. De Sarkar, A. K. Bhowmick, *Journal of Materials Science* **2005**, *40*, 5233.

[99] Minglin Ma, Randal M. Hill and Gregory C. Rutledge, *Journal of Adhesion Science and Technology* **2008**, *22*, 1799.

[100] Larry L. Hench and Jon K. West, *Chem. Rev.* **1990**, *90*, 33.

[101] http://en.wikipedia.org/wiki/Wetting

[102] P. F. Rios, H. Dodiuk, S. Kenig, S. McCarthy and A. Dotan, *Polym. Adv. Technol.* **2008**, *19*, 1684.

[103] D. Mecerreyes, V. Alvaro, I. Cantero, M. Bengoetxea, P. A. Calvo, H. Grande, J. Rodriguez, J. A. Pomposo, *Adv. Mater.* **2002**, *14*, 749.

[104] Yuung-Ching Sheen, Wei-Hsuan Chang, Wen-Chang Chen, Yih-Her Chang, Yuan-Chang Huang, Feng-Chih Chang, *Mater. Chem. Phys.* **2008**.

[105] Bin Ding, Chunrong Li, Yoshio Hotta, Jinho Kim, Oriha Kuwaki and Seimei Shiratori, *Nanotechnology* **2006**, *17*, 4332.

[106] Nadir Kiraz, Esin Burunkaya, Ömer Kesmez, Meltem Asiltürk, H. Erdem Çamurlu, Ertuğrul Arpaç, *J Sol-Gel Sci Technol.*, DOI 10.1007/s10971-010-2298-2.

[107] *Coatings, Adhesives and Sealants*, Bayer MaterialScience, BMS-CAS-Innovation & Business Creation · Bayresit VPLS 2331 · Sales Aid.

[108] http://www.polyurethane.org/s_api/sec.asp?cid=947&did=3727

[109] Shahin Bonakdar, Shahiar Hojjati Emami, Mohammad Ali Shokrgozar, Afshin Farhadi, Seyed Amir Hoshiar Ahmadi, Amir Amanzadeh, *Materials Science and Engineering C* **2010**, *30*, 636.

[110] Friedrich Louis, Anne Schmidt-Tiedemann, Karl-Josef Schirra, *Use of pheromones*

and other semiochemicals in integrated production, IOBC wprs Bulletin **2002**, *25(9)*, 1.

[111] H. H. Shorey, R. S. Kaae, L. K. Gaston, J. R. McLaughlin, *Envir. Ent.* **1972**, *1*, 641.

[112] S.R. Farkas, H. H. Shorey and L. K. Gaston, *Environ. Entomol.* **1974,** *3*, 876.

[113] G. H. L. Rothschild, *Ent. exp. & appt.* **1974,** *17*, 294.

[114] H. Arn, B. Delley, M. Baggiolini and P. J. Charmillot, *Enr. exp. & appl.* **1976,** *19*, 139.

[115] J. C. Keller, E. B. Mitchell, G. McKibben, T. B. Davitch, *J. econ. Ent.* **1964**, *57*, 609.

[116] M. Beroza, B. A. Bierl, E. F. Knipling, R. J. G. Tardif, *J. econ. Ent.* **1971**, *64*, 1527.

[117] E. H. Glass, W. L. Roelofs, H. Am, A. Comeau, *J. econ. Ent.* **1970**, *63*, 370.

[118] H. H. Shorey, R. S. Kaae, L. K. Gaston, J. econ. Ent. **1974**, *67*, 347.

[119] Derek G. Campion, *Pestic. Sci.* **1976**, *7*, 636.

[120] Shinzo Omi, Nobuo Umeki, Hiroaki Mohi, Mamoru Iso, *Journal of Microencapsulation* **1991**, *8(4)*, 465.

[121] A. K. Minks, S. Voerman, and J. A. Klun, *Ent. exp. & appl.***1976**, *20*, 163.

[122] M. Beroza, C. S. Hood, D. Trefrey, D. E. Leonard, E. F. Knipling, W. Klassen and L. J. Stevens, *J. econ. Entomol.* **1974**, *67*, 659.

[123] J. Granett and C. C. Doane, *J. econ. Entomol.* **1975**, *68*, 435.

[124] Meir Ziv, Daniel E. Sonenshine, Robert M. Silverstein, Janet R. West, and Katherine H. Gingher, *Journal of Chemical Ecology* **1981**, *7(5)*, 829.

[125] http://www.modbee.com/2010/08/14/1294766/winegrape-growers-meet-discuss.html

[126] http://www.ccv.cl/reportajes_datos.php?id_reportaje=188

[127] R. Ideses, J.T.Klug, A.Shani, S.Gothilf, and E.Gurevitz, *Journal of Chemical Ecology* **1982**, *8(1)*, 195.

[128] Aristi R. Bachtsi, Costas Kiparissides, *Journal of Controlled Release* **1996**, *38*, 49.

[129] C.A. Finch, *Chemical reactions and stereochemistry of poly(vinyl alcohol), in: Poly(vinyl alcohol) Developments*, John Wiley and Sons, New York **1992**, 286.

[130] B. Gander, R. Gurni, E. Doelker and N. Peppas, *Pharm. Res.***1989**, *7*, 578.

[131] C.J. Kim and P.I. Lee, *Pharm. Res*. **1992**, *9***,** 10.

[132] Fabienne Faÿ, Isabelle Linossier, Gaëlle Legendre, Karine Vallée-Réhel, *Macromol. Symp.* **2008**, *272*, 45.

[133] A. Stoiljkovic, R. Venkatesh, E. Klimov, V. Raman, J. H.Wendorff, A. Greiner, *Macromolecules* **2009**, *42*, 6147.

[134] C. Vauthier, B. Cabane, D. Labarre, *European Journal of Pharmaceutics and Biopharmaceutics*, **2008**, 69, 466.

[135] J. Sun, K. Bubel, F. Chen, T. Kissel, S. Agarwal, A. Greiner, *Macromol. Rapid Commun.* **2010**, *31*, DOI: 10.1002/marc.201000379.

12. Acknowledgements

I would like to express my sincere gratitude to my direct supervisor Prof. Dr. Andreas Greiner for giving me such an interesting topic and also for his continuous support during my research work. He has been actively interested in my work and has always been available for advice.

My special thanks go to PD Dr. Seema Agarwal for her invaluable guidance and encouragement. This thesis would not have been possible without her support.

I would like to show my gratitude to Mrs. Edith Schmidt for taking care of my official and personal documents and for being ever-so polite and helpful.

I am grateful to all the members of our working group for their constant support and advice, not only related to my work but also in helping me to improve my German speaking skills. My special thanks go to my lab colleagues: Elisabeth Giebel, Judith Hehl and Kathrin Bubel for their cooperation and for providing me with a good working environment.

I would also like to thank Lisa Hamel for her help during the initial days of my research work.

I am grateful to Norman Grabe and Stefan Bokern for taking out time to measure my GPC samples and Dr. Marco Gensheimer and Christian Brandl for helping me out with the Infrared spectroscopy measurements.

I would like to thank Martina Gerlach and Anna Bier for the ordering of chemicals and glasswares and thereby ensuring that my work goes on smoothly.

I am thankful to Anna Bier, Claudia Mattheis, Christian Knierim, Christoph Luy, Fei Chen, Dr. Samarendra Maji and Syamkumar V. Mulpuri for helping me correct my Ph.D. thesis. My special thanks go to Kathrin Bubel and Sebastian Paulig for writing the Zusammenfassung.

A big thank you to Dr. Carsten Sinkel for helping me in computer related problems.

My sincere thanks also go to Mr. Michael Hellwig for his help in operating the scanning electron microscope.

I offer my regards to all those who supported me in any respect during the completion of my Ph.D. work and whose names I might have forgotten to mention.

Last but not the least, I owe my deepest gratitude to my father, Mr. Anil Bansal and my mother, Mrs. Aparna Bansal for their unconditional love and support. Without their blessings, this achievement would not have been possible.